DOE/JPL-No. 954698-80/1
Distribution Category UC-63

STUDY OF CURVED GLASS PHOTOVOLTAIC MODULE AND MODULE ELECTRICAL ISOLATION DESIGN REQUIREMENTS

Final Report

June 1980

Work performed under
Jet Propulsion Laboratory Contract No. 954698
for the
Engineering Area of the Low-Cost Solar Array Project

Prepared By

Bechtel National, Inc.
Research and Engineering Operation
50 Beale Street
P.O. Box 3965
San Francisco, California 94119

The JPL Low-Cost Solar Array Project is sponsored by the U.S. Department of Energy and forms part of the Solar Photovoltaic Conversion Program to initiate a major effort toward the development of low-cost solar arrays. This work was performed for the Jet Propulsion Laboratory, California Institute of Technology by agreement between NASA and DOE.

12218

ACKNOWLEDGEMENTS

This study was conducted as a team effort by members of Bechtel National, Inc., Research and Engineering Operation. Overall management responsibility rested with E.Y. Lam, Manager of the Power Technology Group. W.J. Stolte served as the Project Manager and D.J. Rosen was the Project Engineer.

ABSTRACT

Bechtel National, Inc., has conducted a study to evaluate the technical feasibility and cost effectiveness of curved glass superstrate photovoltaic modules for use in large scale applications such as central station power plants. The study also evaluated electrical insulation and isolation design considerations with regard to module encapsulation systems.

The design of a 1.2 by 2.4 m (4 by 8 ft) curved glass superstrate and support clip assembly is presented, along with the results of finite element computer analyses and a glass industry survey conducted to assess the technical and economic feasibility of the concept. Installed costs for four curved glass module array configurations are estimated and compared with costs previously reported for comparable flat glass module configurations.

Electrical properties of candidate module encapsulation systems are evaluated along with present industry practice for the design and testing of electrical insulation systems. Electrical design requirements for module encapsulation systems are also discussed.

TABLE OF CONTENTS

ILLUSTRATIONS

TABLES

Section 1

SUMMARY

This report presents the results of an engineering study conducted by he Research and Engineering Operation of Bechtel National, Inc., for the Engineering Area of the Jet Propulsion Laboratory's Low-Cost Solar Array Project under Contract Number 954698, as a part of the U.S. Department of Energy's Solar Photovoltaic Conversion Program. The objectives of the study were to evaluate the technical and economic feasibility of a curved glass superstrate photovoltaic module design and to assess the electrical isolation requirements of module encapsulation systems.

The study emphasized large scale applications, such as central station photovoltaic power plants. The general design approach and purchase quantities reflected what would be needed for a 200 MW (peak) plant. For study purposes, the plant was located at a 35° latitude, with the array tilt fixed at the latitude angle. An encapsulated cell efficiency of 15 percent, a Nominal Operating Cell Temperature (NOCT) efficiency of 92 percent, and a module packing efficiency of 0.92 were provided by JPL, thereby setting the module surface area required for the plant at 1.58×10^6 m^2. Estimated costs (in both 1975 and 1980 constant dollars) are presented in terms of dollars per square meter of total module surface area.

Based on analyses conducted during this study, the design of a curved glass superstrate module appears technically feasible. Stresses developed in a 1.2 x 2.4 m (4 x 8 ft) curved glass module, consisting of a 0.48 cm (0.187 in.) thick tempered glass plate, are acceptable for loadings of up to ±2.4 kPa (±50 psf) when the module is supported by four 30 cm (12 in.) long clip assemblies.

Comparison of installed costs for equivalent flat and curved glass superstrate array designs (including foundations, support structure and module framing) indicates that the use of curved glass superstrates can result in cost savings in the range of $3.00 to $10.00/m^2 (1980 dollars) for design structural loadings of 1.2 kPa (25 psf) to 2.4 kPa (50 psf). However, these costs are exclusive of fabrication costs for bending the glass.

A survey of glass suppliers and manufacturers indicated that although fabrication of the curved glass superstrates is technically feasible, no large scale production facilities presently exist that are capable of handling this glass size. Fabrication cost estimates (1980 dollars) ranged from about $18.00 to $30.00/m^2 for a production quantity of 4.6 x 10^5 m^2 (5 x 10^6 ft^2) per year.

It is possible that larger production volumes (in the range of 9 x 10^6 m^2 or 100 x 10^6 ft^2 per year) could result in significant reduction of this cost premium. However, at this time, glass

manufacturers are reluctant to speculate on large volume production costs for this type of operation.

Comparison of installed costs for surface type foundations (spread footings) and deep type foundations (caissons) indicates that, for proper soil conditions, caissons can result in costs savings of up to $11.00 (1980 dollars) per square meter of array for a design loading of 2.4 kPa (50 psf).

In the area of electrical isolation requirements, it was determined that the module encapsulation system will most likely be required to provide electrical isolation of energized modules. Therefore, the encapsulation system must maintain acceptable electrical insulating properties throughout the useful life of the module.

Existing industry experience with regard to the design and long-time performance characteristics of solid-dielectric insulating systems results primarily from the cable industry. The majority of this experience relates to operation with ac fields (60 Hz).

The electrical properties of materials are affected by both the physical configuration of the insulation system and the effects of aging. For example, the dielectric strength of most materials is dependent on the duration of voltage application, rate of voltage rise, material thickness, electrode configuration and

other parameters. In addition, corona, ultraviolet light, temperature, and other ambient conditions tend to reduce dielectric strength with time (aging). Therefore, adequate safety factors must be used in the design of an encapsulation system to ensure that electrical stress levels in the materials are sufficiently below those that would cause failure during the life of the module. The long-time dielectric strength of a material is sometimes referred to as the voltage endurance.

The required safety factor, that is the ratio of the measured short-time dielectric strength (the value usually presented on product data sheets) of a material to the maximum acceptable working stress during operation, is somewhat dependent on material properties, configuration and ambient conditions. For example, the cable industry presently specifies a safety factor of about 6 for polyethylene used as an insulator in high voltage ac cables. Although safety factors for module insulation, operating primarily in a dc field, will likely be somewhat lower, present knowledge about the aging mechanisms in dielectric materials over the long-term is not sufficient to formulate definite values.

Calculation of stress levels within module encapsulation systems must account for field intensifications resulting from sharp edges on solar cell interconnects and other conducting surfaces. In addition, for series dielectrics (laminates) ac stress distributes in proportion to the materials' permittivities and

relative thicknesses, while for dc fields the stress distributes in proportion to the materials' resistivities and thicknesses. Therefore, it is possible to develop high stress levels in thin material layers such as primers, adhesives, or cover films.

In addition to dielectric strength, the encapsulation system must maintain an acceptable level of leakage resistance. This requirement becomes more significant as module size increases and/or for increasing system voltages. Some of the candidate encapsulating materials (such as EVA) appear to have relatively low volume resistivities, so that it may be necessary to provide an additional layer of high resistance material (such as a Mylar sheet).

Previous attempts, primarily by the cable industry, to predict long-time insulation performance by means of accelerated aging tests have, at best, been only partially successful. This is especially true with regard to the effects of multiple aging parameters, which are likely to be present in the modules' operating environment. Therefore, it appears prudent that a testing program be established to evaluate the voltage endurance of module encapsulating systems under normal (real time) operating conditions.

Section 2

INTRODUCTION

Commercialization of large-scale terrestrial photovoltaic power systems requires optimization of both solar cell module and balance-of-plant designs, in order to achieve acceptable life-cycle energy costs.

This final report documents an engineering study to evaluate a curved glass photovoltaic module design and to assess the electrical isolation requirements of module encapsulation systems. The study was performed by the Research and Engineering Operation of Bechtel National, Inc., for the Engineering Area of the Jet Propulsion Laboratory's Low-Cost Solar Array (LSA) Project under Contract Number 954698, as a part of the U.S. Department of Energy's Solar Photovoltaic Conversion Program.

Specifically, the use of a curved glass superstrate module design was investigated to identify potential reductions in total installed costs for the module/structure/foundation system, primarily by reducing the required amount of panel steel, when compared to installed costs for flat glass modules as previously reported by Bechtel (Ref. 2-1).

The study also addressed the design procedures and material requirements necessary to ensure that the encapsulation materials

will maintain the required electrical isolation integrity throughout the design life of the module.

The primary emphasis of the study was on the design of large-scale systems such as photovoltaic central station power plants.

2.1 REPORT FORMAT

This report has been prepared in accordance with the format specified by JPL Document Number 1030-26, Rev. B.

2.2 COST BASES

In order to be consistent with current practice in the LSA Project, all costs in this report are presented in 1975 and 1980 constant dollars. Cost estimates were converted to 1975 and 1980 constant dollars by using factors from the LSA Price Deflator Table supplied by JPL.

Cost data are normalized to terms of dollars per square meter ($/m²). The cost data can be translated to other bases by dividing by appropriate conversion factors (e.g., $/W = $/m² divided by W/m², or $/ft² = $/m² divided by 10.764 ft²/m², etc.)

During the course of the study, efforts were made to uniformly apply design criteria as well as design and cost estimating procedures so as to produce unbiased results. The accuracy of

the cost estimates presented herein are consistent with the level of detail in an engineering study.

2.3 UNITS

For the most part, English units were used in performing the study. These units were subsequently converted to SI units for presentation in this report. The SI units were rounded to correspond to nominal values currently being used by the Engineering Area of JPL's LSA Project, as typified by the conversion of panel and array dimensions shown in Table 2-1.

TABLE 2-1

CONVERSION OF DIMENSIONAL UNITS

English Units (feet)	SI Units	
	Precise (meters)	Nominal (meters)
2	0.6096	0.6
4	1.2192	1.2
8	2.4384	2.4
16	4.8768	4.8
32	9.7536	9.8

Section 3

BASELINE PLANT DESCRIPTION

This section presents a brief description of the baseline plant design used in this study, in order to put ensuing discussions of its components into perspective.

3.1 TERMINOLOGY

At present, several institutions are working to establish a consistent set of terms and a hierarchy to describe the components and systems that comprise a photovoltaic power plant. Attempts are being made to have these terms be consistent, as far as possible, for both flat-plate and concentrator array designs.

Figure 3-1 delineates the meanings given to such terms within this report. Primary emphasis in the study described herein is on aspects of module, panel, and array design. However, for completeness, all terms relevant to a photovoltaic power plant are presented.

3.2 BASELINE PLANT FEATURES

The general design approach and purchase quantities used in this study reflect what would be needed for a 200 MWp central station photovoltaic power plant or similar large-scale application. The

SOLAR CELL – The basic photovoltaic device which generates electricity when exposed to sunlight.

MODULE – The smallest complete, environmentally protected assembly of solar cells and other components (including electrical connectors) designed to generate dc power when under unconcentrated terrestrial sunlight.

PANEL – A collection of one or more modules fastened together, factory preassembled and wired, forming a field installable unit.

ARRAY – A mechanically integrated assembly of panels together with support structure (including foundations) and other components, as required, to form a free-standing field installed unit that produces dc power.

BRANCH CIRCUIT – A group of modules or paralleled modules connected in a series to provide dc power at the dc voltage level of the power conditioning unit (PCU). A branch circuit may involve the interconnection of modules located in several arrays.

ARRAY SUBFIELD – A group of solar photovoltaic arrays associated by the collection of branch circuits that achieves the rated dc power level of the power conditioning unit.

ARRAY FIELD – The aggregate of all array subfields that generate power within the photovoltaic central power station.

PHOTOVOLTAIC CENTRAL POWER STATION – The array field together with auxiliary systems (power conditioning, wiring, switchyard, protection, control) and facilities required to convert terrestrial sunlight into ac electrical energy suitable for connection to an electric power grid.

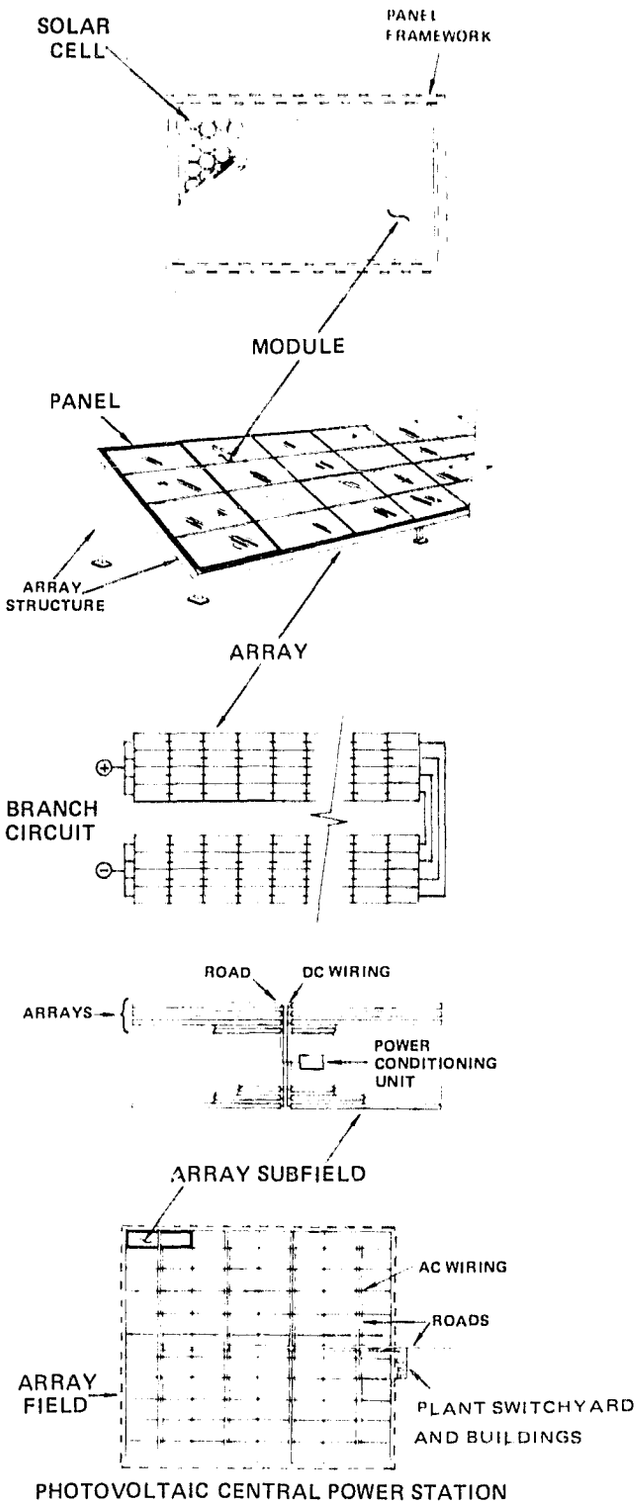

Figure 3-1 DELINEATION OF TERMINOLGY

postulated baseline plant concepts are those developed in previous studies by Bechtel (Refs. 2-1, 3-1, 3-2, and 3-3).

For purposes of this study, the plant is located at a 35° latitude, with the array tilt fixed at the latitude angle. An encapsulated cell efficiency of 15 percent, an NOCT efficiency of 92 percent, and a module packing efficiency of 0.92 are assumed, thereby setting the module surface area required for the plant at 1.58×10^6 m^2 (1.7×10^7 ft^2). Estimated costs are presented in terms of dollars per square meter of module surface area.

The collector unit shipped to the site for installation is a panel and consists of an assembly of one or more modules. The modules, in turn, support and encapsulate the solar cells. The panels are field installed on array structures at the plant site to form an array. Array slant heights of 2.4 m (8 ft) and 4.8 m (16 ft) are evaluated in this study. For the baseline plant, the arrays are approximately 152 m (500 ft) long, with adjacent arrays separated by 1.5 times the vertical height of the array (that is, 2.8 m (9.2 ft) interarray separation for 4.8 m (16 ft) slant heights and 1.4 m (4.6 ft) for 2.4 m (8 ft) slant heights). Additionally, maintenance roads (running parallel to the arrays) separate groups of arrays at spacings of approximately 18 m (60 ft). Main plant roads, transverse to the arrays, connect the maintenance roads.

Modules on pairs of adjacent arrays are wired in series to form a branch circuit with a nominal operating voltage of 1500 volts dc for the baseline plant. Higher branch circuit voltages would result in proportionately longer arrays. Several adjacent branch circuits are wired in parallel to obtain a current of approximately 300 amps. The 300 ampere dc feeder cables are brought to a power conditioning unit (pcu) within the array subfield. The dc feeder cables are direct buried and run alongside the main plant roads.

Each one of 36 power conditioning units is rated at approximately 6 MW at 1500 Vdc and includes all components (e.g., converter, harmonic filters, control circuitry, etc.) necessary to convert the dc output of the arrays into a 34 kV, 60 hertz waveform compatible with electric utility standards. Higher branch circuit voltages would result in use of fewer, but higher power rated units operating at the same current to obtain the same total power.

The filtered outputs of the power conditioning units in the array field are collected at 34 kV and brought to the plant switchyard by direct buried cables running parallel to the main plant roads. At the switchyard, the voltage is stepped up to 230 kV for connection to the utility transmission line.

The control and data acquisition system consists of microcomputers located within the power conditioning units and

connected by a serial data link to a central computer located in the central control room. The system monitors converter and array operating parameters and controls the converters to track the arrays' maximum power point with variations in insolation and temperature.

The plant design also includes switchgear, protective relaying, grounding and lightning protection systems, and other auxiliary systems required for proper plant operation and protection. Shops, warehouses, and other maintenance facilities are provided as required.

Section 4

CURVED GLASS MODULE DESIGN

This section presents a discussion of the curved glass superstrate module design including: design bases, module geometry, support clip design, a summary of finite element structural analyses and the results of a glass industry survey conducted to assess the feasibility and cost of large-scale manufacturing of curved glass modules.

As shown in Figure 3-1, a module is defined as a series-parallel interconnected set of solar cells terminating in two dc power leads (plus and minus) brought out through an encapsulant system. The encapsulant system provides environmental protection for the solar cells and may also provide structural support.

The majority of present and proposed module configurations may be divided into two broad categories: 1) superstrate, in which structural support is provided by a rigid transparent cover sheet such as glass and 2) substrate, in which structural support is provided by a rigid element behind the solar cells such as metal, plastic or wood.

This study is specifically concerned with the superstrate configuration using a glass cover sheet. Typically, a glass superstrate module consists of a glass sheet with an interconnected solar cell assembly fastened to it by an adhesive.

The cells are covered by a pottant material such as silicone rubber, polyvinyl butyral (PVB) or ethylene vinyl acetate (EVA). A back cover film, such as Mylar or Tedlar is often included to provide a moisture barrier.

As previously reported by Bechtel (Ref. 2-1), the optimum size for a glass superstrate module for use in large scale applications is about 1.2 x 2.4 m (4 by 8 ft). This is based on total installed costs per unit of collector area. Computer aided, finite element stress analyses (Ref. 2-1) indicate that a flat glass sheet of this size must be continuously supported around its perimeter (picture frame support) in order to be structurally sound under the projected loading conditions. Reference 2-1 also indicates that, depending on the specific design considered and the design loading, the cost for this type of module frame is in the range of 30 to 40 percent of the total module support (foundation, structure and frame) costs. Therefore, significant array cost savings may be realized if the panel (module) framing requirements can be reduced.

Attempts to reduce framing costs by putting the flat plate on four discrete clip supports instead of on the continuous support result in reaction forces concentrated in the region of the clips. This is because bending occurs in the glass at the corners of the clips, giving rise to unacceptably high local stress concentrations in the plate (Ref. 2-1).

One potential method of reducing the localized stress concentrations is to use a slightly curved glass sheet for the superstrate. The use of a slightly curved superstrate results in an arching action which reduces the magnitude of the bending moment in the glass at the support clip interfaces. This reduction occurs because a portion of the applied load (assumed to be normal to the glass) is reacted by a membrane force in the plane of the glass. This effect can be likened to that of a structural arch.

Aside from the glass sheet, the module materials contribute little structural strength to the assembly. In addition, these material requirements are essentially the same for both the flat and curved glass module assemblies. Therefore, to simplify the comparison between the two configurations, characteristics of the interconnected solar cell assembly and module encapsulating materials (aside from the glass) are not addressed in detail in this section.

4.1 DESIGN BASES

This section presents the design bases utilized for the design and evaluation of the curved glass superstrate module.

- Based on the results of previous Bechtel studies (Refs. 2-1 and 3-2) the module size is 1.2 by 2.4 m (4 by 8 ft).
- The thickness of the glass superstrate is constrained to be greater than 3.2 mm

(0.125 in.) for reasons of hail resistance, manufacturability and handling considerations (Ref. 2-1).

- The applied loads are 0.96, 1.7, and 2.4 kPa (20, 35, and 50 psf) and are uniform. In accordance with agreements with JPL, loads are assumed to act in either of the directions normal to the module surfaces and are not differentiated into dead and live load fractions relating to phenomenon which cause the loads.

4.2 MODULE DESIGN

The configuration of the curved glass module is illustrated in Figure 4-1.

As shown in the figure, the module consists of a 1.2 by 2.4 m (4 by 8 ft) glass sheet, 0.48 cm (0.187 in.) thick, which is curved to form a section of a cylinder. This is accomplished by heating the glass, either during initial manufacture or as a separate process. The glass is then bent, by sagging or use of a form, to the desired curvature and cooled. The axis of the cylinder is parallel to the long (2.4 m) edge of the glass and the radius of curvature is 2.4 m (8 ft). The glass is supported at four "discrete points" on the perimeter. The initial design analyzed in this study had support clips that were each 15 cm (6 in.) long, as shown in Figure 4-1. However, as reported in this section, computer aided stress analyses indicate that longer clips, on the order of 30 cm (12 in.), may be necessary to limit stress concentrations at the support clip/glass module interfaces to acceptable levels. The four support points are located on the

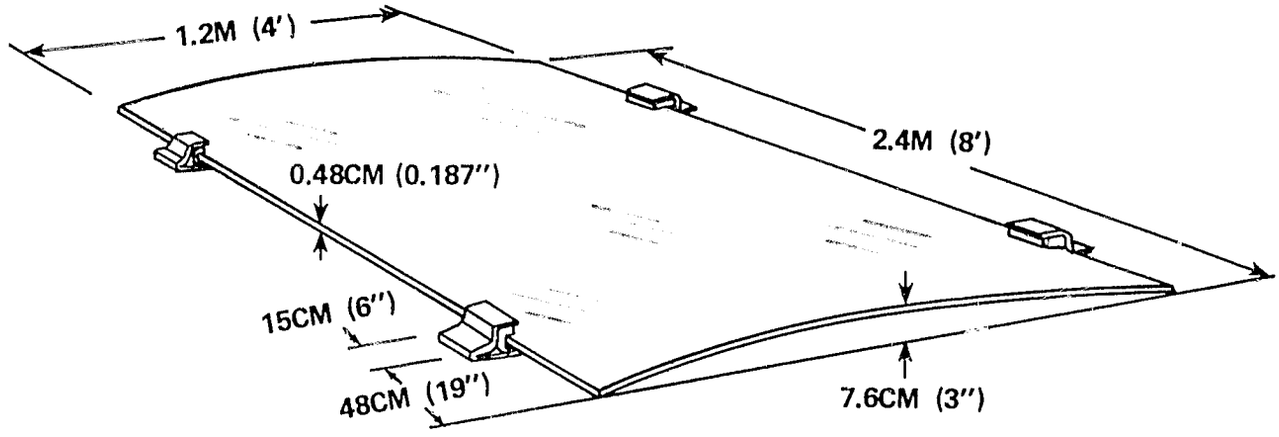

Figure 4-1 CURVED GLASS MODULE

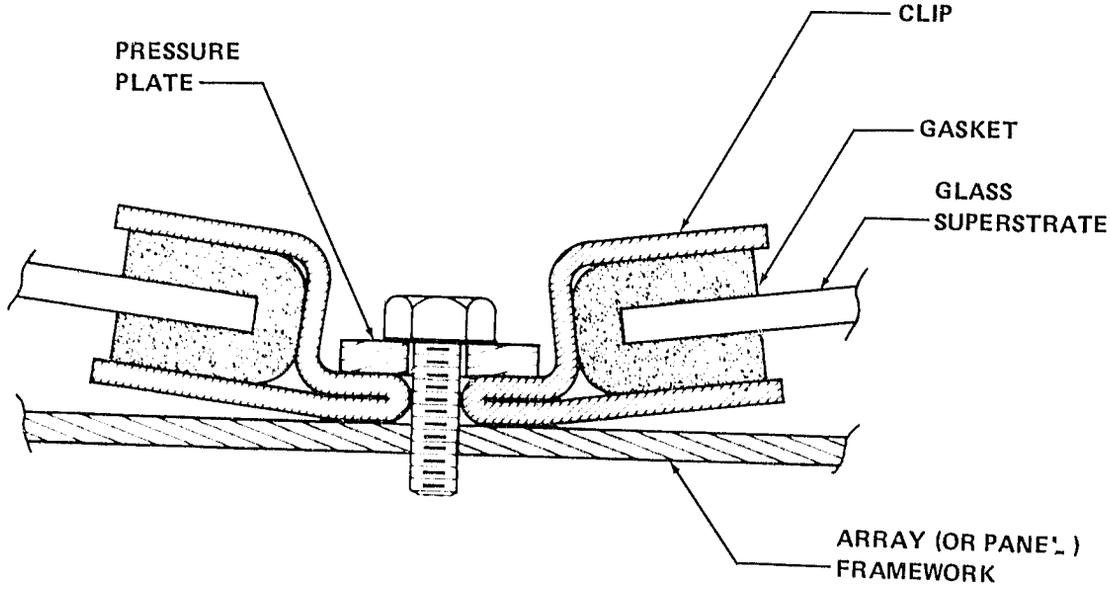

Figure 4 - 2 MODULE SUPPORT CLIP

long edges of the glass, approximately 20 percent (48 cm) in from each corner.

Loads applied to the module are transmitted to the support structure via the clip assemblies illustrated in Figure 4-2. With this design, membrane action will occur with loading of either surface of the module. That is, loading of the convex surface (in the case of downward loading) results in a compressive membrane force, while loading of the concave surface (in the case of uplift) results in a tensile membrane force. The designer need only insure that the allowable working compressive and tensile stresses of the glass are not exceeded at the design load.

Each support clip consists of a galvanized cold rolled steel section (12 gage). A 6.4 mm (0.25 in) thick gasket of 70 $\pm$ 20 durometer rubber surrounds the glass and provides the interface between the glass superstrate and the steel support clip. The gasket is attached to both the metal clip and the glass superstrate by an adhesive, such as any one of a number of commercially available epoxies.

The adhesive restrains relative movement between the glass and the gasket/clip assembly. This is especially important in the case of uplift (negative loading) on the curved glass module configuration, as discussed in Section 4.3. Movement resulting

from downward loading is constrained primarily by the design of the clip.

The clip overlap on the glass was selected to be 2.5 cm (1.0 in.). Therefore, the total contact surface between the curved glass superstrate and the four support clips is 310 cm^2 (48 in^2). The maximum loading is 2.4 kPa (50 psf), or 7130 newtons (1600 lbs.) for the module. Under these conditions, the average shear stress between the glass/gasket and the gasket/clip interfaces is 235 kPa (33 psi). This appears to be within the capabilities of available adhesives (Ref. 4-1) and gasket materials.

It may be necessary to provide an edge seal around the entire perimeter of the glass module. This requirement will likely depend on the characteristics of the encapsulating material(s) used to protect the back of the cells. Edge sealing could be accomplished using techniques presently under investigation (Ref. 4-2). This sealing is not expected to contribute to the structural support of the module.

The module/support clip assembly can be factory assembled onto panel frames or shipped to the field for direct installation on the array structure. This is discussed further in Section 5.

The modules are fastened to the array structure (or panel frame) by bolts and metal pressure plates, as illustrated in Figure 4-2.

The use of pressure plates to clamp the clip assemblies to the array structure will likely ease manufacturing and construction tolerances by eliminating the need for alignment between mounting holes on the support structure and module clips.

4.3 COMPUTER ANALYSES

The curved glass module design was evaluated using finite element computer analyses to determine the stresses in the glass and deflections resulting from uniform loading. These analyses were conducted to refine and supplement previous evaluations made by Bechtel (Ref. 2-1). Refinements include a finer mesh in the vicinity of the support clips, modeling of the rubber support gaskets and use of the MSC/NASTRAN program instead of the ANSYS program used in the previous work.

Finite element analysis techniques are widely used to provide approximate solutions to complex structural problems. Basically, the technique involves dividing the structure to be analyzed into a number of discrete (finite) elements, whose structural properties can be modeled via mathematical equations. By using appropriate numerical techniques, sets of equations representing each of the elements are solved simultaneously to determine the response of the structural system. The accuracy of the solution depends, to a large part, on the boundary conditions (the method used to model the characteristics of the support clip/gasket

assembly) as well as the number of elements used in the model. The latter is defined by the finite element mesh.

The MSC/NASTRAN computer program was selected for these analyses, rather than the ANSYS program used in the previous evaluations.

One reason for this change is that the NASTRAN output was felt to be better formatted than the ANSYS output, thereby facilitating evaluation of the results. In addition, the NASTRAN program provides output data which makes the evaluation of the degree of convergence to the theoretical solution easier during a nonlinear analysis.

It is generally necessary to utilize non-linear analyses when evaluating plates and shells that undergo deflections which are larger than the plate thickness. This is indeed the case for the flat glass module configurations reported on in Ref. 2-1. Therfore, to provide consistency, as well as the same level of accuracy, initial analyses of the curved module were also conducted using non-linear techniques. However, as will be illustrated in the following discussion, the curved geometry of this configuration results in significant membrane action, even at relatively low loading levels. Therefore, structural deflections are significantly less than those occuring in flat plate configurations. As a result, it was concluded during this study that, within the specified loading (±2.4 kPa), linear

(small deflection) analyses are generally adequate for evaluation of the curved glass module.

Since the nonlinear analysis capability was a new release by MSC/NASTRAN, it was felt necessary to verify its performance. The programs were compared for a 1.2 x 2.4 m (4 by 8 ft) flat plate with continuous edge support in a "picture frame" module. This was done to allow comparisons to be made with existing experimental data and previous analyses.

The results are compared in Figures 4-3 and 4-4. Figure 4-3 shows total and membrane stresses as a function of loading for the center of the flat plate with a hinged boundary condition. Within the accuracy of the plot, the ANSYS and NASTRAN solutions for total stress are represented by a single (dashed) line. This is also true of the data presented in Figure 4-4 which shows total stress at the center and corners of the plate. As shown in the figures, good agreement was obtained between the ANSYS and NASTRAN results, as well as with the experimental data.

4.3.1 Model Development

Development of the finite element mesh was based on the following criteria:

- In regions of high stress gradients the mesh should be fine enough to accurately model the behavior.

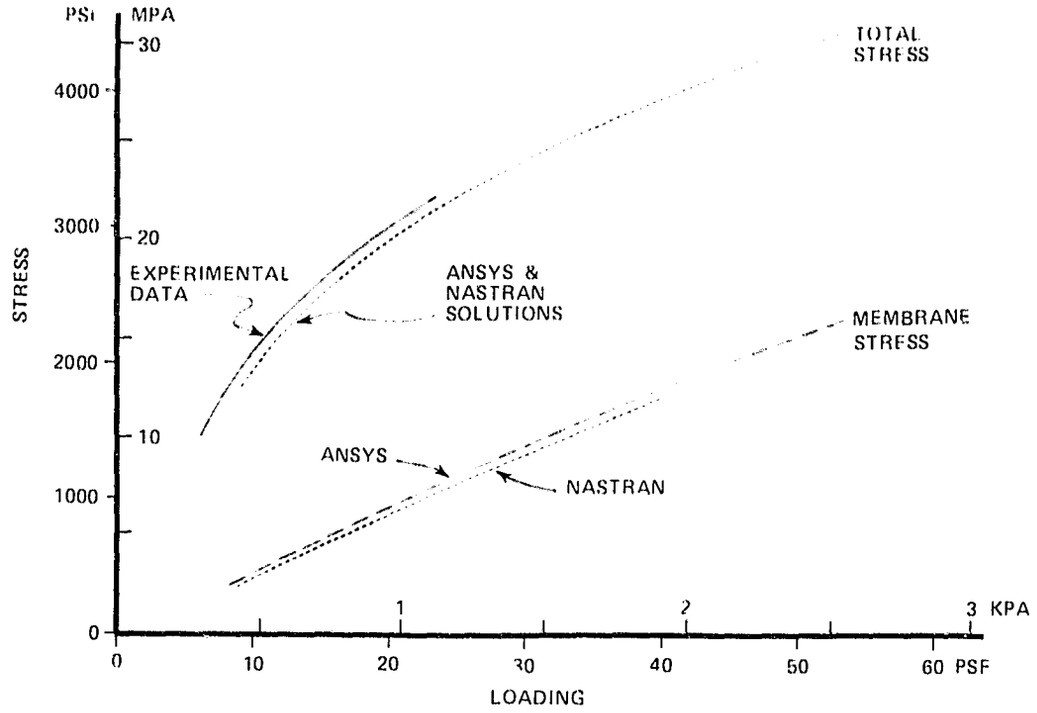

Figure 4-3 STRESS AT CENTER OF FLAT PLATE

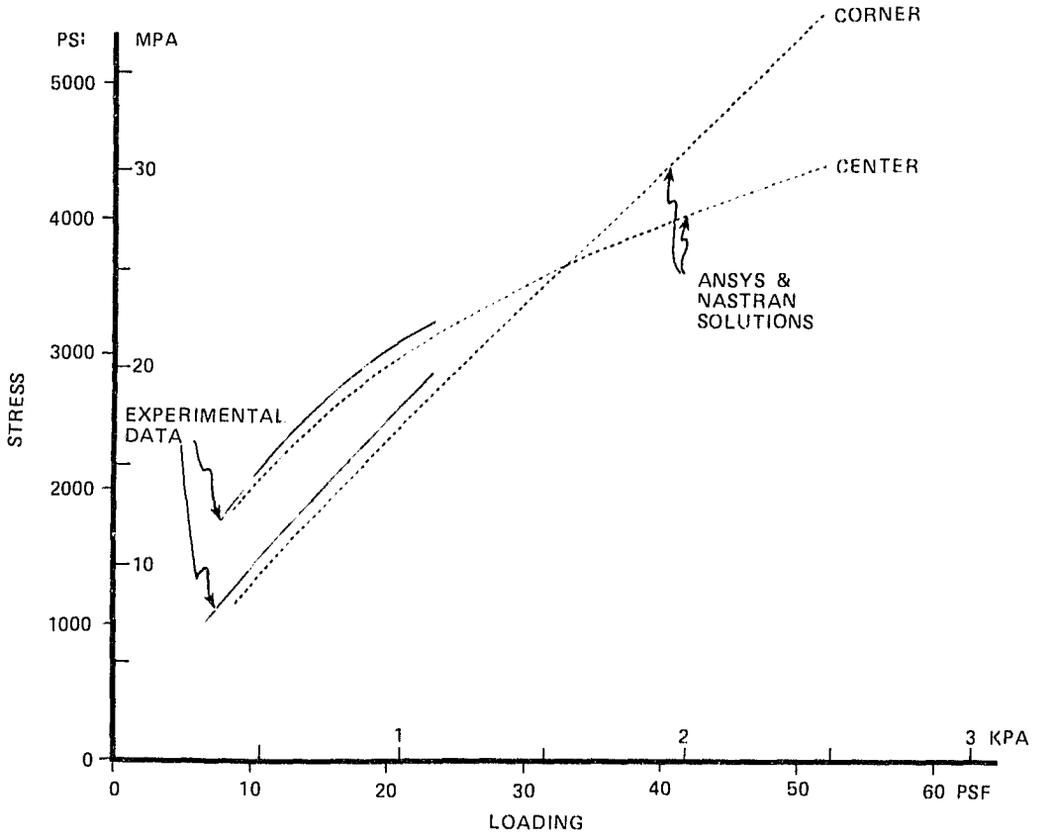

Figure 4-4 STRESS VERSUS LOADING—FLAT PLATE

- There should be no large aspect ratios for the elements.
- There should be no abrupt or discontinuous changes in the mesh.
- Symmetry should be used so that only one quarter of the plate is analyzed to minimize the computational effort

The finite element mesh developed for these analyses is illustrated in Figure 4-5. Taking advantage of symmetry to reduce computational costs, the mesh models one quarter of the 1.2 x 2.4 m (4 by 8 ft) module and includes one support clip/gasket assembly. As shown in the figure, a significantly finer mesh is used in the region of the support clip, where the highest stresses are anticipated.

This finer mesh is illustrated in Figure 4-6, which shows the mesh used to model the gasket material. A 1.27 cm (1/2 in.) mesh is used in the area of the glass/gasket interface, as compared to a 5.1 cm (2 in.) mesh used in previous analyses (Ref. 2-1). A 5.1 cm (2 in.) mesh is used in the other areas of the glass sheet, as compared to a 10.2 cm (4 in.) mesh used previously.

The gasket was modeled using three dimensional solid finite elements with properties specified to represent the rubber material. Several hardnesses of rubber were examined, as discussed further in Section 4.3.5. The metal support clip was modeled using finite elements (not illustrated).

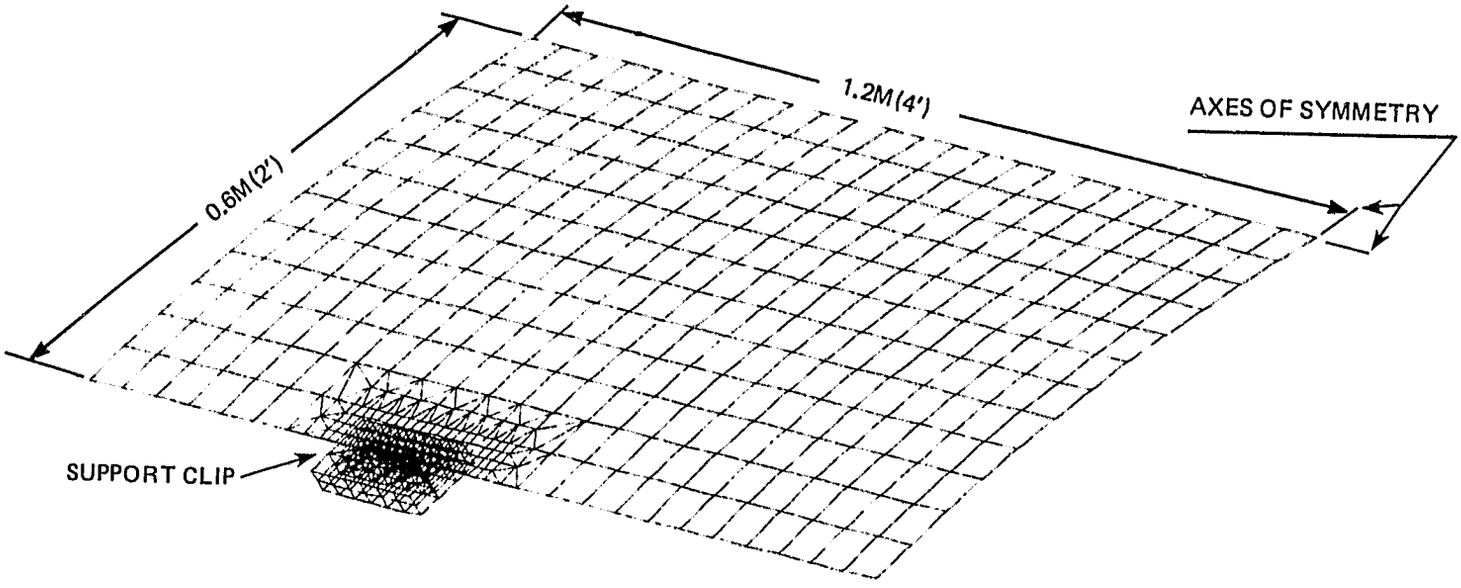

Figure 4-5 FINITE ELEMENT MESH

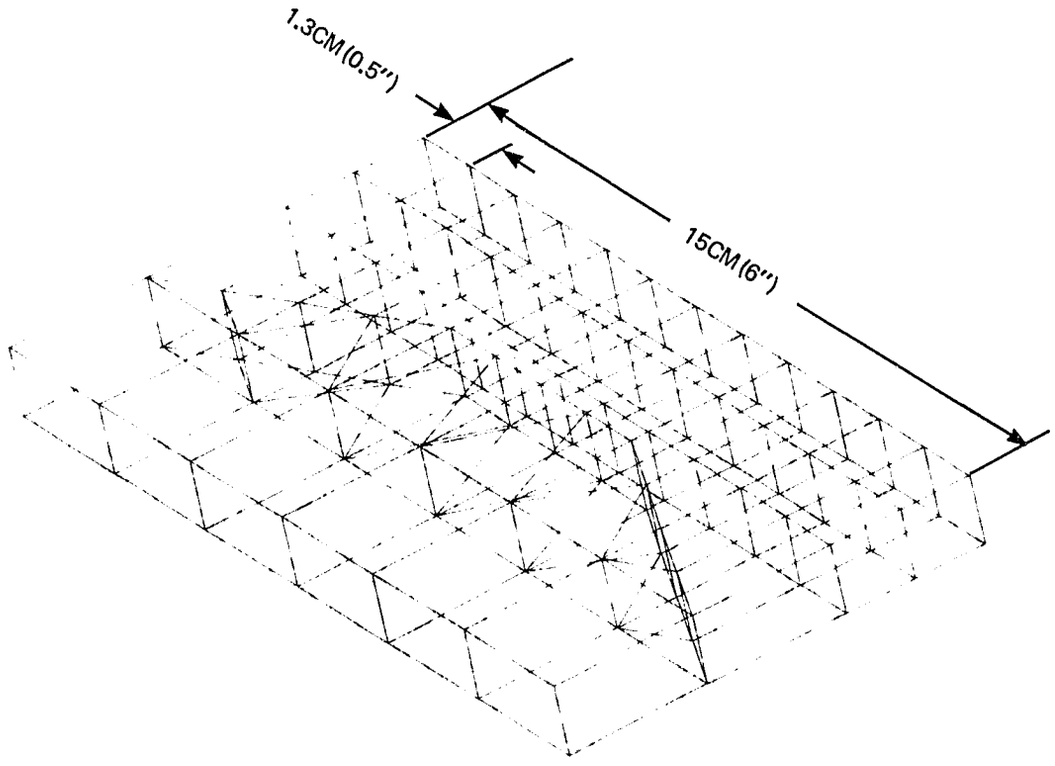

Figure 4-6 LOWER PORTION OF SUPPORT GASKET

Points on the bases of the support clips are fixed against motions. In addition, as discussed in Section 4.2, relative motion between the glass/gasket and gasket/clip interfaces is not permitted. This is done to ensure that the glass sheet is restrained and can not be "sucked-out" of the support clips with uplift loading. In practice, this means that the gasket would be fastened to the glass and clips by an adhesive. For these analyses, a perfect adhesive was assumed. This simplification does not affect the results because in an actual module, the elasticity of the adhesive would be much less than that of the rubber gasket.

4.3.2 Nonlinear Analysis

Attempts to analyze the curved glass superstrate design using the NASTRAN nonlinear analysis capability were unsuccessful. The failure to complete the analyses using these techniques resulted from numerical instabilities which occurred as the program attempted to reach a converged solution.

Nonlinear structural analysis routines utilize iterative mathematical techniques and are therefore expensive to run. The limited resources of the project did not allow a complete evaluation of the problem or identification of the source of the error. Knowledgeable consultants, both within and outside the Bechtel organization, having considerable experience with the NASTRAN program were also unable to specify remedies.

It was decided that one potential cause of the difficulty could be a structural instability of the glass plate. Therefore, a buckling analysis was conducted to evaluate the stability of the design.

4.3.3 Buckling and Snap-Through Analyses

A glass plate, unlike ductile plates made of metals and plastics, cannot survive the buckling transition from one stable form to another. For the design being investigated, there are two forms of elastic instability. One is symmetric and, for shallow shells and arches, is referred to as snap-through buckling. The other is antisymmetric and the deformed shape is referred to as the buckled shape. Obviously, if the design is unstable at a load below the design load, then the module would fail catastrophically when the loading exceeds the critical buckling or snap-through load.

The stability of the curved module was investigated by performing a buckling analysis of a simply supported module configuration (hinged supports). The MSC/NASTRAN program was used to calculate the buckling eigenvalues and eigenvectors. The lowest buckling eigenvalue, for an applied load of 0.48 kPa (10 psf) on the module is 9.75. Consequently, the buckling load is estimated as 4.67 kPa (97.5 psf). The buckled shape of the module is shown in Figure 4-7.

Because the actual support would be flexible, two other support conditions more closely resembling the rubber gasket were also investigated. Both involved a model simply supported against motion in the direction normal to the shell and with springs of arbitrary stiffness in the tangential direction. For spring constants of 60,000 and 6,000 psi, the estimated buckling loads are 102 and 109 psf respectively.

A check of the computer results was made by calculating approximate buckling loads using equations from Ref. 4 3. It was found that the buckling load for a continuously supported arch lies between 6.98 and 13.25 kPa (146 and 277 psf) depending on the fixity of the supports. Thus, the value of 4.67 kPa (97.5 psf) given by the NASTRAN program appears to be reasonable for an arch shell supported by four 15 cm (6 in.) long clips. This indicates that the curved glass superstrate module would be stable under the 2.4 kPa (50 psf) uniform design load. The snap-through load was calculated to be 9.58 kPa (200 psf) by using equations given in Ref. 4-4.

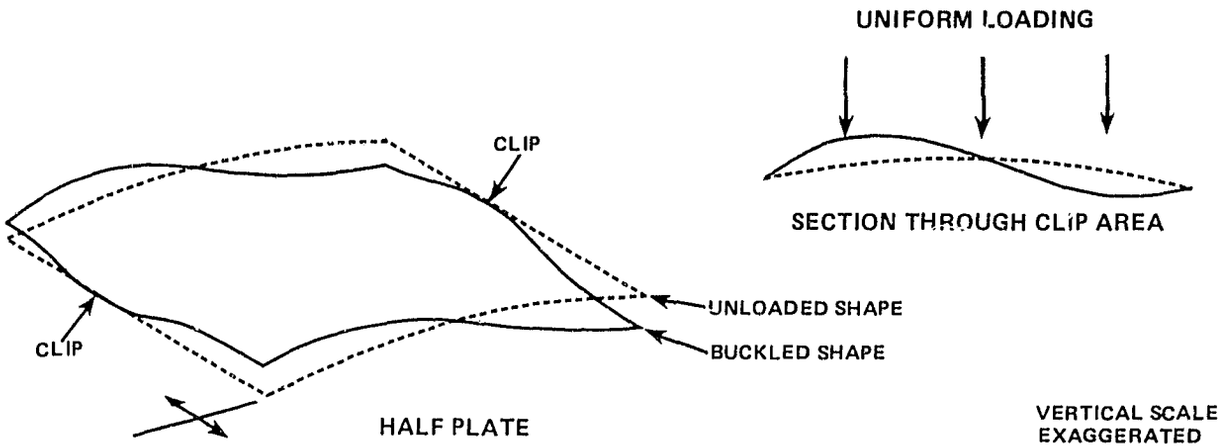

Figure 4-7 BUCKLED SHAPE FOR CURVED GLASS PLATE UNDER UNIFORM LOADING

4.3.4 Assessment of Nonlinearity

Previous nonlinear analyses of the curved glass module indicated that the maximum deflection would be only slightly greater than the plate thickness at a loading of 2.4 kPa (50 psf), thus indicating that nonlinear analyses might not be required. A recently developed technique (Ref. 4-5) was utilized to assess the degree of nonlinearity of the curved glass module under the design loading conditions of ±2.4 kPa (±50 psf).

The technique is based on measuring the difference in the load vector as determined by a regular stiffness analysis and a differential stiffness analysis. The latter is a first order

approximation of the geometric nonlinear approach. A general mathematical description of the method follows.

$$[Kxx] = [Kaa + Kdaa]$$

$$(Px) = [Kxx] (Ulv)$$

$$(Py) = (Px) \cdot (Px)$$

$$(Pz) = (Pl) \cdot (Pl)$$

$$\text{ratio} = \frac{(Py)}{(Pz)}$$

where

[Kaa] = stiffness matrix for a linear elastic static analysis

(Ulv) = displacement matrix

(Pl) = load vector

[Kdaa] = differential stiffness matrix

(Px) = revised load vector

(Py) = 1x1 matrix or scalar measure of (Px)

(Pz) = 1x1 matrix or scalar measure of (Pl)

A ratio close to 1.0 indicates that there has not been much change in the stiffness matrix after making first order corrections, so that significant error will not result from ignoring the effects of geometric nonlinearities.

Table 4-1 is a listing of the load vectors and their ratios for 3 cases using different mesh sizes and loadings. One case uses the 7.6 cm (3 in.) square mesh that was used to determine the buckling load. The remaining two cases use a 5.1 cm (2 in.)

square mesh (as shown in Figure 4-5) and 2.4 kPa (50 psf) loading in the downward and upward directions (negative loading indicates uplift). As can be seen from the table, the nonlinearity is somewhat greater with upward loading. This is due to the fact that with an upward pressure the curved module responds by trying to assume the shape of a funicular curve.

TABLE 4-1

MEASURE OF NONLINEARITY

Mesh Size (cm)	(in)	Loading (kPa)	(psf)	Py (psf)	Pz (psf)	Ratio Py/Pz	Deviation
7.6x7.6	3x3	0.48	10	92.23	93.11	0.9905	0.0095
5.1x5.1	2x2	2.4	50	495.92	512.96	0.9668	0.0332
5.1x5.1	2x2	-2.4	-50	580.11	512.85	1.1309	0.1309

Based on the data presented in Table 4-1, it was decided that linear analyses would generally be acceptable for the present purposes.

4.3.5 Analytical Results

The following cases were evaluated using the MSC/NASTRAN linear analysis capabilites:

- Six inch clip, hard (91 durometer) rubber gasket, ±50 psf loadings

- Six inch clip, soft (49 durometer) rubber gasket, ±50 psf loadings
- Twelve inch clip, hard (91 durometer) rubber gasket, 50 psf loading

All stresses are reported as principal stresses. Positive stresses are tensile and negative stresses are compressive. Principal stresses calculated at the neutral surface of the shell provide a direct reading of the tension (or compression) in the module and the tension (or compression) induced at the support by the wind load. Major (most positive) and minor (most negative) principal stresses at the top and the bottom surfaces provide a measure of the bending induced by normal loads.

Six Inch Clip-Hard Gasket. This model uses a "hard" rubber gasket and a 5.1 x 5.1 cm (2 x 2 in.) mesh. The term "hard" is used to denote rubber with a Young's modulus of 20.7 MPa (3000 psi). This is approximately equivalent to 91 durometer (as given by Figure 1 in ASTM D 1415).

The deformed shape of the module under a 2.4 kPa (50 psf) downward load is illustrated in Figure 4-8. The figure presents an isometric projection of the displaced shape of the quarter module analyzed and is overlayed on the unloaded shape. The displacements have been greatly magnified for graphic presentation. The figure also presents a displacement contour plot showing the actual magnitudes of the displacements. The maximum displacement occurs at the center of the long edge and is

0.6 cm (0.237 inches), 26 percent greater than the thickness of the plate.

Contour plots of the major and minor principal stresses are presented in Figures 4-9 and 4-10, respectively. As shown in Figure 4-9, the highest tensile stress occurs at the edge of the clip, on the top surface of the plate and is 16.2 MPa (2345 psi). The tensile stress on the bottom of the plate at the center of the long edge is 15.1 MPa (2190 psi). Although the maximum tensile stresses appear to be within acceptable limits, Figure 4-10 indicates that a relatively high (75.1 MPa or 10,900 psi) compressive stress occurs on the bottom of the plate at the corner of the support clip. While this may be an acceptable condition for downward loading, the same may not hold true for an uplift condition. This is because changing the direction of the loading force in this manner will generally result in the previous compressive stresses becoming tensile stresses and vice versa.

Evaluation of the same model for a -2.4 kPa (-50 psf) (uplift) loading essentially resulted in a reversal of stresses and deflections. Figure 4-11 illustrates the deformed shape. The principal significance is that the 75.1 MPa (10,900 psi) compressive force at the corner of clip becomes a tensile force. It should be remembered that these results are based on a linear analysis and that geometric nonlinearities would actually result in some differences in deflections and stresses between the two

DEFORMED SHAPE
(DISPLACEMENTS MAGNIFIED)

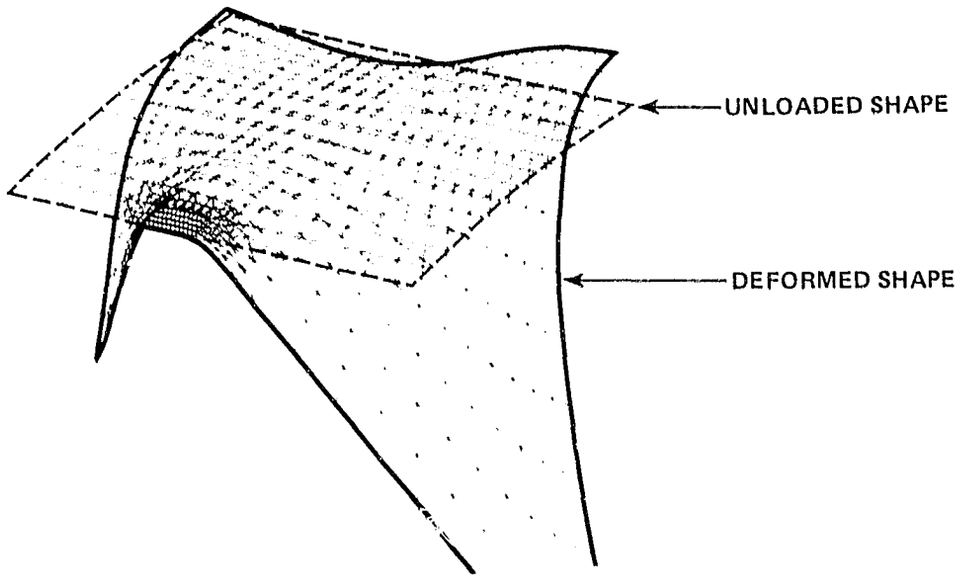

DISPLACEMENT CONTOURS

DISPLACEMENTS

Contour	cm	inches
1	0.0005	0.0002
5	0.127	0.050
10	0.284	0.112
15	0.444	0.175
20	0.600	0.237

Figure 4-8 DEFORMED SHAPE FOR DOWNWARD LOADING

TOP SURFACE

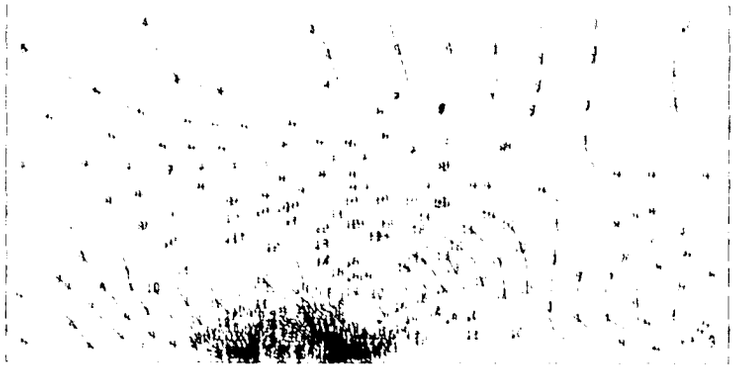

Contour	STRESS MPa	psi
1	-3.65	-530
5	0.48	70
10	5.72	830
15	10.96	1590
20	16.17	2345

MIDDLE SURFACE

Contour	STRESS MPa	psi
1	-2.14	-310
5	0.34	50
10	3.45	500
15	6.62	960
20	9.72	1410

BOTTOM SURFACE

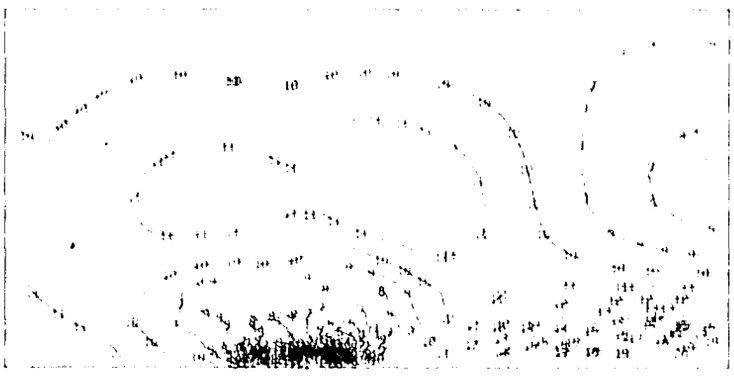

Contour	STRESS MPa	psi
1	-13.51	-1960
5	-7.45	-1080
10	0.52	75
15	7.58	1100
20	15.13	2195

Figure 4-9 MAJOR PRINCIPAL STRESSES—SIX INCH CLIP—HARD GASKET

TOP SURFACE

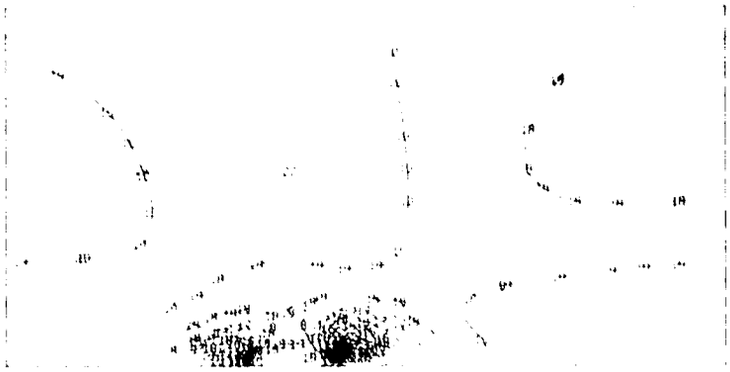

Contour	STRESS MPa	psi
1	-13.31	-1930
5	-9.10	-1320
10	-3.83	-555
15	0.14	20
20	0.69	100

BOTTOM SURFACE

Contour	STRESS MPa	psi
1	-75.15	-10900
5	-59.16	-8580
10	-39.16	-5680
15	-19.24	-2790
20	0.69	100

Figure 4-10 MINOR PRINCIPAL STRESSES–SIX INCH CLIP–HARD GASKET

loading conditions. However, the high stress occurs at the edge of the clip, where deflections are relatively small. Therefore, it may be assumed that the effects of geometric nonlinearities are also small.

Six Inch Clip - Soft Gasket. Based on the preceding results, an attempt was made to make the support more flexible by reducing the gasket material stiffness by a factor of ten and reducing the support plate thickness from 0.48 cm (3/16 in.) to 0.32 cm (1/8 in.). The soft rubber has a Young's modulus of 2.07 MPa (300 psi) and is equivalent to 49 durometer hardness.

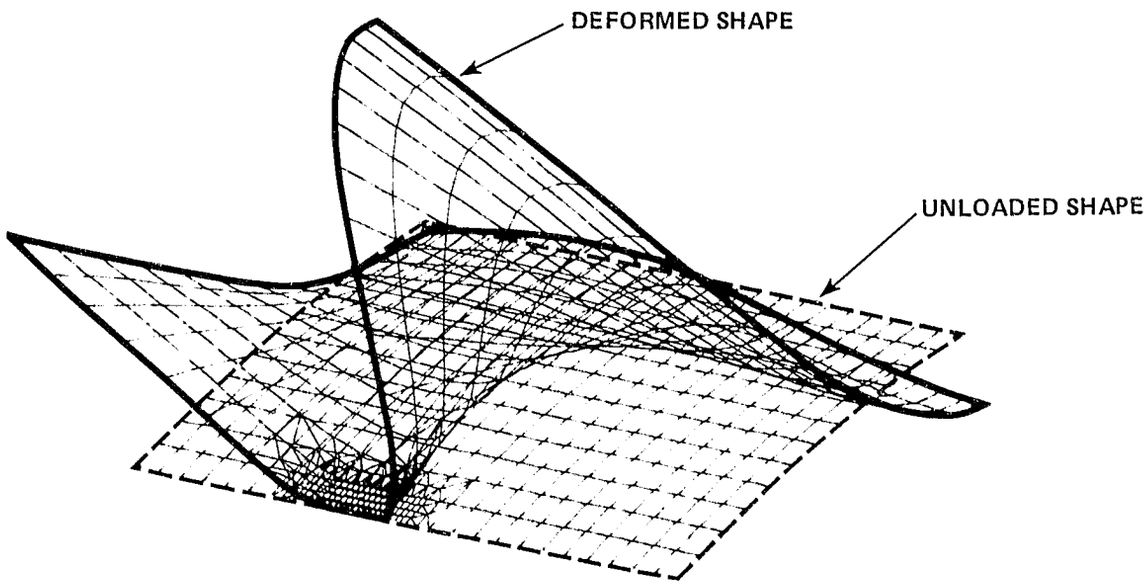

Figure 4-11 DEFORMED SHAPE FOR UPLIFT

It was hoped that this would reduce the high stress concentrations at the edge of the clip by transferring some of the load to the inner part of the gasket.

The maximum displacement at the center of the long edge increased 2.7 percent to 0.62 cm (0.243 in.). A review of the stress contour plots (Figures 4-12 and 4-13) shows some transfer of stresses occurred and the inner part of the gasket and clamped plate are taking some of the load. This resulted in a 2.4 percent increase in tensile stress on the bottom of the plate at the center of the long edge. The tensile stress on the top of the plate at the edge of the clip was essentially unchanged. However, as indicated in Figure 4-13, the compressive stress (for downward loading) on the bottom of the plate at the edge of the clip increased by about 1 percent to 75.9 MPa (11,000 psi). Based on this data, it appears that for the 15 cm (6 in.) clip, both hard and soft gaskets result in unacceptably high stresses.

Twelve Inch Clip - Hard-Gasket. The effect of clip size on the stress distributions was investigated by modifying the 2 x 2 in. mesh model to incorporate a 12 in. support clip with a hard rubber gasket. The maximum deflection at the center of the long edge was 0.47 cm (0.186 in.) for a downward loading of 2.4 kPa (50 psf). This compares well with the results obtained for a 12 in. clip model analyzed using the ANSYS computer program nonlinear capability (Ref. 2-1), which indicated a maximum deflection of 0.50 cm (0.195 in.).

TOP SURFACE

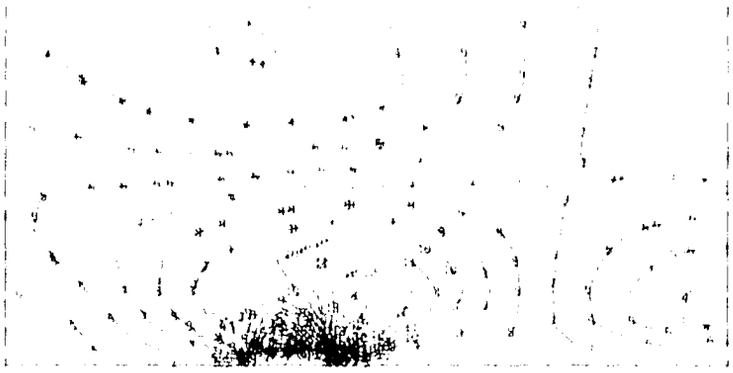

Contour	STRESS MPa	psi
1	-4.14	-600
5	1.65	240
10	8.89	1290
15	16.13	2340

MIDDLE SURFACE

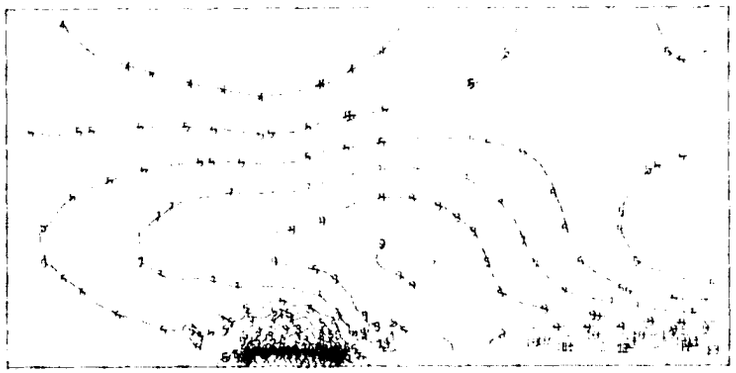

Contour	STRESS MPa	psi
1	-3.58	-520
5	0.90	130
10	6.48	940
15	12.17	1765

BOTTOM SURFACE

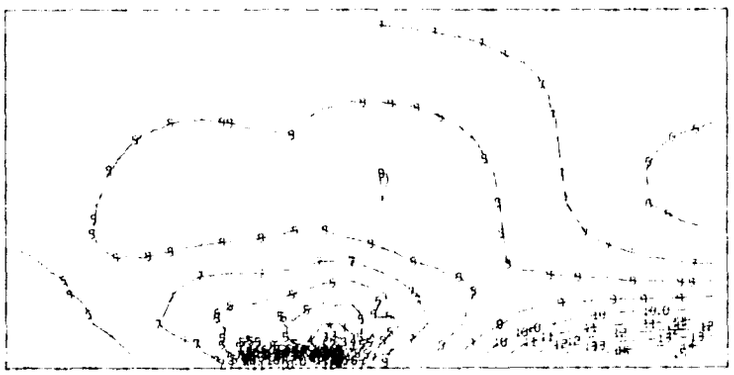

Contour	STRESS MPa	psi
1	-13.17	-1910
5	-4.96	-720
10	5.24	760
15	15.51	2250

Figure 4-12 MAJOR PRINCIPAL STRESSES—SIX INCH CLIP—SOFT GASKET

TOP SURFACE

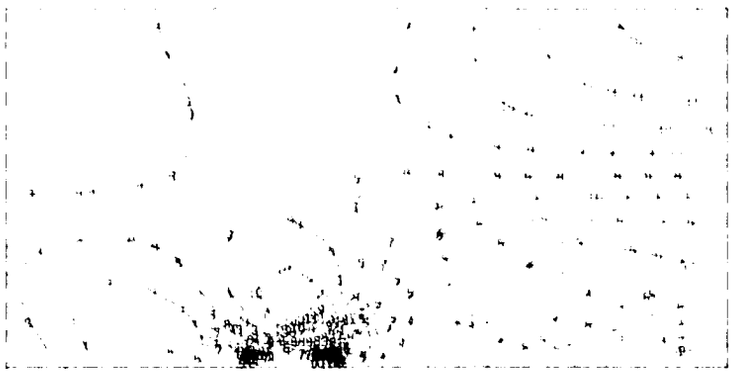

Contour	STRESS MPa	psi
1	-13.41	-1945
5	-7.38	-1070
10	0.10	15
15	7.58	1100

BOTTOM SURFACE

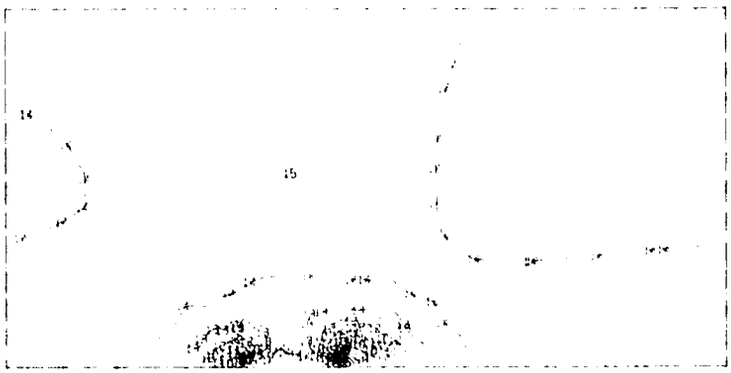

Contour	STRESS MPa	psi
1	-75.84	-11000
5	-53.92	-7820
10	-26.48	-3840
15	1.03	150

Figure 4-13 MINOR PRINCIPAL STRESSES–SIX INCH CLIP–SOFT GASKET

Contour plots of the principal stresses are presented in Figures 4-14 and 4-15. The maximum tensile stress on the top of the plate, at the corner of the clip, is 10.6 MPa (1540 psf). The ANSYS analysis resulted in a stress at this point of 14.2 MPa (2070 psi). The tensile stress on the bottom of the plate at the center of the long edge is 14.3 MPa (2080 psi). This compares with 18.6 MPa (2700 psi) for the ANSYS nonlinear analysis. It is interesting to note that the maximum tensile stress (24.8 MPa or 3600 psi) occurs in the middle surface of the plate, at the center of the long edge and is therefore a membrane stress.

The maximum compressive stress (downward loading) occurs on the bottom of the plate, at the corner of the clip, in the same relative position as with the six inch clip. However, as shown in Figure 4-15, the value has been reduced to 32.1 MPa (4650 psi). This compares with 31.0 MPa (4500 psi) obtained from the ANSYS analysis.

The results of the twelve inch clip analysis indicate that the maximum stress concentrations have been reduced to generally acceptable levels. In addition, the reasonably good agreement between the results of the linear NASTRAN and nonlinear ANSYS results lends further credence to the belief that linear analyses provide an acceptable level of accuracy for the evaluation of this design.

TOP SURFACE

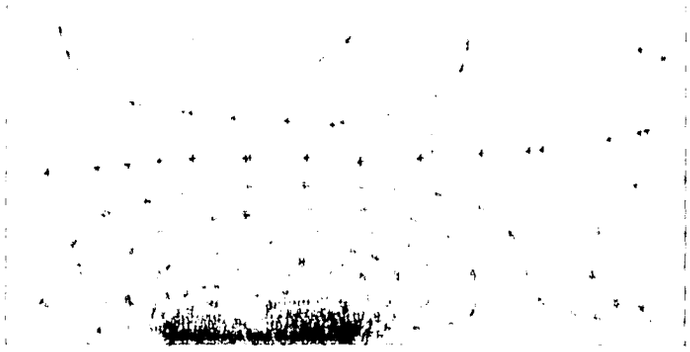

Contour	STRESS MPa	psi
1	-2.17	-315
5	1.45	210
10	6.00	870
15	10.55	1530

MIDDLE SURFACE

Contour	STRESS MPa	psi
1	-5.31	-770
5	3.28	475
10	14.00	2030
15	24.82	3600

BOTTOM SURFACE

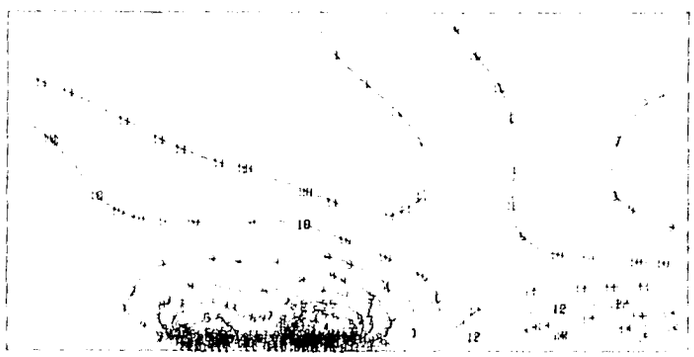

Contour	STRESS MPa	psi
1	-21.93	-3180
5	-11.58	-1680
10	1.38	200
15	14.34	2080

Figure 4-14 MAJOR PRINCIPAL STRESSES—TWELVE INCH CLIP—HARD GASKET

TOP SURFACE

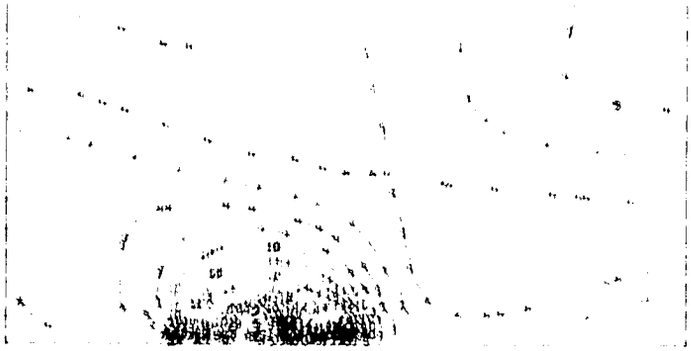

Contour	STRESS MPa	psi
1	-15.10	-2190
5	-6.83	-990
10	3.52	510
15	13.79	2000

BOTTOM SURFACE

Contour	STRESS MPa	psi
1	-32.10	-4650
5	-22.41	-3250
10	-10.27	-1490
15	1.86	270

Figure 4-15 MINOR PRINCIPAL STRESSES—TWELVE INCH CLIP—HARD GASKET

4.3.6 Differential Stiffness Analysis

As an additional check on the significance of geometric nonlinearities (particularly in the case of uplift), a differential stiffness analysis was conducted in order to obtain a first order nonlinear approximation.

The same model used in the buckling analysis (nominal 3 x 3 in. mesh and hinged supports) was evaluated for an uplift loading of 2.4 kPa (50 psf).

In the region of higher stress levels around the support, there was very little change in stress levels as a result of the differential stiffness correction, generally in the range of 1 to 3 percent. However, along the longitudinal center line and the long edge, there were considerable changes in stresses.

Although the percentage change in stresses was great, 25 to 41 percent, the stress magnitudes were not large, i.e., 152 psi changed to 260 psi. The most significant change occurred in the stress component representing bending at the center of the long edge. The percent change in stress was 25 percent but the stress changed from -17.1 MPa (-2482 psi) to -21.3 MPa (-3085 psi). This is a compressive stress which, at this magnitude, does not endanger the structural integrity of the module.

4.3.7 Design Evaluation

Evaluation of the data obtained from the preceding analyses results in the following conclusions:

- Linear static analyses of future curved module and support clip designs will be adequate to assess the design performance for both positive and negative loadings (i.e. downward forces and uplift).
- From a stress standpoint, the curved glass module supported by 4 discrete gasket/clip support assemblies will withstand normal loads in either direction of at least 2.4 kPa (50 psf). However, to minimize stress concentrations at the edges of the clips, the clip assemblies may have to be on the order of at least 30 cm (12 in.) long.
- The gasket/glass interface must be able to transfer an average force of 235 kPa (33 psi) through either friction, adhesion or a combination of the two.

4.4 GLASS INDUSTRY SURVEY

A number of glass manufacturers and specialty fabricators were surveyed, by Bechtel, to assess the technical feasibility and large volume manufacturing costs for the curved glass superstrate module design. The glass manufacturers contacted included:

- ASG Industries, Inc.
- PPG Industries, Inc.
- Libby-Owens-Ford (LOF).
- Schott

The specialty fabricators contacted, included:

- California Glass Bending Corp.
- Standard Bent Glass
- Eagle Convex Glass Co.

Based on the results of this survey it appears that the 1.2 by 2.4 m (4 by 8 ft) module size is beyond the present capabilities of existing large volume production (glass bending) facilities. Currently, large sheets of curved glass are used primarily for architectural purposes and are produced by the speciality fabricators. Due to the relatively low volume of production for any particular shape (from a few to several hundred sheets), fabrication is at best a semi-automated procedure and results in high production costs.

The remainder of this section discusses the technical comments received from the manufacturers regarding the module design and presents a summary of cost estimates for large volume production.

4.4.1 Design Feasibility

In general, the glass suppliers responding to the survey indicated that the curved glass module design appears to be technically feasible.

Specific comments and suggestions from the suppliers include:

- Direct glass to metal contact should be avoided. At least 3.2 mm (1/8 in.) of elastomer (gasket material) should be located between glass surfaces and metal framing sections.

- The elastomer (gasket material) should maintain a hardness of 70 $\pm$ 20 durometer under all ambient operating conditions for the life of the module.

- At present, the minimum glass thickness that can be given a full temper (four to five times the bending strength of annealed glass) after bending is 4.8 mm (3/16 in.). Partial tempering can be achieved with thinner glass, 3.2 mm (1/8 in.).

4.4.2 Large Volume Production Costs

Low cost glass manufacturing and fabrication is only achievable with large production volumes. This is because the automated equipment necessary to reduce per unit labor costs is capital intensive. These costs must be amortized over a large number of units in order to realize potential savings.

Since at present there are no large volume automated bending facilities capable of accommodating the 1.2 x 2.4 m (4 x 8 ft) module size, a sufficient market would have to be demonstrated before a manufacturer would be willing to invest in such equipment.

Estimated fabrication costs for curving the glass superstrate are presented in Table 4-2. These costs are the additional costs (above that of the glass and other module materials) to curve the

glass. These budgetary cost estimates are based on responses to the industry survey previously discussed and essentially represent extrapolations from existing production experience with smaller glass sizes.

As shown in Table 4-2, fabrication costs drop with increasing production volume. However, for production volumes in the range of 4.6×10^5 m^2/year (5×10^6 ft^2/year, or about 60 MWp/year) fabrication costs appear to be unacceptable. This is discussed further in Section 5.3. Table 4-2 also shows that with present production methods, costs for a smaller module, 1.2 by 1.2 m (4 by 4 ft) are likely to be somewhat lower than for the 1.2 by 2.4 m (4 by 8 ft) module size used as the baseline in this study. However, the additional array structure and module handling requirements would probably negate any reduction in fabrication costs.

Table 4-2

CURVED GLASS FABRICATION COSTS

PRODUCTIVITY RATE		ESTIMATED COST[1]			
M^2/YEAR	FT^2/YEAR	1975 $		1980 $	
		$/$M^2$	$/$FT^2$	$/$M^2$	$/$FT^2$
Prototype (<1000)	Prototype[2]	53.58-61.43	5.00-5.71	75.00-86.00	7.00-8.00
4.6×10^2	5×10^3[2]	17.11-37.66	1.59-3.50	23.99-52.70	2.23-4.90
4.6×10^5	5×10^6[2]	13.13-21.20	1.22-1.97	18.40-29.70	1.71-2.76
4.6×10^5	5×10^6[3]	7.32-15.39	0.68-1.43	10.22-21.52	0.95-2.00

1) Excludes the cost of the glass

2) 1.2 by 2.4 m (4 by 8 ft) module

3) 1.2 by 1.2 m (4 by 4 ft) module

As previously mentioned, low cost fully automated glass manufacturing facilities require large production rates. For example, a single production line for the manufacture of sheet glass by the float method is typically capable of production volumes in the range of 9×10^6 to 18×10^6 m^2/year (100×10^6 to 200×10^6 ft^2/year). It is conceivable that such a production facility could be modified to directly produce the slightly curved sheets. Therefore, production rates higher than those presented in Table 4-2 might result in additional per unit cost reductions. At this time, glass manufacturers are reluctant to speculate on truly large volume production costs. This results in large part from the lack of experience with automated facilities capable of handling the required glass size and configuration

Another technique available for the fabrication of the curved glass is sag bending. Sag bent glass is not bent to a mold surface. The bending operation might possibly be accomplished in a manner similar to that used for tempering ordinary flat glass sheets. The present costs for tempering 1.2 by 2.4 m (4 by 8 ft) glass sheets is on the order of $2.00/m^2$ ($0.20/ft^2$) in 1980 dollars for production volumes of several million square meters per year (Ref 2.1). The implications on total installed array costs of bringing the glass fabrication premium into this cost range are discussed further in Section 5.3.

Section 5

ARRAY STRUCTURE AND FOUNDATION DESIGN

This section presents a discussion of array structure and foundation designs capable of supporting the curved glass module described in Section 4. Section 5.1 lists the array design bases. Section 5.2 presents design descriptions and data on installed costs for the four array configurations evaluated in this study. Total array costs are summarized in Section 5.3, which also presents a comparison between the curved glass module array costs and conventional flat glass module array costs (Ref. 2-1).

5.1 DESIGN BASES

This section lists the requirements, adopted conventions, and other bases pertinent to the design of the arrays and the estimation of array costs.

In order to facilitate comparison of the total installed costs for flat and curved glass module configurations, the design and cost bases used in this study were selected so as to be consistent with those used by Bechtel to estimate the flat glass module array costs presented in Ref. 2-1.

The reader is cautioned that, because the purpose of this study, as well as the study reported in Ref. 2-1, was to identify major cost drivers and to compare design configurations, several sources of inaccuracies may be present. These include: inaccuracies due to engineering approximations and subsequent utilization of available non-optimized structural shapes, and cost estimation inaccuracies due to the unavailability of data on similar construction projects and their historical costs.

Therefore, although these inaccuracies do not affect the general comparison of array configurations, they are inherent in the cost data presented in the following sections. Detailed design and cost estimating studies are required to better define the absolute values of installed costs for specific array configurations and site conditions.

5.1.1 Requirements

The following requirements are incorporated into the study:

- The four array configurations evaluated herein were evolved through a collaborative effort between JPL and Bechtel.
- Loads are normal to and uniformly distributed on the solar collector surfaces in both upward and downward directions.
- Three loads are considered: 0.96, 1.7 and 2.4 kPa (20, 35, and 50 psf). This load range represents a departure from the requirements used in Ref. 2-1, where loadings of 1.7, 2.4 and 3.6 kPa (35, 50 and 75 psf) were used. The lower range of loadings used in this study

was selected by Bechtel and JPL as being more representative of actual array loadings.

- The loads are to be considered as combined live loads and dead loads with no differentiation between the two. This requirement, together with the load direction requirement, tends to overemphasize lift and drag forces. However, for these array designs, the superstructure weight per square meter is relatively small compared to the 0.96, 1.7, and 2.4 kPa (20, 35, and 50 psf) required load magnitudes. Consequently, major cost drivers are not likely to be obscured by this combined load requirement.

- Uniform Building Code (UBC) 1976 Edition, Class 3 site soil conditions are assumed. Class 3 materials are characterized by the UBC as sandy gravel to gravel. The soil load resistance values specified by the UBC for the class are neither the highest nor the lowest that the UBC specifies. The values are: 96 kPa (2000 psf) bearing pressure downward, 9.6 kPa (200 psf) lateral bearing pressure, and a sliding resistance coefficient of 0.35. Increases in the values are permitted for increased depths below grade by step function statements. The values are considered reasonable for establishing consistency for study design work. As discussed later, a site soils investigation is considered advisable for final optimization.

- The vertical distance between grade and the panel's lower edge is required to be two ft in order to avoid rain splatter of soil onto the modules.

- A 35° latitude array tilt angle was used for this study and is implied in further discussions unless otherwise stated.

- The construction materials are to be concrete for foundations and steel for the superstructure.

5.1.2 Assumptions and Conventions

- The foundation design methods and equations are those specified and permitted by the UBC. This convention was adopted to assure consistency between the UBC "allowables" and

the methods for predicting values for comparison with the allowables.

- Commercially available steel shapes were selected. This convention was adopted to assure the greater cost estimating reliability usually possible with a wide base pricing system. Since this study was intended as a screen to compare array configurations, it was assumed that any later optimization of the arrays would include detailed calculations to refine the specific member dimensions.

- Simply supported end conditions are assumed for connections between members. Later optimizations may show that moment connections are more cost effective. However, moment connections are usually cost effective only when the connection costs are a small part of the total cost (e.g., the material cost for long steel members with a large weight per meter is much higher than the cost of connecting such members).

- The panel strength (Case 2 only) is not relied on to brace the array on the basis that array structure and panels are erected and installed during two different time periods.

- Allowable stresses, design methods, and equations specified by the American Institute of Steel Construction (AISC) code are adopted. An exception is the adoption of the American Metal Manufacturers Association (AMMA) specified deflection for metal members that directly support glass. Implicit in this experimental and experience based specification is the assumption that the glass is supported by an elastomer and does not bear directly on the metal support member. The adoption of these conventions was made for consistency throughout the study and to conform with accepted practices for the materials used. One exception, of a judgmental nature, was a restriction of the slenderness ratio (L/r) to less than or equal to 120 for cantilevered posts whose free ends are not guided.

- As a convention, American Concrete Institute Code requirements were adopted for concrete foundation members.

5.1.3 Cost Bases

The array structure and foundation costs are presented in terms of both 1975 and 1980 constant dollars and are normalized to dollars per square meter of total module surface area.

These costs include shipping and installation. Also, the steel costs include the cost of galvanizing to protect the steel and the foundation costs include the cost of excavating and backfilling trenches when required. Costs for clearing and grading the site are excluded. Also excluded are the costs of distributables, engineering, and contingency. Any cost benefit to the total plant that may accrue from using the foundation excavations to install electrical ground mat wiring are not included.

5.2 ARRAY CONFIGURATIONS

This section presents design descriptions and cost data for four array configuration cases. The four configurations investigated in this study are designated as Cases 10 through 13 to avoid confusion during subsquent comparisons with the nine cases reported on in Ref. 2-1 (designated as Cases 1 through 9).

A design for each of the four cases was developed for ±0.96 kPa (20 psf), ±1.7 kPa (35 psf) and ±2.4 kPa (50 psf) loading.

5.2.1 Case 10 Design

The configuration or the Case 10 array design is illustrated in Figure 5-1. This design is for a 2.4 m (8-ft) slant height and 1.2 by 2.4 m (4 by 8 ft) panels.

This configuration is similar to the Case 3 configuration evaluated in Ref. 2-1 for flat glass panels. It was included in this study to facilitate the comparison of installed array costs for equivalent flat and curved glass array configurations.

As illustrated in Figure 5-1, the support structures consist of front and back vertical posts and front and back horizontal girders. The foundations consist of partially buried precast concrete spread-footings having a center to center spacing of 4.8 m (16 ft) in the east-west direction. The slant distance between the front and back girders is 1.29 m (4.23 ft) to permit direct connection between the panel (module) clips and the support structure.

The panel consists of a single 1.2 by 2.4 m (4 by 8 ft) curved glass module and four support clips, as described in Section 4.2. The panel also includes steel bracing members connected between the clips in the short (1.2 m) dimension. The braces may consist of steel rods or other light structural members to prevent damage to the glass from "flattening-out" during panel handling, shipping and installation.

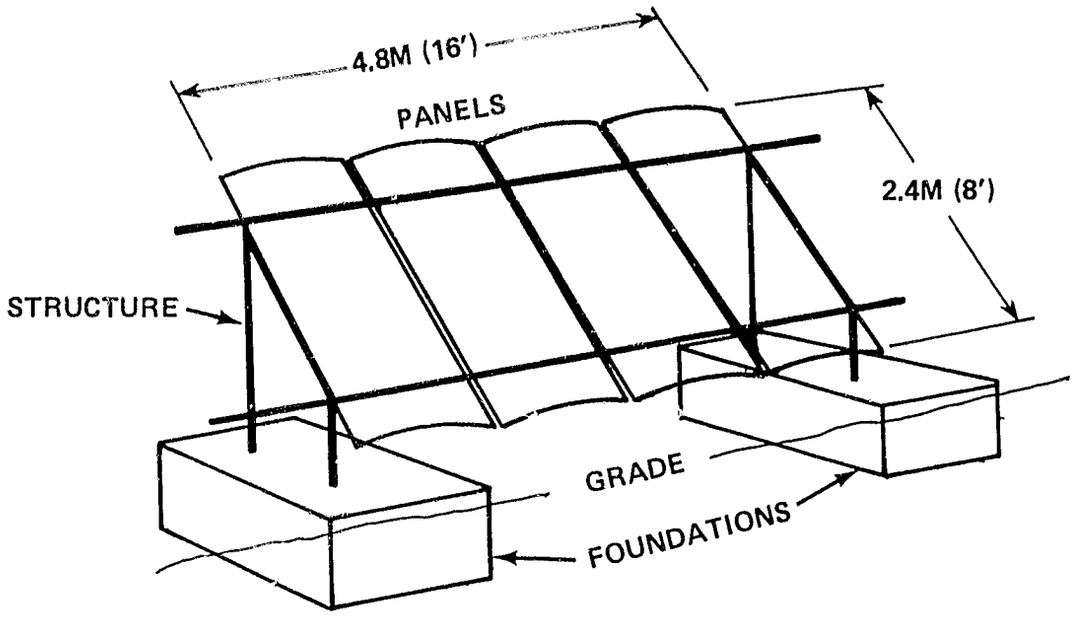

Figure 5–1 CASE 10 ARRAY CONFIGURATION

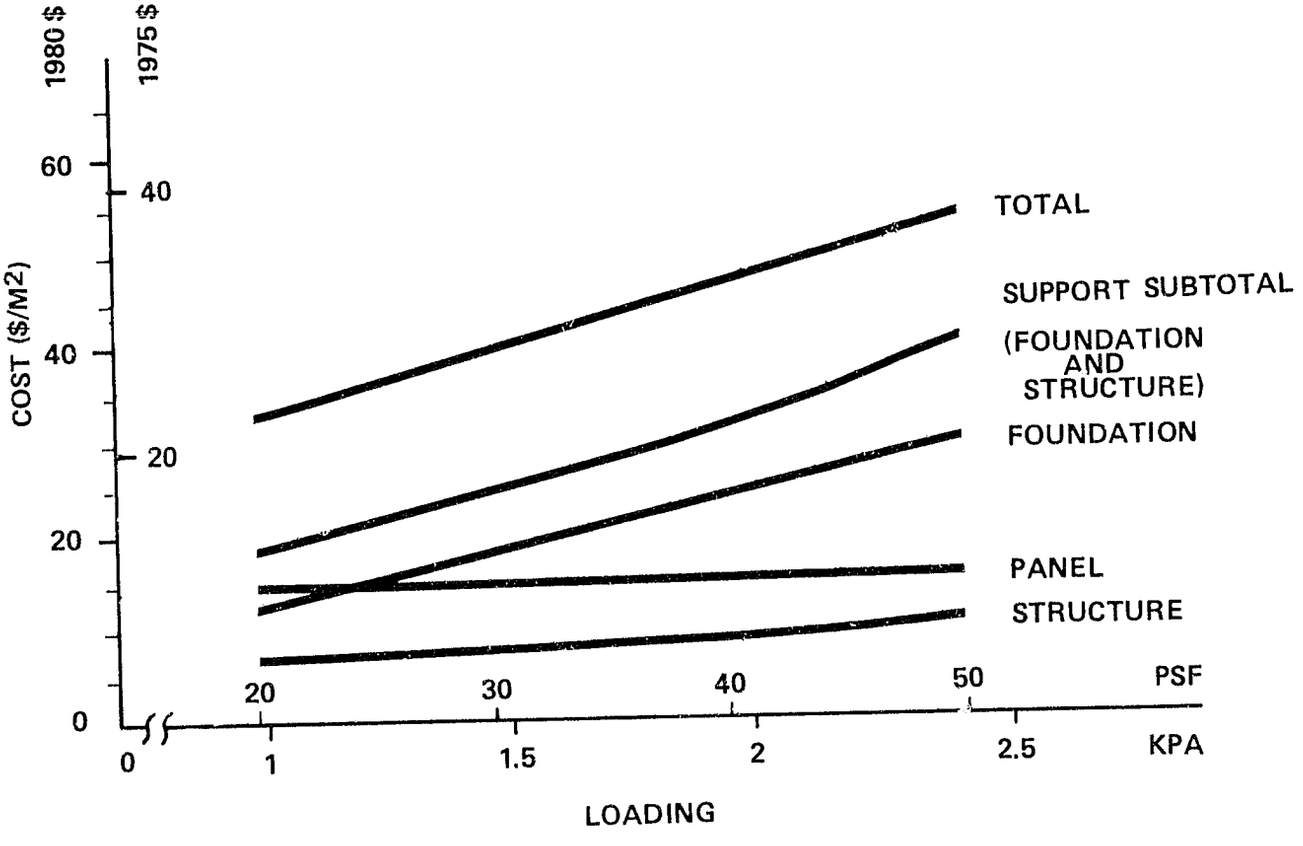

Figure 5-2 CASE 10 ARRAY COSTS

Cost data for the Case 10 design are presented in Figure 5-2 as a function of structural loading. As discussed in Section 5.1.3, the cost data are normalized to dollars per square meter of module area and are presented in terms of 1975 and 1980 dollars.

5.2.2 Case 11 Design

The configuration of the Case 11 array design is illustrated in Figure 5-3. This design is similar to the Case 10 design discussed in Section 5.2.1 except that in this case the slant height is 4.8 m (16 ft) and 2.4 by 4.8 m (8 by 16 ft) panels are used.

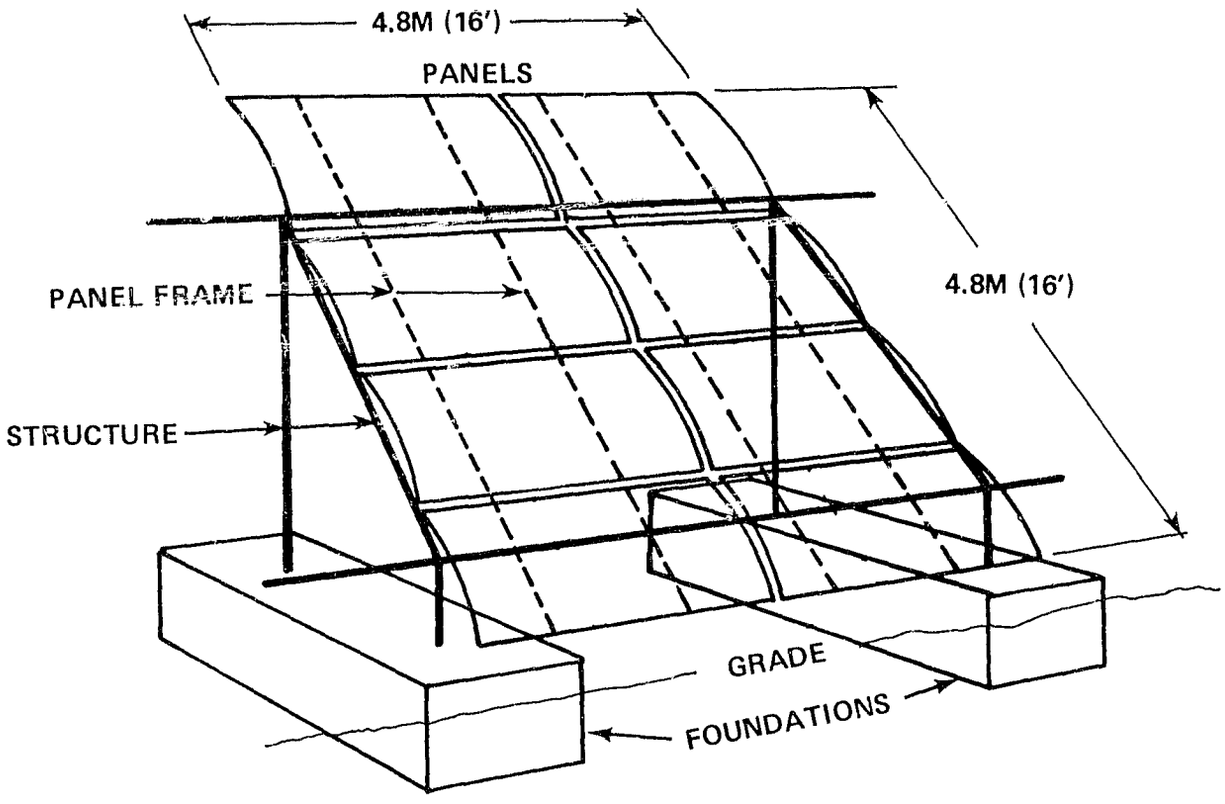

Figure 5–3 CASE II ARRAY CONFIGURATION

This configuration is also similar to the Case 7 configuration evaluated in Ref. 2-1 for flat glass panels.

The panel configuration is illustrated in Figure 5-4. As shown in the figure, the panel consists of four 1.2 by 2.4 m (4 by 8 ft) curved glass module and support clip assemblies, as described in Section 4.2, factory assembled onto a support frame. The frame provides rigidity for the glass during handling, shipping and installation, as well as structural support for the modules after installation on the support structure.

Cost data for the Case 11 design are presented in Figure 5-5.

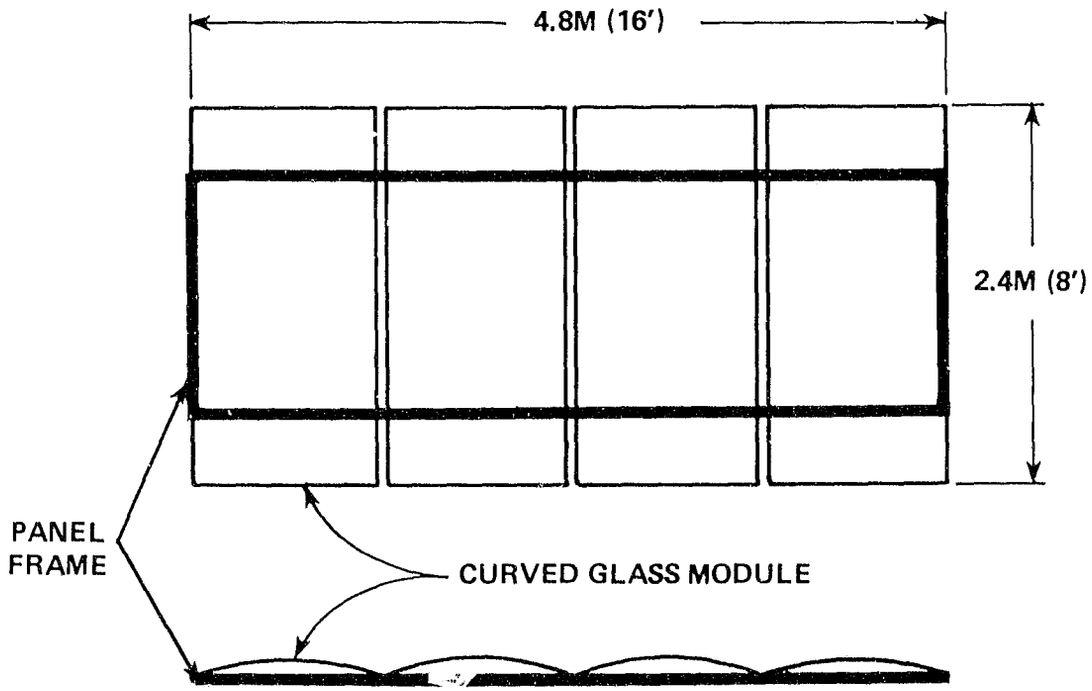

Figure 5-4 CASE11 PANEL CONFIGURATION

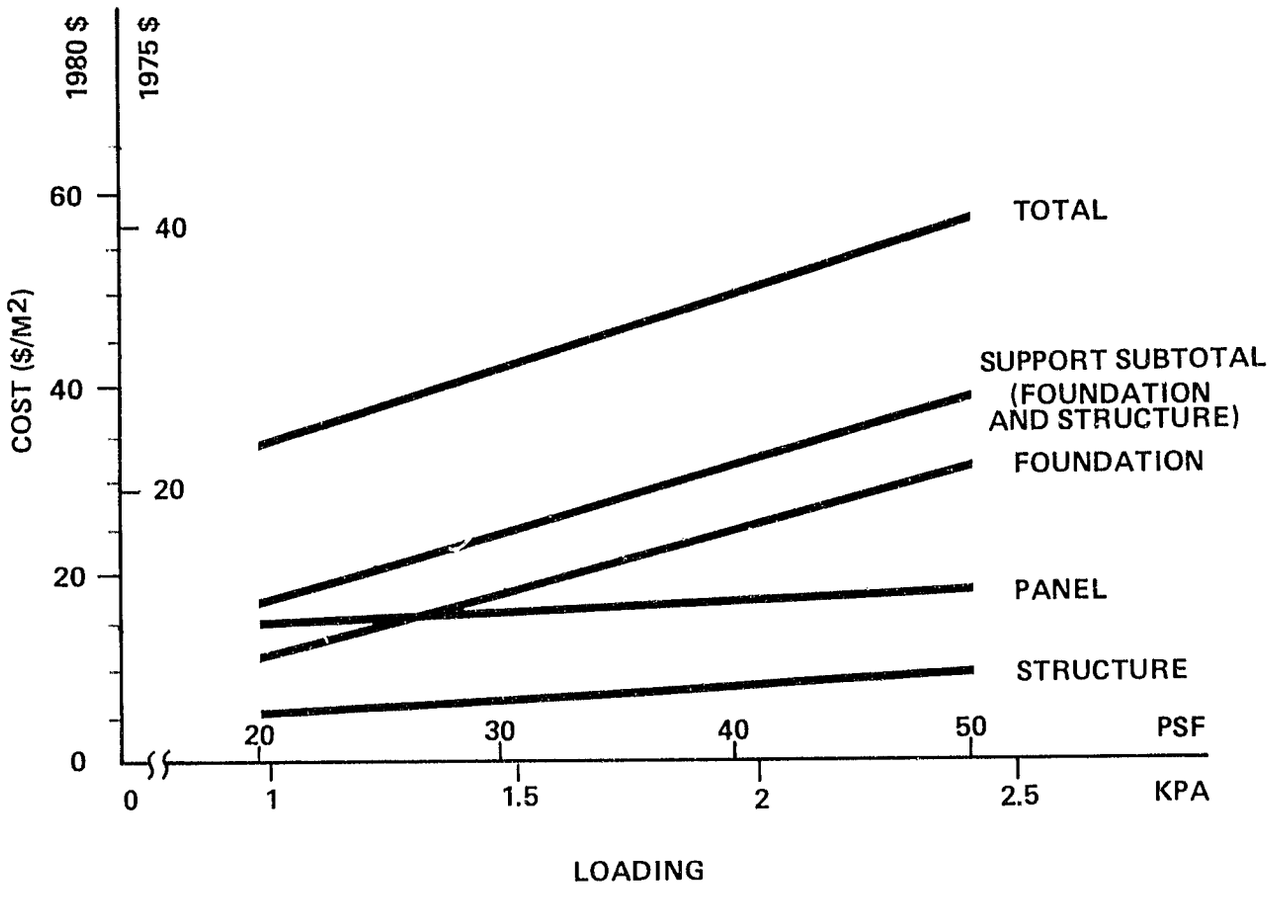

Figure 5—5 CASE 11 ARRAY COSTS

5.2.3 Case 12 Design

The configuration of the Case 12 design is illustrated in Figure 5-6. This design is for a 2.4 m (8 ft) slant height and 1.2 by 2.4 m (4 by 8 ft) panels.

As can be seen in the figure, this design differs from the first two cases presented in this study (and the nine cases presented in Ref. 2-1) in that caisson type foundations and pedestal mounted structures are used. This configuration was included in the study to provide a cost comparison between spread-footing and caisson supported array designs.

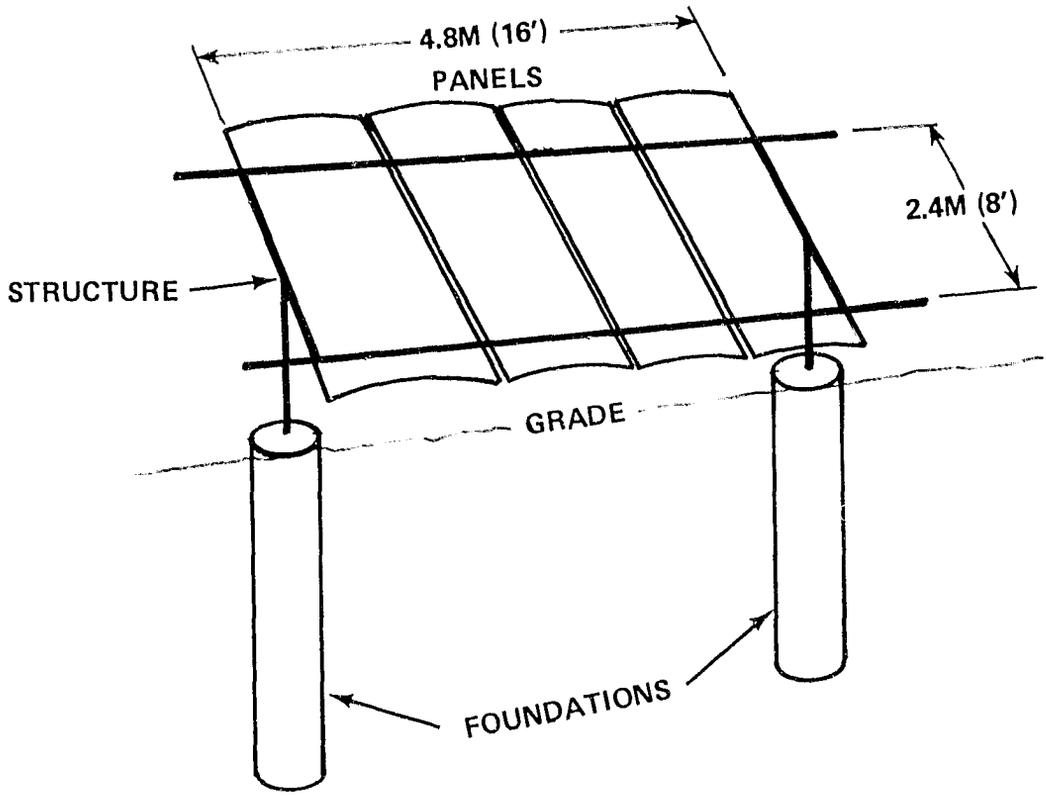

Figure 5–6 CASE 12 ARRAY CONFIGURATION

As illustrated in Figure 5-6, the support structures consist of vertical posts, front and back horizontal girders and siderails.

Installed costs for caisson foundations are generally more sensitive to soil type (Ref. 5-1) than are equivalent spread-footing foundations. This results primarily from the installation requirements imposed by the nature of the soil. That is, if the soil is adequately cohesive, the caisson can be installed by simply augering a hole, placing the reinforcing bar and pouring the concrete. However, less cohesive soils such as gravel or dry sand often require that the holes be cased to prevent cave-in during construction (Ref. 2-1 and 5-1). Unfortunately, due to the variable nature of soils, it is not

possible to make a simple table, such as provided by the UBC, that adequately describes all site soil values.

During this part of the study, it was assumed that no casing was required during foundation installation. The effects of varying soil conditions on caisson foundations are discussed further in Section 5.3.2.

The panel configuration is identical to that used for the Case 10 array, as discussed in Section 5.2.1.

Cost data for the Case 12 design are presented in Figure 5-7.

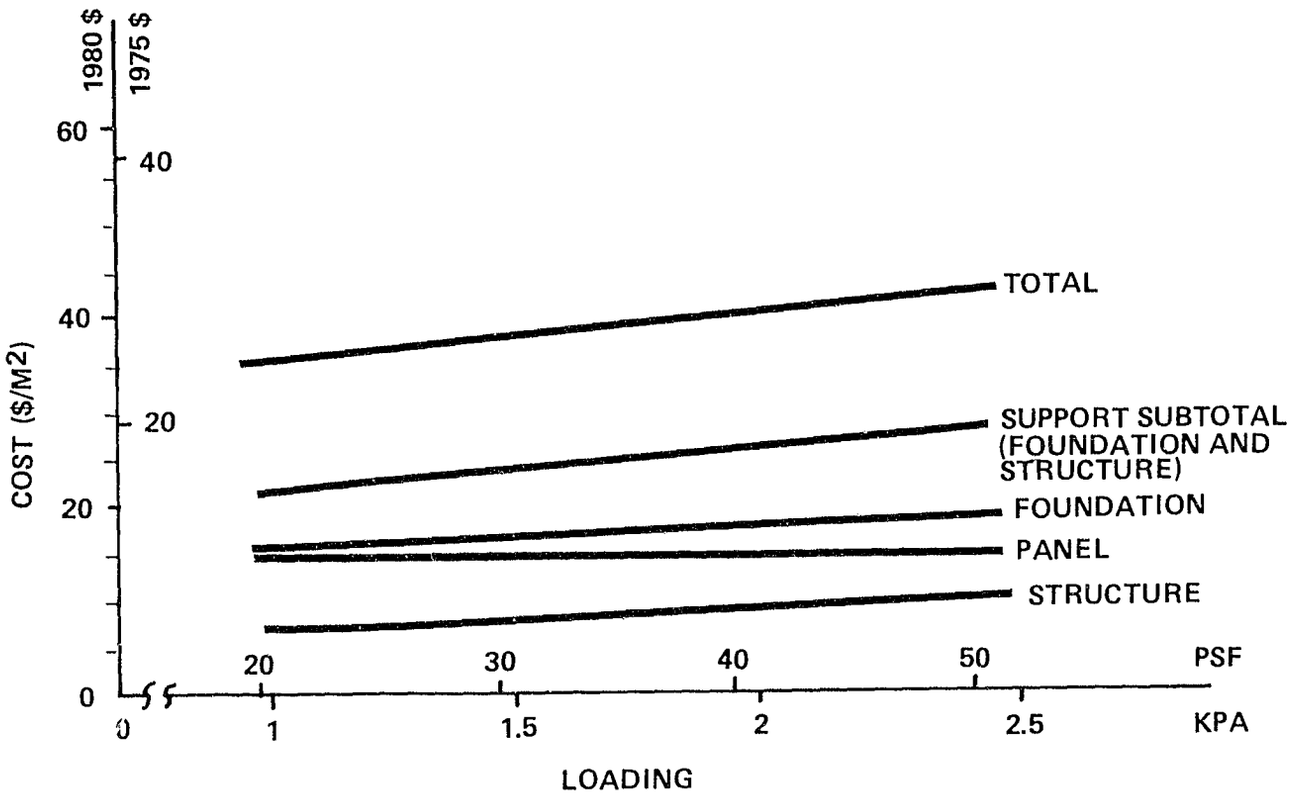

Figure 5—7 CASE 12 ARRAY COSTS

5.2.4 Case 13 Design

The configuration of the Case 13 design is illustrated in Figure 5-8. This design is for a 2.4 m (8 ft) slant height and 1.2 by 2.4 m (4 by 8 ft) panels. This configuration is similar to Case 12 in that it is a pedestal mounted structure using caisson foundations. However, as can be seen in Figure 5-8, the Case 13 structure consists of a single horizontal member attached to vertical posts. The foundations are of the caisson type, spaced at 4.8 m (16 ft) between centers.

This configuration was reported (in Ref. 5-1) to have a low installed cost compared with more conventional support structures, such as Cases 1 through 12. However, the study reported in Ref. 5-1 considered only foundation and support structure costs. Therefore, the configuration was included in the present study to facilitate evaluation and comparison of total costs, including foundations, support structures and module (panel) framing requirements.

The panel configuration is illustrated in Figure 5-9. As shown in the figure, the panel consists of a single 1.2 by 2.4 m (4 by 8 ft) curved glass module, as described in Section 4.2. However, in order to facilitate connection of the panel to the single support girder, additional framing was provided as shown in Figure 5-9.

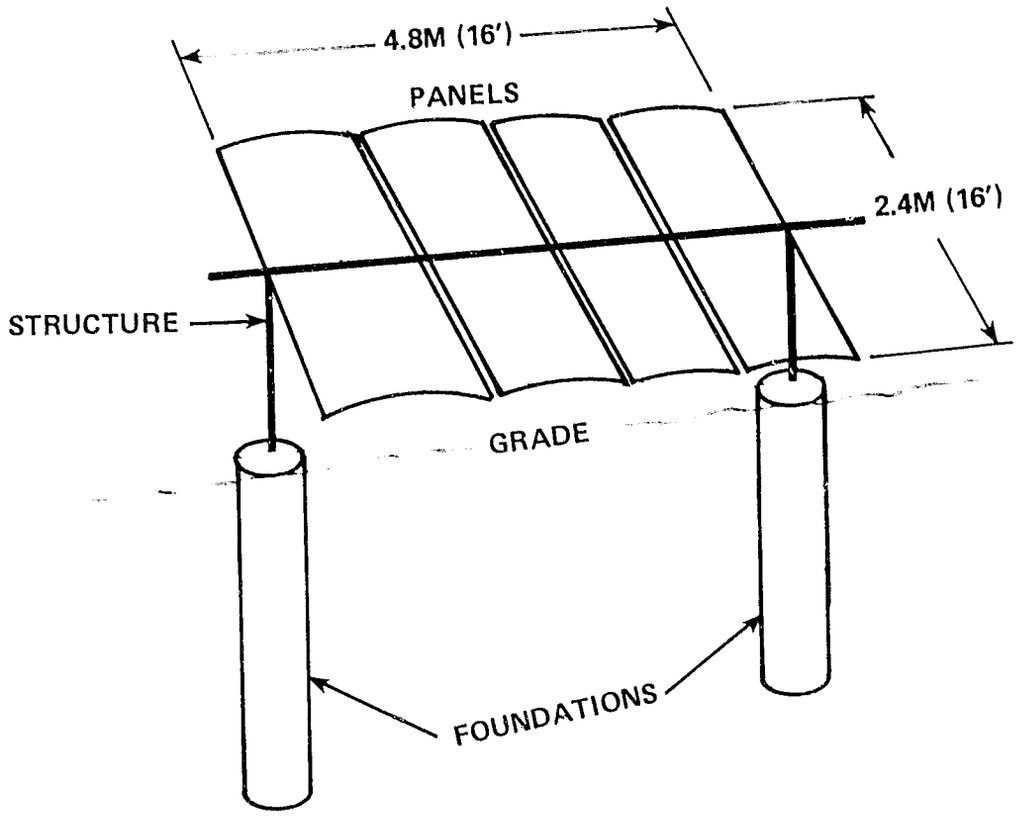

Figure 5–8 CASE 13 ARRAY CONFIGURATION

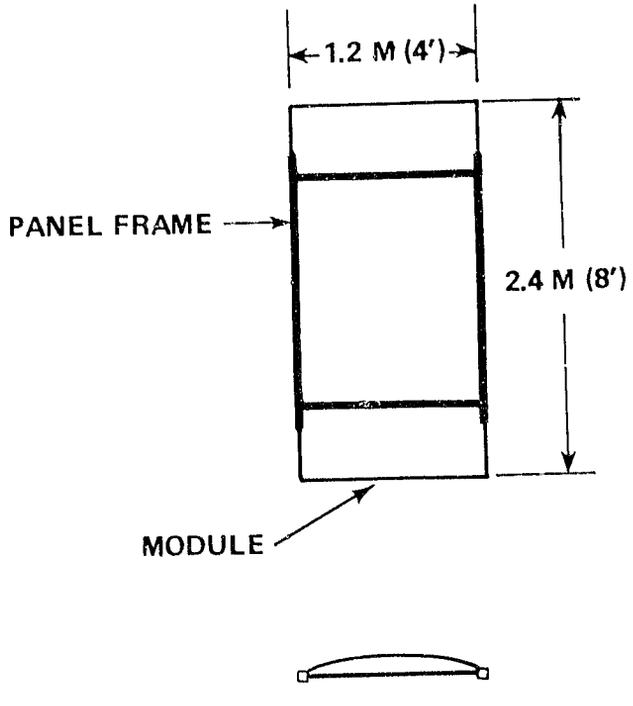

Figure 5–9 CASE 13 PANEL CONFIGURATION

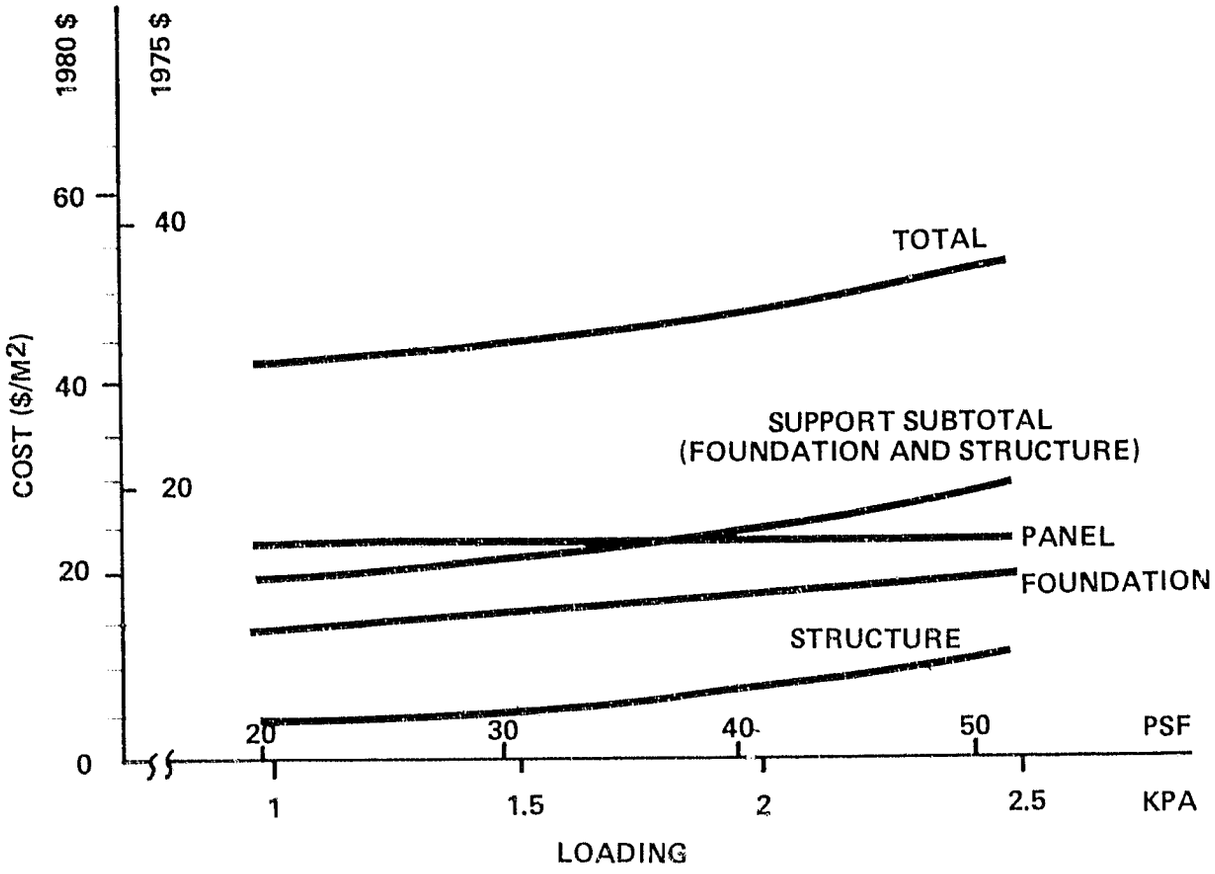

Figure 5–10 CASE 13 ARRAY COSTS

Like the Case 10 and Case 12 panels, the Case 13 panel design also includes steel bracing members connected between the clips to prevent glass damage during handling, shipping and installation.

Cost data for the Case 13 design are presented in Figure 5-10.

5.3 COST COMPARISONS

This section presents a cost comparison between the four array designs (Cases 10, 11, 12 and 13) discussed in Section 5.2. The economic viability of the curved glass superstrate module design is also evaluated, via comparison with equivalent flat glass module array costs as presented in Ref. 2-1. A comparison

between the use of caisson and spread-footing type foundations is also presented.

5.3.1 Curved Glass Module

In order to establish a reference with which to compare the costs of the curved glass module array configurations, two flat glass module array configurations are briefly reviewed here. The two configurations selected for the cost comparison are illustrated in Figures 5-11 and 5-12. These array configurations, designated as Case 3 and Case 7, were reported in a previous Bechtel study (Ref. 2-1). Of the nine flat glass module array configurations investigated in Ref. 2-1, Cases 3 and 7 represent the lowest total installed costs over the load range investigated. Loadings investigated in Ref. 2-1 were 1.7, 2.4 and 3.6 kPa (35, 50 and 75 psf) as compared with the range of 0.96, 1.7 and 2.4 kPa (20, 35 and 50 psf) used in the present study.

As shown in Figure 5-11, Case 3 is similar to Case 10 in that the support structure consists of front and back vertical posts and front and back horizontal girders. The foundations consist of partially buried precast concrete spread-footings. The array slant height is 2.4m (8 ft) and the array supports 1.2 by 2.4m (4 by 8 ft) panels which in turn contain 1.2 by 2.4m (4 by 8 ft) modules. Case 7, shown in Figure 5-12, is similar to Case 11 in that the support structure also consists of front and back

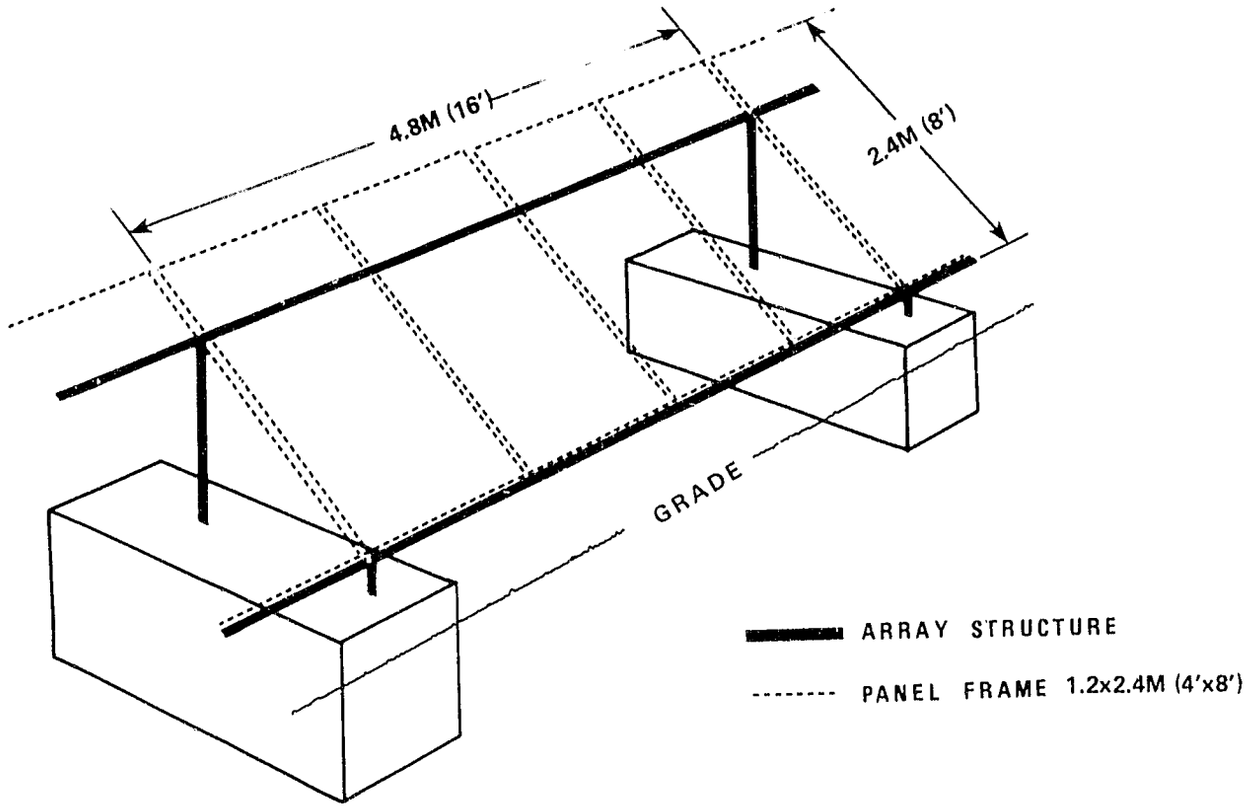

Figure 5-11 CASE 3 ARRAY CONFIGURATION

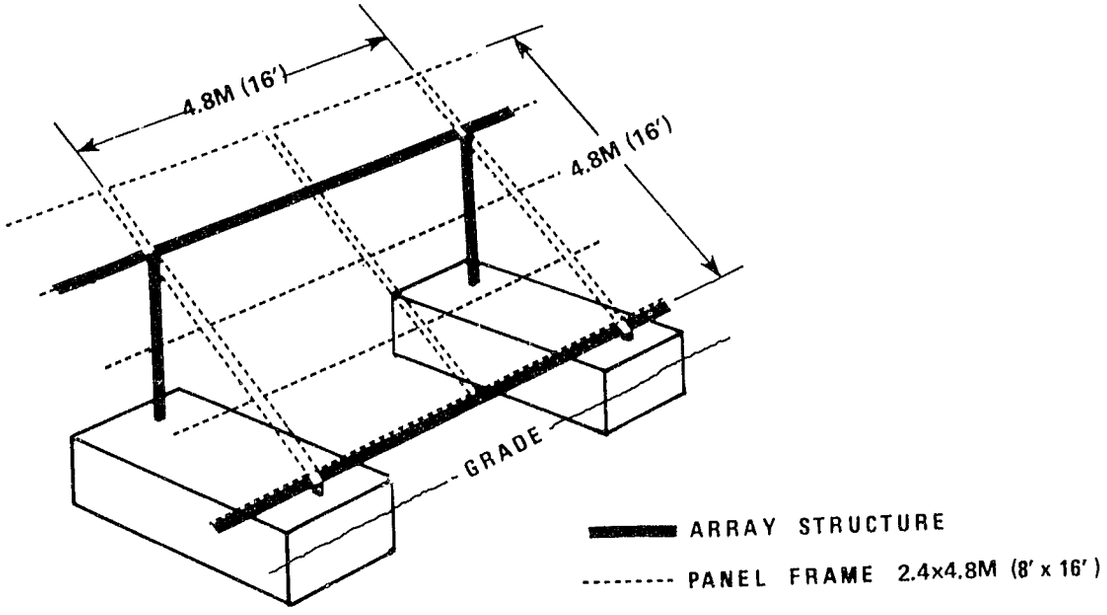

Figure 5-12 CASE 7 ARRAY CONFIGURATION

vertical posts and front and back horizontal girders. The foundations are again composed of precast concrete spread footings. The Case 7 array has a slant height of 4.8m (16 ft) and supports 2.4 by4.8m (8 by 16 ft) panels. The panels in turn consist of 1.2 by 2.4m (4 by 8 ft) modules.

Estimated costs for the Case 10, 11, 12 and 13 array configurations are presented in Figure 5-13 for the loading range of 0.96 to 2.4 kPa (20 to 50 psf). Figure 5-13 also presents the costs for the Case 3 and 7 configurations (costs for Cases 3 and 7 were not escimated for 0.96 kPa (20 psf)). All costs in Figure 5-13 are presented in terms of $/m^2$ of installed module area and are normalized to both 1975 and 1980 dollars. The cost data (in 1980 dollars) is also summarized in Table 5-1.

All costs include array foundations, support structures and panels. The costs exclude module costs (solar cells, interconnects, glass superstrate and other encapsulating materials). In addition, costs for Cases 10, 11, 12 and 13 are exclusive of any premium incurred for curving the glass superstrate.

It should be pointed out that the nine array configurations investigated in Ref. 2-1, of which Cases 3 and 7 resulted in the lowest costs, all used spread-footing foundations. Therefore, comparison of installed costs for Cases 12 and 13, which use caisson foundations, with the previously reported array costs

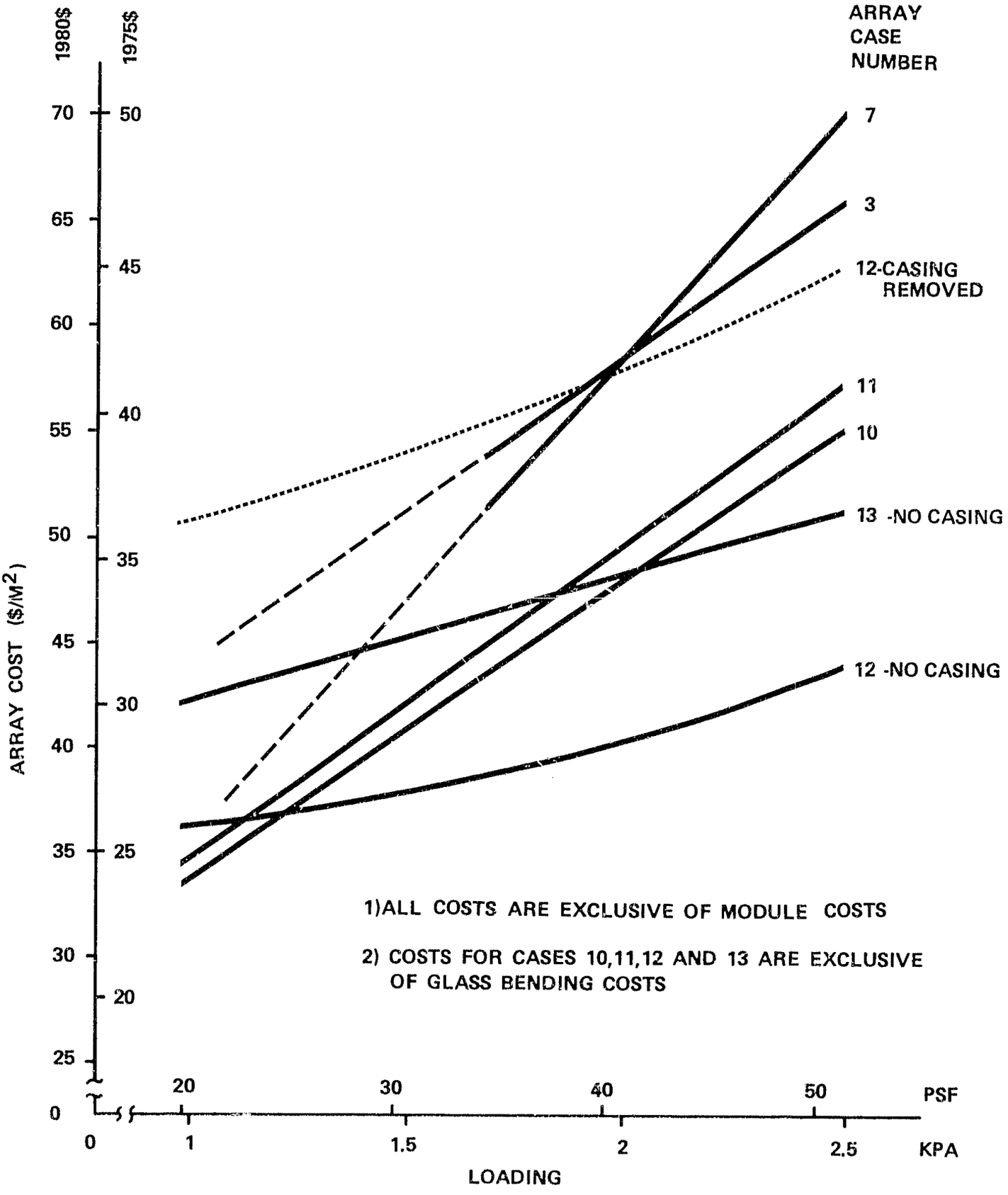

Figure 5-13 ARRAY COST COMPARISON

TABLE 5-1

ARRAY COST ESTIMATE SUMMARY (1980 $/m^2)

ARRAY CASE	0.96 KPA (20 PSF) LOADING				1.7 KPA (35 PSF) LOADING				2.4 KPA (50 PSF) LOADING			
	ARRAY		PANEL FRAME	TOTAL(1)	ARRAY		PANEL FRAME	TOTAL(1)	ARRAY		PANEL FRAME	TOTAL(1)
	STRUCTURE	FOUNDATION			STRUCTURE	FOUNDATION			STRUCTURE	FOUNDATION		
10	7.20	12.20	14.20	33.60	7.60	21.20	14.20	43.00	9.90	30.40	14.20	54.50
11	5.10	12.50	17.10	34.70	7.30	21.20	17.10	45.60	8.40	30.40	17.50	56.30
12	7.00	14.70	14.20	35.90	7.80	16.80	14.20	38.80	10.30	18.80	14.20	43.30
13	4.40	14.70	23.00	42.10	6.70	16.80	23.00	46.50	9.00	18.80	23.00	50.80

(1) Module costs increase this total by approximately $84/m^2, plus glass bending cost.

does not fairly assess the cost differences attributable to the curved glass module. An evaluation of spread-footing versus caisson foundation costs is presented in Section 5.3.2.

The difference in the costs for the flat glass module array configurations (Cases 3 and 7) and the equivalent curved glass module array configurations (Cases 10 and 11), as presented in Figure 5-13, therefore represents the breakeven or allowable cost premium for curving the glass.

As expected, reductions in panel material result in reduced array costs for the curved glass model configurations. Unfortunately, the cost savings do not appear sufficient to offset the estimated glass bending costs, as discussed in Section 4.4.2. This is further illustrated in Figure 5-14, which compares breakeven costs with estimated glass bending costs (for production volumes of 4.6×10^5 m²/year) as reported in Table 4-2.

However, if further reductions in glass bending costs could be realized through large volume production, the outlook would change considerably. For example, if glass bending costs could be reduced to the same level as the present cost for tempering flat glass ($2.00/m² in 1980 dollars) the curved glass module configuration becomes attractive for loadings above about 1.2 kPa (25 psf). As shown in Figure 5-14, if glass bending costs were $2.00/m² (1980 dollars), the Case 10 curved glass module array configuration would result in a savings of about $3.00/m² (1980

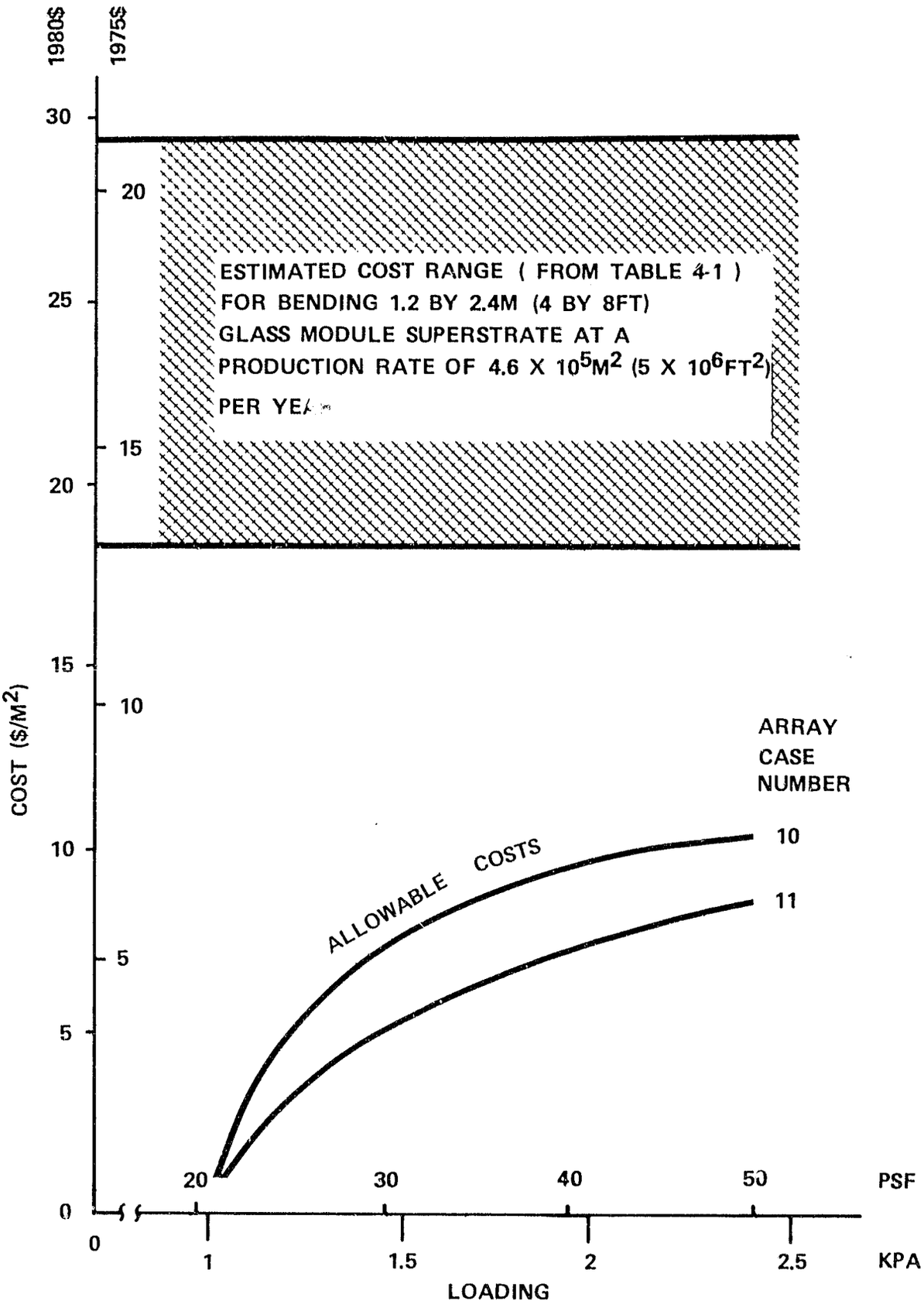

Figure 5-14 ALLOWABLE GLASS BENDING COSTS

dollars) at 1.2 kPa (25 psf) when compared to the installed cost of an equivalent flat glass array. The cost savings would increase, to about $10.00/m² (1980 dollars) at 2.4 kPa (50 psf). For a 13 percent module efficiency these savings are equivalent to $0.02/peak watt (1980 dollars) at 1.2 kPa (25 psf) and $0.08/peak watt (1980 dollars) at 2.4 kPa (50 psf).

5.3.2 Foundation Cost Comparison

As previously mentioned, Array Cases 1 through 9 (reported in Ref. 2-1) and Cases 10 and 11 of the present study all used spread-footing foundations. This was done because the variability of soil conditions results in uncertainties with regard to design requirements and installed costs for other foundations, such as the caisson type.

However, it appears that for proper soil conditions, the caisson type foundation can result in lower installed costs compared to spread-footings. This is illustrated by comparing the array costs for Cases 10 and 12 presented in Figure 5-13. As shown in Figures 5-1 and 5-6, Cases 10 and 12 are similar in design except that Case 10 uses spread-footing foundations while Case 12 uses caissons. The installed costs presented in Figure 5-13 for Case 12 (no casing) assume soil conditions such that no casing is required during construction (as discussed in Section 5.2.3). Under this assumption, Figure 5-13 indicates that for loadings above about 1.25 kPa (25 psf) the caisson design (Case 12)

results in a lower cost than an equivalent spread-footing design (Case 10). At 2.4 kPa (50 psf), the cost difference is about $11.00/m² ($1.00/ft²) in 1980 dollars. For a 13 percent module efficiency this saving is equivalent to about $0.08/peak watt (1980 dollars).

The cost advantage of the caisson foundation may vanish, however, for different soil conditions. For example, if UBC soil classes 1 or 2 (crystaline or sedimentary rock) conditions are assumed, the drilling costs for caisson foundations would likely be prohibitive. In this case, spread-footings, rock anchors or other designs would be appropriate. Also, some types of UBC classes 3 and 4 soil conditions (loose sand or gravel) would likely require casing of the hole during construction. As shown in Figure 5-13, the estimated costs for Case 12 rise significantly when temporary casing is required during construction.

The array costs for Case 12 with casing removed were estimated using foundation cost data presented in another Bechtel study (Ref. 5-1). These costs assume the use of removable steel casings and are based on existing construction practices. These practices are generally not optimized for the repetitive, high-volume installation requirements of large photovoltaic power systems. It is therefore possible that specially designed equipment and/or inexpensive (cardboard) left-in-place casings might result in lower installation costs.

It should be concluded from the above discussion that array foundation design and, therefore, array costs are likely to vary with site soil conditions.

5.3.3 Array with Single Horizontal Support (Case 13)

As previously discussed, the use of a single horizontal support results in a low cost support structure, as might be expected. However, the advantage disappears when panel framing requirements are included in the evaluation. This is illustrated for the curved glass module in Figure 5-13. Comparison of array costs for Cases 12 and 13 (no casing) indicates that the single horizontal support configuration results in higher installed costs at all loadings investigated. For the curved glass module designs this results from the increased panel framing material needed in Case 13 to support the module and to facilitate attachment to the support structure.

Although not specifically analyzed in the present study, a single horizontal support might still be attractive if used with flat glass modules. The flat glass modules would be completely framed in either case, so that the additional panel framing requirements might not be as severe as when curved modules are used.

5.3.4 Comparison Summary

From the cost comparisons made in the preceding portion of Section 5.3, it can be concluded that:

- The use of 1.2 by 2.4 m (4 by 8 ft) curved glass modules results in a reduction in installed costs for the array panel/structure/foundation when compared to equivalent flat glass module designs. However, significant reductions in presently estimated glass bending costs must be achieved for the curved glass module design to result in overall cost savings.

- For proper soil conditions, caisson (deep) foundations result in lower installed costs than equivalent spread-footing (surface) designs.

- Array designs using a single horizontal support (torque tube) result in higher array costs than equivalent designs using two (upper and lower) supports when used with curved glass modules.

Section 6

CURVED GLASS MODULE TEST PLAN

This section discusses a test plan to experimentally evaluate the curved glass module design presented in Section 4.

Simulated windload tests on full sized prototype curved glass module assemblies would generate data necessary for verification of the finite element stress analyses discussed in Section 4.4. In addition, prototype testing would facilitate further optimization of the support clip design, including optimization of: clip length, clip location, gasket material and gasket thickness.

Fabrication and testing of full size prototype modules would also generate useful data concerning handling, shipping, and installation requirements for large (1.2 by 2.4 m) solar cell panels.

The basic elements of the test program would include:

- Fabrication of 1.2 by 2.4 m (4 by 8 ft) curved glass superstrate(s).
- Fabrication of rolled steel support clips.
- Assembly of prototype curved glass module(s).

- Simulation of uniform wind loading (using techniques developed by JPL and described in Ref. 6-1) and measurement of stress distributions in the glass.
- Parametric evaluation of support design including clip length and clip location.

6.1 REQUIREMENTS

The primary purpose of the test plan is to experimentally measure the stress distributions and deflections for a curved glass module under simulated wind loading. It would therefore be necessary to fabricate several curved glass modules as described in Section 4.2. This would include procurement and bending of the glass, as well as fabrication and assembly of the gasket/clip supports.

The test program would be aimed at verifying the previous analytical work rather than determining ultimate strength or breaking stress. This implies that a large number of test sample units would probably not be required. Further, a functioning module is not necessary since the solar cells, interconnects, and other encapsulating materials do not contribute to the strength of the module. Thus it would probably not be necessary to include these components in the test prototype. However, future tests might be conducted on complete solar cell modules to determine any possible effects of bonding the cells to the glass (e.g., cell cracking due to flexing of the glass).

The test sample could therefore consist of a few (six for example) curved glass sheets. In these quantities, the curved glass could be obtained from any of the specialty fabricators listed in Section 4.4.

Tempering of the curved glass test panels would not be required because this does not affect the stress distributions occuring below the breaking stress. Testing of tempered, or partially tempered superstrates might be considered if these are obtainable. Testing of various glass thicknesses, such as 3 and 5 mm (1/8 and 3/16 in.) would also provide useful data.

The simple steel support clip could be easily fabricated. Clips of various lengths should be produced in order to facilitate optimization of support design.

The required data on stress distributions within the module under loading would be obtained via appropriately located strain gages. Strain gages should be mounted on both the top and bottom surfaces of the glass in the expected areas of maximum stress.

Uniform wind loading of the glass module could be simulated using pressure application techniques developed at JPL (Ref. 6-1) for pressure cycle testing of solar panels.

Basically, uniform pressure is applied to the panel by inflation of an air bag in contact with the surface of the panel. By

appropriate configuration of the pressure application system a uniform pressure, equal to the pressure in the air bag, is transmitted to the panel.

The existing apparatus, located at JPL, can accept a maximum panel size of only 1.2 by 1.2 m (4 by 4 ft). In addition, small modifications to the existing configuration would likely be required to facilitate mounting of the curved glass module and for measurement of glass deflections.

Fortunately, the design and construction of the apparatus is relatively simple. Therefore, modifications to existing equipment or construction of a specially designed unit would not represent a major effort.

Alternately, testing of reduced size (half-scale) modules could also be considered. This scaling technique would require thinner glass which may be difficult to fabricate.

Assuming that initial testing verifies the technical feasibility of the concept, design optimization could be accomplished utilizing the same test apparatus and curved glass superstrates.

6.2 COST

As mentioned in Section 4.4, several of the specialty glass fabricators surveyed during this study have indicated the ability

to produce 1.2 by 2.4 m (4 by 8 ft) curved glass superstrates in prototype quantities.

The estimated costs for the prototype superstrates are in the range of $56.00/m^2$ to $86.00/m^2$ ($5.20/ft^2$ to $8.00/ft^2$). These costs are in mid-1979 dollars and include the price of the glass, the fabrication (bending) costs and, in some cases, packaging for shipment. This results in a cost of between $166.00 and $256.00 for each 1.2 by 2.4 m (4 by 8 ft) superstrate. A total of six superstrates would therefore cost approximately $1,000 to $1,500, in mid-1979 dollars. The cost of a glass superstrate is lower than the cost of a nonlinear analysis computer run.

Prototype clips should have the shape shown in Figure 4-2 but need not be fabricated as a rolled section. The costs of module/clip assembly, module instrumentation and the test fixture, as well as the actual conduct of the testing and data collection program, will depend on the organization conducting the tests.

For example, the test program might be conducted at the Jet Propulsion Laboratory. In this case, the existing pressure cycle testing apparatus could be modified to accommodate the curved glass superstrate. Costs to accomplish the necessary modifications would depend on the present status and configuration of the equipment as well as the particular personnel assigned to the program. Similarly, the cost of

conducting the experimental work and collecting and analyzing the data would also depend on the type of personnel assigned to the project. Therefore, except for the curved glass superstrates, specific costs for the test plan were not estimated during this study.

Section 7

MODULE ELECTRICAL INSULATION

This section presents a discussion of electrical insulation design considerations with regard to module encapsulation systems. The intent is to create an awareness of factors that influence electrical insulation performance and to show that electrical properties of module materials should be considered along with optical, mechanical and other properties during module development, design and testing programs. It is not intended to unnecessarily restrict the selection of materials or configurations by module manufacturers, but rather to provide information that will help to ensure long-term module performance and life.

Gases, liquids and solids are all commonly used as electrical insulators. However, existing and proposed module encapsulation designs are essentially solid dielectric systems. Therefore, the characteristics and design requirements of solid dielectric insulating systems are emphasized in this study.

In addition to weathering, the module encapsulating system will, during operation, be stressed by electric fields resulting from normal dc system operating voltages, transient overvoltages and

ac ripple (if an inverter is used). Therefore, the module encapsulating system must maintain acceptable electrical insulating properties throughout the useful life of the module, both to prevent premature failure and to protect personnel against shock hazards.

General characteristics of insulation materials are discussed in Section 7.1, along with factors that affect insulation performance. Section 7.2 discusses current industry practice regarding the design, testing and selection of insulating materials and systems. A brief listing of encapsulant material electrical properties is presented in Section 7.3. Factors affecting module design are discussed in Section 7.4 and Section 7.5 presents a discussion of design requirements and cost implications with regard to system voltage level. Testing procedures are suggested in Section 7.6.

7.1 INSULATION CHARACTERISTICS

The following simplified definitions are included for readers unfamiliar with terms used in describing insulation characteristics. These terms are discussed in detail in the remainder of this section.

aging - a permanent change in insulating properties with time

dielectric strength - electric field which causes insulation failure under specified test conditions

- intrinsic dielectric strength - maximum (theoretical) dielectric strength of ideal sample
- impulse dielectric strength - electric field which causes insulation failure after being applied for a very short time (microseconds)
- short-time dielectric strength - electric field which causes insulation failure after being applied for a "short-time" (several minutes)
- long-time dielectric strength (voltage endurance) - electric field which causes insulation failure after being applied for a "long-time" (several years)

electric field (voltage gradient) - limit of voltage difference per unit distance at a point

insulation - a material in which an applied electric field produces a very small or negligible current

insulation failure (breakdown) - loss of insulating properties, generally evidenced by a relatively high current with applied electric field

safety factor - empirical factor applied to short-time dielectric strength to determine a suitably conservative value for long time design stress

working (design) stress - electric field to which the insulation material will be exposed during the working lifetime

Electrical insulation materials are used to confine system voltages to the desired portions of a module. Some or all of these materials may concurrently serve other functions such as mechanical support, bonding, weatherproofing, etc. By accepted definition, dielectric strength is that voltage which an insulating material can withstand before breakdown (loss of

C-2

insulating property) occurs. This is usually expressed as an electric field (voltage gradient) in terms of voltage per unit distance (such as volts per mil or kilovolts per mm).

The ability of a material to act as an insulator depends on its ability to inhibit the acceleration of electrons within the material. In other words, when a material is acting as an insulator, there is an insufficient quantity of free electrons in the material to provide conduction. The fact that practical insulating materials exhibit finite resistivities indicates that some conduction occurs. For example, the volume resistivity for Mylar, a good insulating material, is on the order of 10^{18} ohms/cm^3 as compared to 10^{-8} ohms/cm^3 for copper. Conduction in insulators is primarily ionic. However, if the electric field within an insulating material is increased to a level at which electrons begin to accelerate through the material, breakdown and loss of insulating properties will result. As electrons begin to accelerate, they collide with the atoms in the material and can release more electrons. This avalanche condition leads to a rapid breakdown in insulating properties and, in many cases, results in physical damage to the material and permanent loss of insulating strength.

Electrical breakdown appears to require not only sufficient electric field, but also a certain minimum amount of energy (Ref. 7-1). Breakdown strength varies with many factors, including material thickness, size and shape of electrodes used

in applying the electric field, shape or distribution of the electric field in the material, frequency of the applied voltage, rate and duration of voltage application, fatigue with repeated voltage applications, temperature, moisture content, and chemical changes over time.

The maximum uniform field to which a homogeneous material can be subjected without breakdown is referred to as the intrinsic dielectric strength of the material. However, in actual insulating materials, many factors intercede to significantly reduce attainable dielectric strength. This is illustrated in Figure 7-1 for polyethylene, a material commonly used for insulating electric power cables.

As can be seen in Figure 7-1, the dielectric strength of polyethylene decreases with increasing time under electrical stress. For this material, the impulse strength is on the order of 25 percent of the intrinsic strength. The short-time strength, which is the value of dielectric strength generally reported on manufacturer's product data sheets, is about 12 percent of the impulse strength and about 3 percent of the intrinsic value. Finally, the maximum permitted stress level for the design of ac cable insulation is about 16 percent of the short-time strength and only 0.5 percent of the intrinsic strength. The maximum value of electric stress used in the design of insulation systems is sometimes referred to as the voltage endurance. It is the voltage endurance of the insulating

materials that is of prime importance in determining the long-time performance of the system.

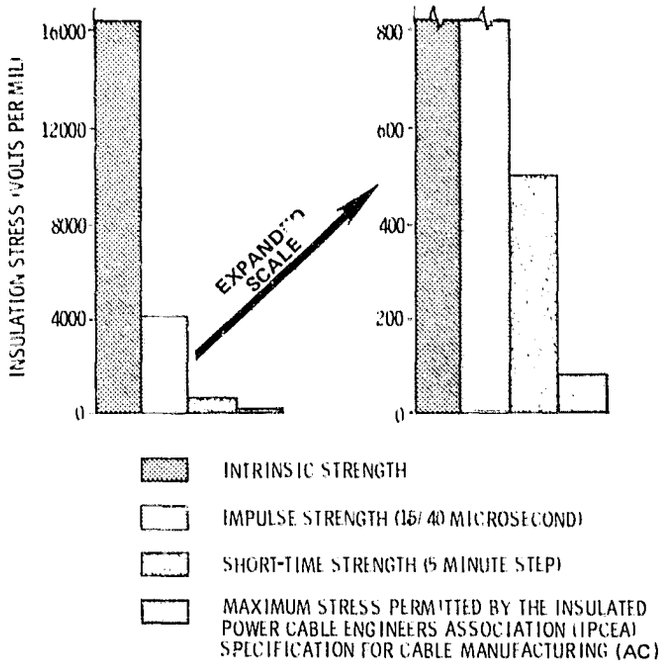

Figure 7-1 EFFECT OF TIME ON DIELECTRIC STRENGH OF POLYETHYLENE

7.1.1 Short-Time Dielectric Strength

As previously mentioned, material manufacturers usually specify dielectric strength in terms of short-time strength. Test methods for the determination of short-time dielectric strength are commonly based on the American Society for Testing and Materials Standard Methods of Test of Dielectric Breakdown of Electrical Insulating Materials (ASTM D149) (see Section 7.2.1).

In general, one of three methods is used. All three methods involve placing a sheet of the material to be tested between two

electrodes. The short-time test is conducted by increasing the voltage applied across the electrodes at a uniform rate until failure occurs. The slow-rate-of-rise test is conducted by applying an initial voltage equal to about 50 percent of the expected breakdown voltage. The voltage is then increased at a uniform rate until breakdown occurs. In the step-by-step test an initial voltage of 50 percent of the expected breakdown voltage is applied, as in the slow-rate-of-rise test. In this test, however, the voltage is increased in equal increments and is held at each voltage level for a specified period of time (for example, five minutes) until breakdown occurs. A manufacterer's published value for dielectric strength should be qualified as to method of test (usually ASTM D-149), manner and rate of applying voltage and other attendant conditions.

In addition to the method of voltage application, several other factors affect the dielectric strength of a material. These include:

- Field intensification
- Voids and imperfections
- Material thickness
- Relative humidity
- Temperature
- Frequency of the applied voltage

Field Intensification. Sharp edges or points on electrodes, such as those occurring on solar cells, solder and interconnecting conductors, result in localized field-concentrations. This is illustrated by Figure 7-2. This effect can increase the electric field by a factor of two to three times over that which would occur between parallel flat electrodes. This is further illustrated by Figure 7-3 (Ref. 7-2) which relates spark gap breakdown voltages in air to gap lengths for needle points as one extreme to smooth spherical surfaces of increasing diameter as the other extreme. The maximum intensification of this type is approximately a factor of three. Therefore, when calculating electrical stress levels in insulating materials, it is important that field intensifications resulting from electrode configuration be accounted for.

A second type of field intensification can occur for dielectric materials in series (laminated). The voltage applied across two series insulating materials is distributed nonuniformly according to the materials' permitivities for ac voltages and according to the materials' resistivities for dc voltages. This effect is discussed in detail for representative module material configurations in Section 7.4.

Voids and Imperfections. Material imperfections result in small localized distortions of the electric field within the insulation as discussed above under Field Intensification. For example, if a conducting particle is entrapped in the insulation, the voltage

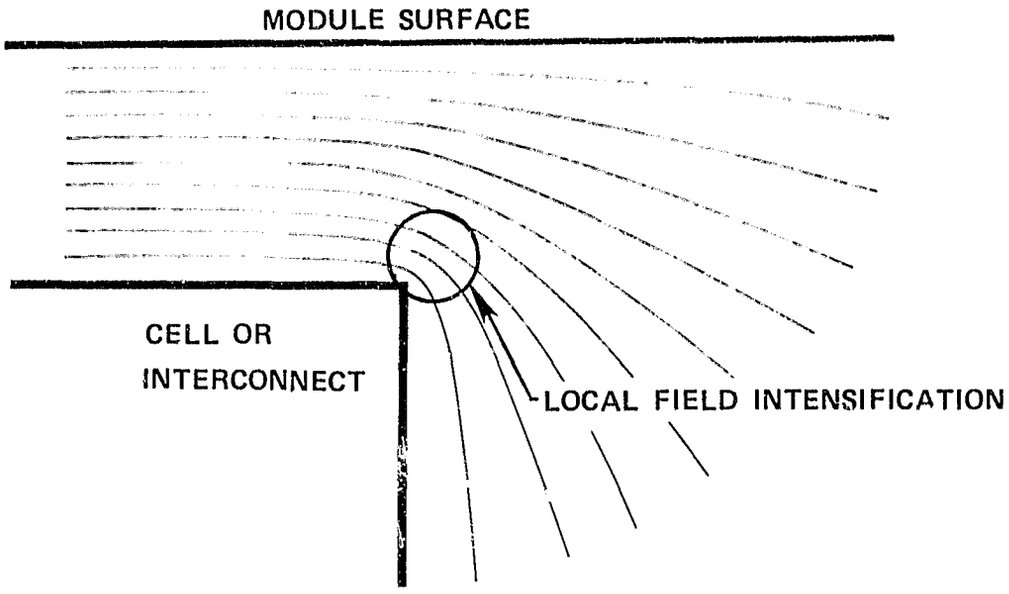

Figure 7-2 POTENTIAL DISTRIBUTION AT SHARP CORNER

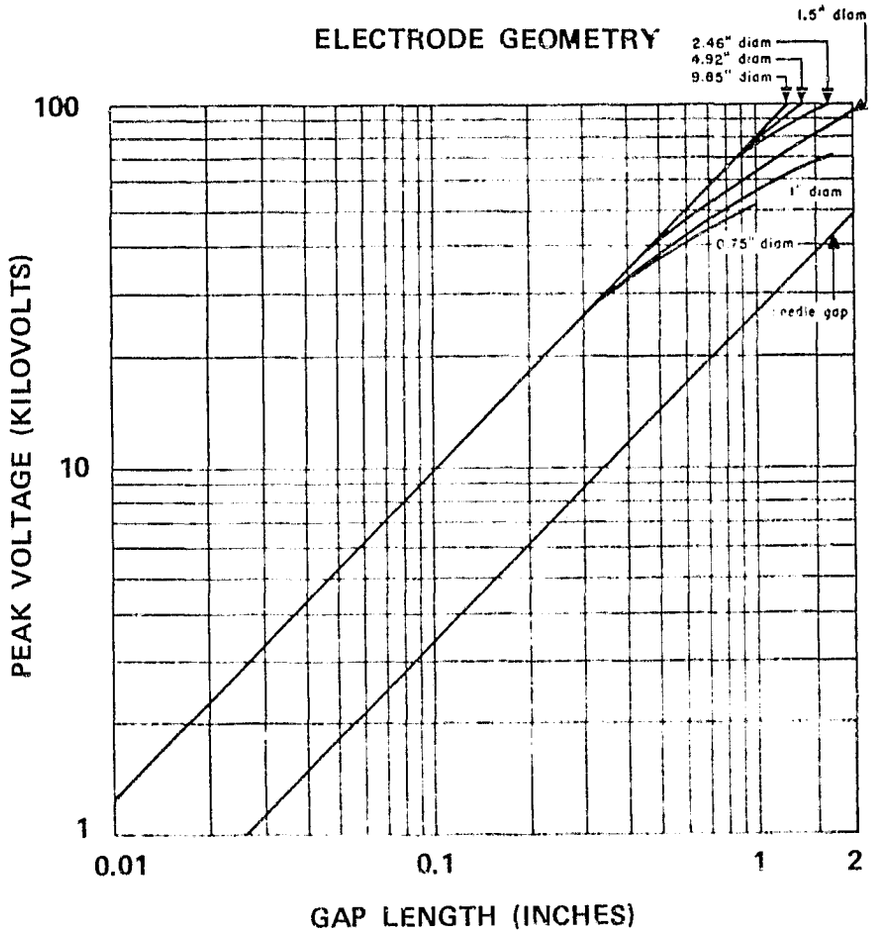

Figure 7-3 GAP BREAKDOWN VOLTAGES IN AIR

gradient across the particle will be negligible, thereby forcing a local increase in the voltage gradient to appear in the surrounding insulation. Such imperfections can be introduced during the manufacturing process. Similar effects result from voids, holes and bubbles that may be formed during manufacture, as the result of thermal cycling or by other processes.

Insulation Thickness. Dielectric strength is generally not a constant with the thickness of a solid or semi-solid material, but varies inversely as a fractional power of the material thickness. In general, for certain valid ranges and depending upon the particular insulating material, the ratio of the dielectric strength of two different thicknesses of the same insulator has been found to be equal to the reciprocal of the square root of the ratio of the two thicknesses ($E_1/E_2 = (t_2/t_1)^{0.5}$). For example, this relationship holds true for Mylar and can be readily determined from the curve shown in Figure 7-4 (Ref. 7-3).

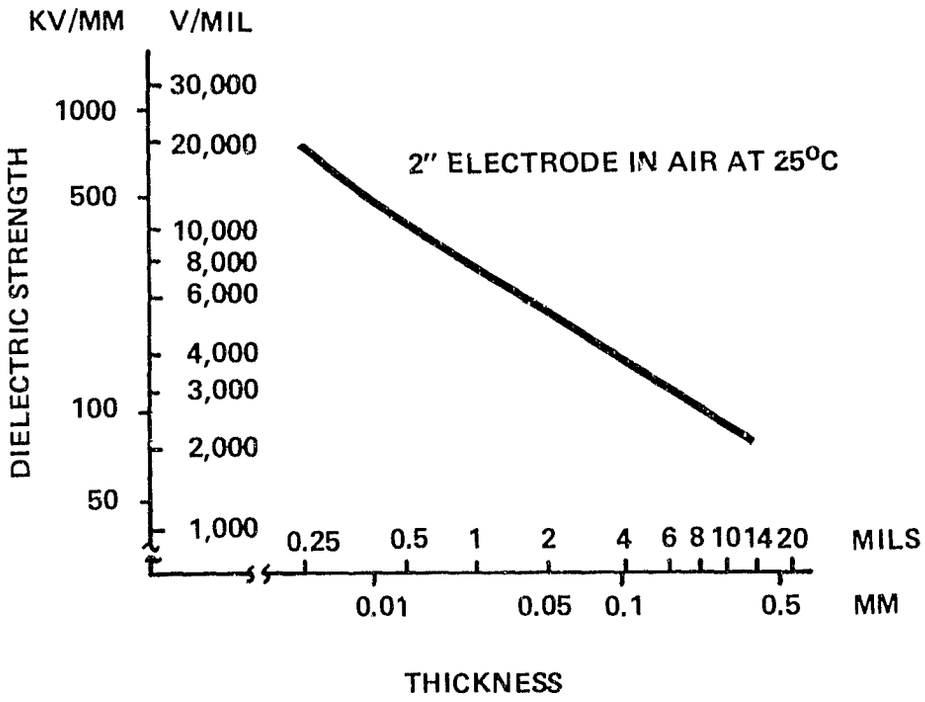

Figure 7–4 DIELECTRIC STRENGTH OF MYLAR AS A FUNCTION OF THICKNESS (60 Hz)

Therefore, for a given dielectric material, the maximum working or design electric stress may decrease for increasing insulation thickness.

Relative Humidity. Relative humidity influences dielectric strength to the extent that moisture (absorbed by or on the surface of the material) affects the materials volume and surface resistivities. The effect of moisture on the dielectric properties varies considerably with the nature of the material.

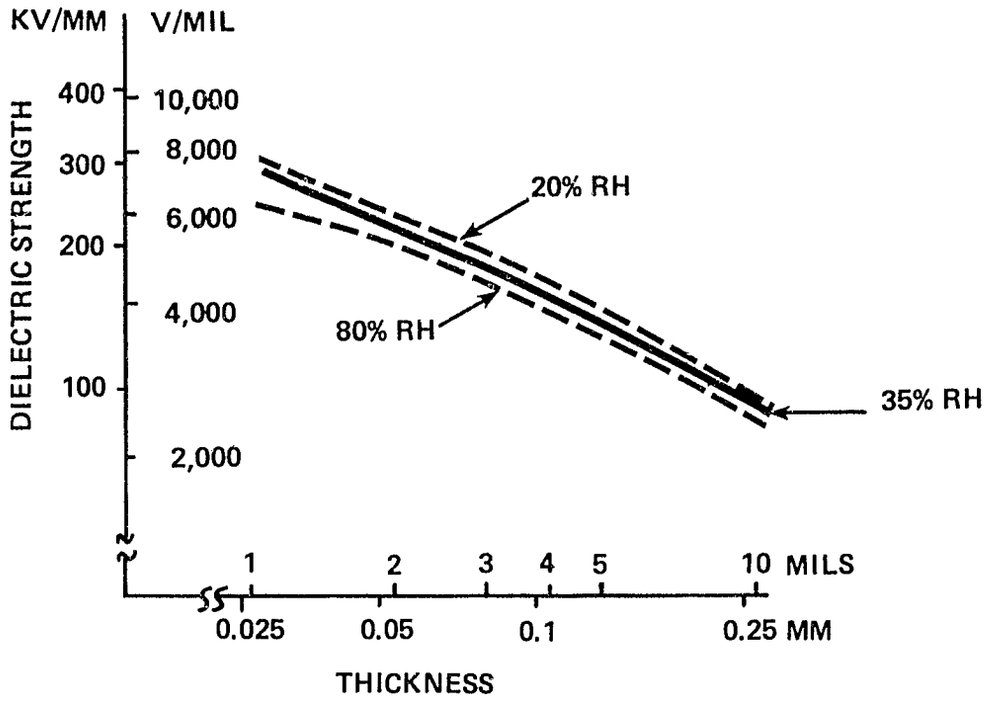

Figure 7–5 DIELECTRIC STRENGTH OF MYLAR AT VARIOUS HUMIDITIES (60 Hz)

Figure 7-5 (Ref. 7-3) illustrates the effect of humidity on the dielectric strength of Mylar for various thicknesses.

Temperature. The temperature of the dielectric material influences the dielectric strength and generally causes it to decrease with increasing temperature. For most materials, the change is small over the normal module operating temperature range. The thinner the material, the more pronounced is the effect. Figure 7-6 (Ref. 7-3) shows the effect of temperature on the short-term dielectric strength of Mylar for several thicknesses.

Frequency. The deterioration of dielectric strength with time has been shown to be greater under conditions of ac stress than

for dc stress. Figure 7-7 (Ref. 7-4) illustrates the phenomenon of frequency dependence on the life of polystyrene in a homogeneous field. The illustrated behavior is typical of most solid dielectrics.

7.1.2 Voltage Endurance

The value of measured short-time dielectric strength is useful and necessary in designing an insulation system. Short-time dielectric strength is used for specification purposes to show insulation quality and to compare one insulation with another of roughly similar thickness. However, the dielectric strength of most insulators decreases with age. Aging generally refers to long-term effects (years). The term "voltage endurance" is

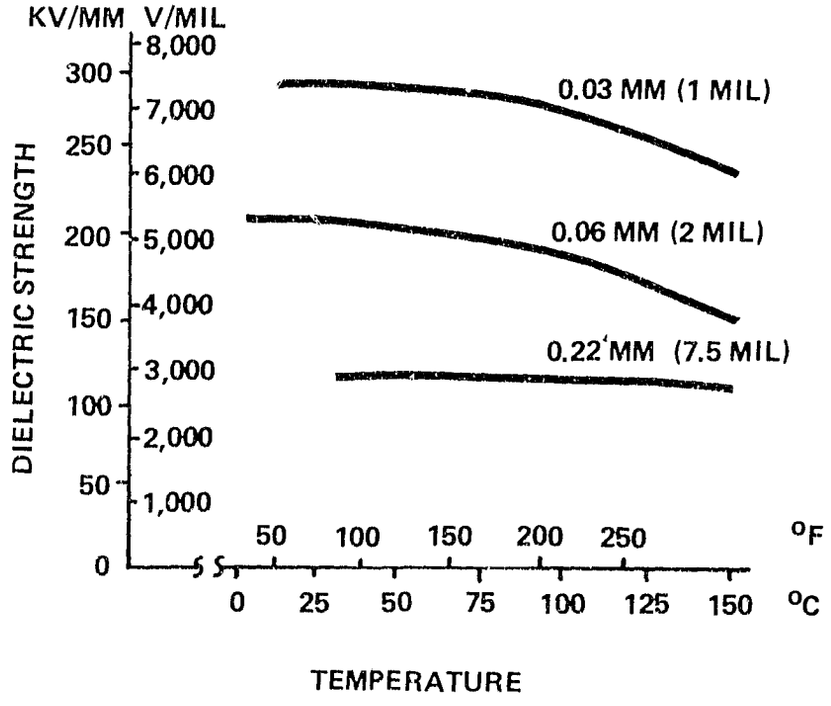

Figure 7–6 DIELECTRIC STRENGTH OF MYLAR AS A FUNCTION OF TEMPERATURE (60 Hz)

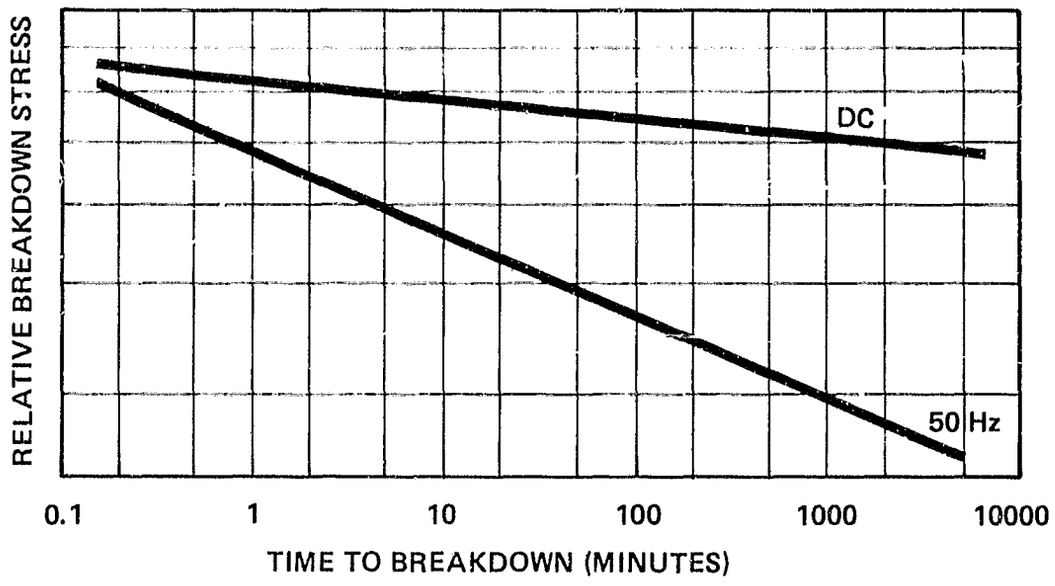

Figure 7–7 EFFECT OF STRESS LEVEL ON INSULATION LIFE

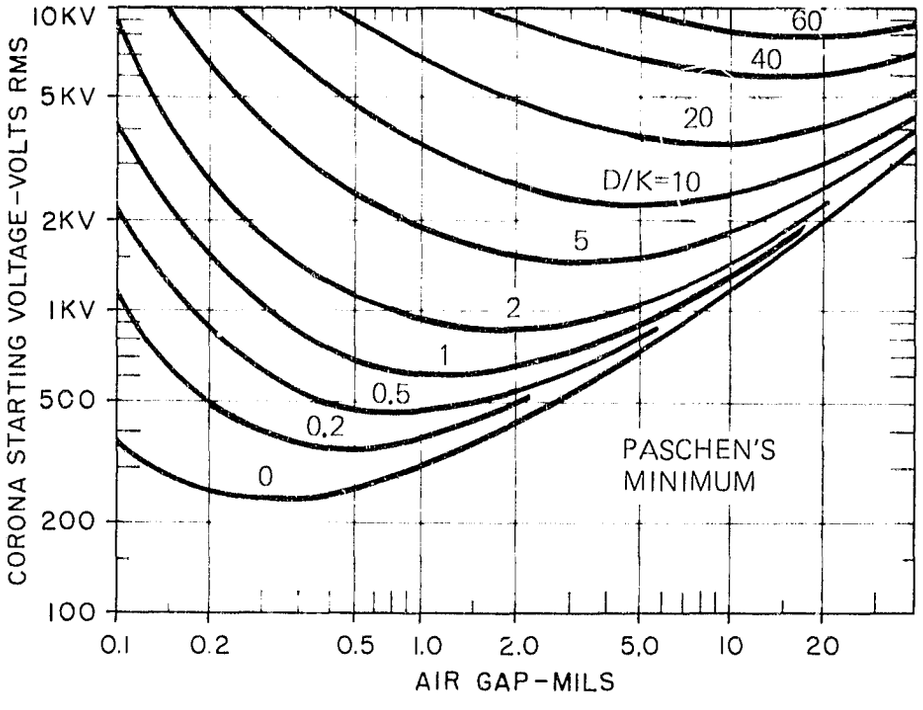

Figure 7-8 CORONA STARTING VOLTAGE (AC)

sometimes used in this regard and refers to the breakdown voltage or field for the insulation after several years of service.

It has been shown by Simoni and Pattini (Ref. 7-5) that aging and life are governed by inverse power laws. At time t_1, under an electric field E_1, aging is equal to that for time t_2 under an electric field E_2 ($E_1^N \times t_1 = E_2^N \times t_2$). The coefficient N of voltage endurance is influenced by the various factors that result in degradation of the insulation material. The effect of these factors is cumulative with time and determines the value of dielectric strength to which an insulation system must be designed for a required life.

Factors that affect the voltage endurance of insulating materials include:

- Corona
- Environmental conditions
- Mechanical cycling
- Treeing
- Other factors.

Corona. The presence of corona discharge, located either at the conductor-insulation interface or in voids within the insulation, produces a slow but steady degradation of insulator properties which can, in time, lead to failure. The corona starting voltage for dc is generally higher than for ac. With a steady direct

voltage, corona discharges appear very intermittently. When corona starts in a dc insulation system a charge is built up in the insulation which prevents further corona discharge until the applied voltage increases further, decreases or reverses, or until the charge leaks off by surface or volume resistivity. It is significant that photovoltaic power system inverters can superimpose an ac ripple voltage on the dc output of the solar cell modules. Although the ac ripple is usually limited to five percent or less, its effect may be such as to sustain corona.

Insulation life degradation due to corona is rapid. For uniform fields the corona starting voltage (ac) is determined by the Paschen Law Curve. Paschen's minimum curve for discharge voltage at one atmosphere of air pressure as a function of air gap length shows that the minimum void voltage at which a discharge can occur is about 230 volts rms (325 volts peak). This minimum occurs for a gap of 0.0076 mm (0.3 mil). The required voltage stress in the gap is therefore nearly 31.5 kV/mm (800 volts/mil). The lowest corona starting or inception voltage in practical insulation is related to the ratio of thickness to relative dielectric constant. A family of curves can be calculated and plotted above Paschen's minimum curve as shown in Figure 7-8 (Ref. 7-6). The corona starting voltage may be calculated as follows:

$$V = V_0 \times (B/T + 1)$$

where:

V = Corona Starting Voltage

V_o = Paschen's Minimum Voltage

$B = D/K$ = $\frac{\text{Thickness of Dielectric}}{\text{Relative Dielectric Constant}}$

T = Air Gap Length

For example, assume a 0.127 mm (5 mil) thickness of Mylar having a relative dielectric constant of 3.3. With a 0.0254 mm (1 mil) void or air gap, the minimum corona starting voltage is 750 volts. For these conditions the electric field in the insulation is only 5.9 kV/mm (150 volts mil) (0.75 kV divided by 0.127 mm).

Reference 7-12 presents a more thorough treatment of this subject, including the effect of pressure and various types of gases.

Voids in the insulation or encapsulation system are extremely influential upon the corona inception voltage. The shape and orientation of the voids are also important. The electric field in a long, flat void oriented perpendicular to the field is increased over that in the insulating material by a factor equal to the material's dielectric constant. The same void oriented parallel to the electric field results in insignificant field intensification. The field intensification factor for a spherical void is approximately 1.5. Particular attention must be given to material quality and fabrication of solar modules to

assure corona free insulation under long-term operating electrical stress levels.

The effect of corona on 60 Hz voltage endurance is illustrated for Teflon, in Figure 7-9 (Ref. 7-25).

Environmental Conditions. Environmental conditions, such as ultra-violet radiation, high temperature, moisture and atmospheric pollutants tend to reduce the breakdown strength of insulating materials. This likely results from physical or chemical changes occurring within the material. The degrading effects of these and other environmental conditions are usually cumulative with time. The net result is that the longer an

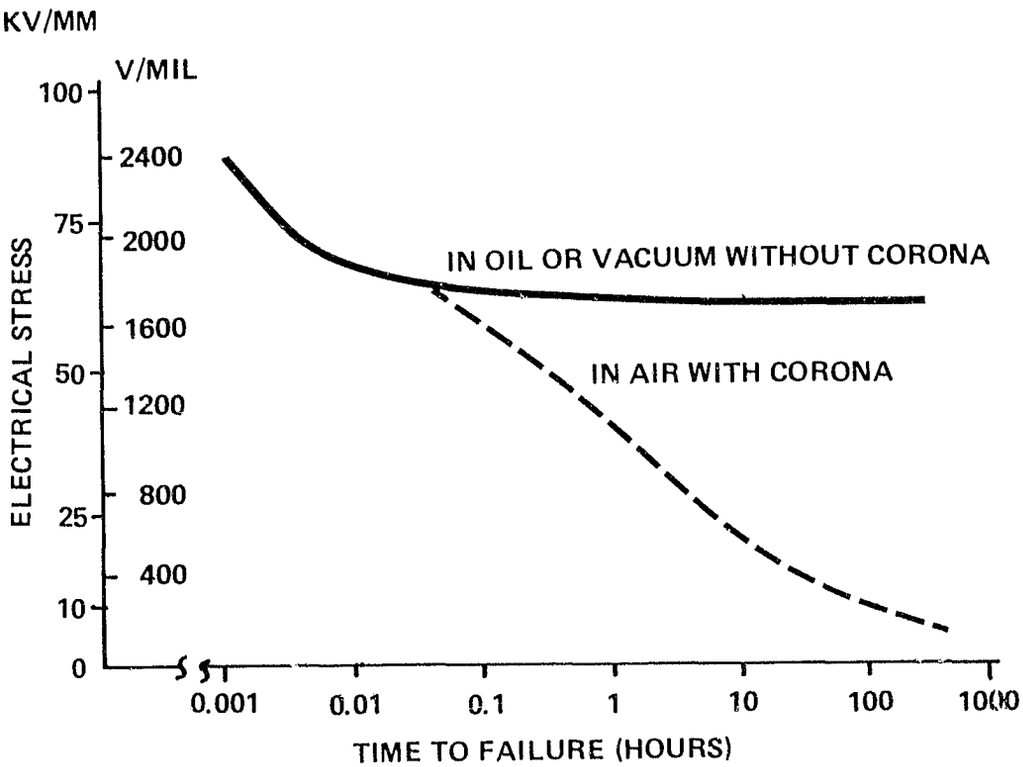

Figure 7–9 EFFECT OF CORONA ON LIFE OF TEFLON (60 Hz)

insulating material is exposed to adverse ambient conditions, the greater the degradation and the lower the voltage endurance.

The effects of individual environmental conditions, such as temperature, on insulation degradation are discussed further in Section 7.2, along with the effects of multiple simultaneous factors.

Mechanical Cycling. Mechanical cycling or other types of physical abuse can also result in decreased dielectric strength over long periods of time.

Treeing. Research on transparent polymeric insulation has revealed the formation of tree-like networks of incipient breakdown channels, which invariably start at an external or internal surface of the dielectric or at an interface between the dielectric and another material (Refernce 7-4). The breakdown channel ultimately leads to failure of the insulation.

Investigation of treeing phenomena has been spurred by the failures in buried cables using extruded dielectric insulation and is just beginning to be understood. Despite the best conservative past design practices employed by cable manufacturers, treeing-caused failures have shown up in buried cables after 5 or 10 years of service.

There are three general categories of treeing: electrical, water, and electrochemical. It is believed that treeing results in localized reductions of dielectric strength within the material, which ultimately leads to dielectric breakdown.

As discussed in Section 7.2.2, treeing in high voltage power cables is a significant cause of premature failure and has thus far eluded attempts by the cable industry at prediction via accelerated aging tests.

Other Factors. Many other factors, unique to a particular insulating material and/or application, can also result in material degradation and reduction in dielectric strength.

For example, the literature indicates that initially unsuspected deleterious chemical reactions can occur between an insulating material and other materials that it contacts. Dupont's Bulletin #M-4D (Ref. 7-3) states that some companies "have developed coatings which result in improvement of the electrical properties of Mylar," including significant increases in corona resistance and dielectric strength. However, the bulletin also states that some varnishes and potting compounds produce a "severe reduction in dielectric strength" and cautions users to evaluate coatings and pottants before they are incorporated into a manufactured product. This could have specific implications for module designers with regard to the use of primers or adhesives.

7.2 INDUSTRY PRACTICE

This section presents a discussion of existing industry practice in the areas of electrical insulation testing and system design procedures.

For purposes of this study, insulation testing is considered to include: short-time material testing, accelerated aging (life tests), and manufacturing quality control/acceptance (QA) tests. Design procedures include the methods of selecting design (working) stress levels, safety factors used in various types of applications and the correlations between predicted life (from accelerated aging data) and actual field experience.

7.2.1 Test Procedures

The major area of interest in this portion of the present study is the dielectric strength of an insulator as it relates to module design. Dielectric strength is measured by applying a voltage to a material sample or piece of equipment and increasing the voltage until indications of breakdown are observed. Breakdown may be indicated by visual observance of damage to the material or by a very rapid increase in current as a function of voltage.

Voltage breakdown (dielectric strength) is usually measured by a destructive test. Material samples are placed between electrodes

and subjected to a voltage. As the voltage is increased, leakage current increases and eventually breakdown occurs. This is illustrated by Figure 7-10. As shown in the figure, the leakage current is initially linearly proportional to the applied voltage. In this region the leakage current is determined by the voltage and the ionic conductivity of the material. The slope of the voltage versus leakage current curve, between points A and B in Figure 7-10, is therefore a measure of the material's leakage resistance. Eventually, the rate of current rise begins to increase. This occurs at point C on the curve in Figure 7-10 and indicates that breakdown is imminent. Further increase in voltage past this point (the knee of the curve) leads to an exponential increase in current. Past the knee of the curve, conduction within the material is primarily by free electrons and in most cases results in permanent damage to the material. In some cases, the test may be terminated as soon as the knee of the leakage current versus voltage curve is determined, so as to save the sample or equipment (nondestructive testing).

As previously discussed, several methods and/or rates of applying the test voltage are used. The voltage may be increased linearly, in uniform steps, in large initial steps followed by smaller steps near the breakdown voltage or in one step. Reflecting general industry applications, a majority of testing is done at the powerline frequency of 60 Hz. In addition, dc (of prime interest herein) and pulse voltages are also used, but less frequently.

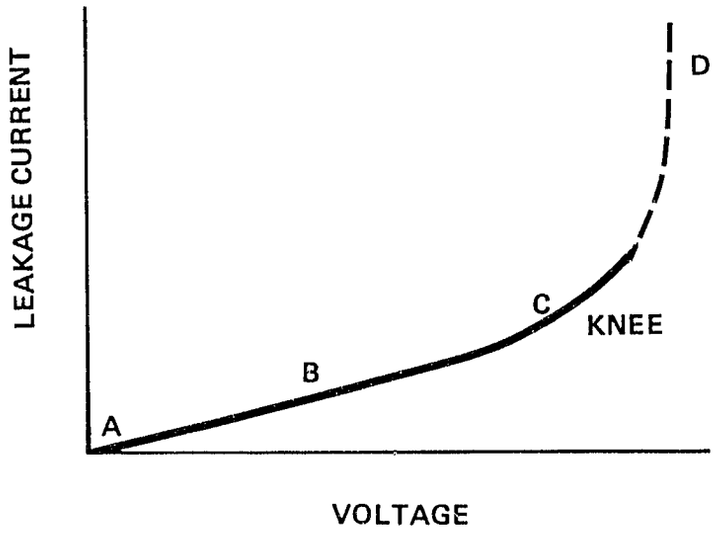

Figure 7–10 LEAKAGE CURRENT VERSES VOLTAGE

Standardized industry procedures for determining dielectric strength and other material properties and for qualifying products have been established by the American Society for Testing and Materials (ASTM). In addition to the ASTM test procedures, the Institute of Electrical and Electronics Engineers (IEEE) and Underwriters Laboratories (UL) have issued specific and applicable standards. Generally, these standards reference ASTM standards. Following is a listing of tests in general use by the industry.

ASTM - The number following the dash indicates the year in which the standard was established. Numbers in parenthesis indicate the year of latest reapproval or modification.

D149-75	Dielectric Breakdown Voltage and Dielectric Strength of Electrical Insulating Materials at Commerical Power Frequencies
D150-74	AC Loss Characteristics and Dielectric Constant (Permittivity) of Solid Electrical Insulating Materials
D176-77	Solid Filling and Treating Compounds Used for Electrical Insulation
D202-77	Sampling and Testing Untreated Paper Used for Electrical Insulation
D229-77	Rigid Sheet and Plate Materials Used for Electrical Insulation
D257-76	DC Resistance or Conductance of Insulation Materials
D374-74	Thickness of Solid Electrical Insulation
D618-61 (77)	Conditioning Plastics and Electrical Insulating Materials for Testing
D669-59 (72)	Dissipation Factor and Dielectric Constant Parallel with Laminations of Laminated Sheet and Plate Insulating Materials
D1371-68 (72)	Cleaning Plastic Specimens for Insulation Resistance, Surface Resistance and Volume Resistivity Testing
D1389-62 (77)	Dielectric Proof-Voltage Testing of Thin Solid Electrical Insulating Materials
D1711-75	Standard Definitions of Terms Relating to Electrical Insulation
D1868-73	Detection and Measurement of Discharge (Corona) Pulses in Evaluation of Insulation Systems
D2132-68 (75)	Dust and Fog Tracking and Erosion Resistance of Electrical Insulating Materials
D2275-75	Voltage Endurance of Solid Electrical Insulating Materials Subjected to Partial Discharges (Corona) on the Surface
D2302-75	Differential Wet Tracking Resistance of Electrical Insulating Materials with Controlled Water-to-Metal Discharges
D2304-68 (72)	Thermal Evaluation of Rigid Electric Insulating Materials

D2305-72 Polymeric Films Used for Electrical Insulation

D2381-68 (74) Flexible Composite Materials Used for Electrical Insulation

D2865-71 (76) Calibration of Standards and Equipment for Electrical Insulating Materials Testing

D3151-73 Thermal Failure Under Electric Stress of Solid Electrical Insulating Materials

D3426-75 Dielectric Breakdown Voltage and Dielectric Strength of Solid Electrical Insulating Materials Using Impulse Waves

Underwriters Laboratory

UL Standard 746A - Polymeric Materials -- Short-Term Property Evaluations

UL Standard 746B - Polymeric Materials -- Long-Term Property Evaluations

UL Standard 746C - Polymeric Materials -- Used in Electrical Equipment Evaluations

Institute of Electrical and Electronic Engineers

IEEE Standard 1 - General Principles for Temperature Limits in the Rating of Electric Equipment

IEEE Standard 98 - Guide for the Preparation of Test Procedures for the Thermal Evaluation and Establishment of Temperature Indices of Solid Electrical Insulating Materials

IEEE Standard 99 - Guide for the Preparation of Test Procedures for the Thermal Evaluation of Insulation Systems for Electric Equipment

IEEE Standard 101 - Guide for the Statistical Analysis of Thermal Life Data

IEEE Standard 101A - Simplified Method for Calculation of the Regression Line (Appendix to IEEE Standard 101)

The primary measurements are covered in ASTM-D 149 (dielectric strength), ASTM-D 150 (permittivity and losses) and ASTM-D 257 (dc conductance). Most of the other standards refer back to these three.

7.2.2 Accelerated Aging

Accelerated aging techniques are sometimes used to predict voltage endurance and to estimate the long-time performance of insulation system designs. As discussed in Section 7.1, the successful design of electrical insulating systems requires that electrical stress levels be kept below those that will cause breakdown during the life of the equipment. The voltage endurance of the insulation is determined by the magnitude of the degrading (aging) factors to which the insulation is exposed and the length of exposure time.

Accelerated testing is used to facilitate evaluation of the service life of insulation materials or systems by increasing the intensity of one or more factors that age the material. A difficulty in conducting such tests is that care must be taken not to introduce failure mechanisms that would not occur naturally in the type of service for which the material is intended. Therefore, testing should duplicate the actual service environment as closely as possible.

Generally, the aging effects of temperature are known and somewhat predictable. The effects of voltage are less known. The effects of other factors and the effect of multiple factors acting concurrently are much less understood and difficult to predict.

For example, a recently published review of insulation aging phenomenon (Ref. 7-7) stated that "accelerated life tests have been performed for many years and yet their validity is still questioned. This uncertainty is believed to be a reflection of our ignorance regarding the significance of the interaction of the various stresses." Similarly, the power cable industry has accumulated a vast amount of operating and test data on the voltage endurance of insulation under ac stress conditions. However, as previously mentioned, attempts to utilize extruded dielectric insulating materials (such as polyethylene) in high voltage cable insulation have been frustrated by the phenomenon called "treeing." A rash of failures in 5-10-year old 15 kV polyethylene insulated cables revealed the problem of "trees." This phenomenon of partial breakdown, having the appearance of a small tree, was entirely unexpected and exemplifies the trouble one may run into when introducing a new system.

The following is a brief discussion of present accelerated aging techniques.

Temperature. As discussed in Section 7.1, higher temperatures generally decrease insulation life. The experimental data seem to correlate with equations relating chemical reaction rate to temperature. Thermal aging, in this context, excludes thermal failure due to temperatures that cause the insulation material to melt, flow or otherwise deform mechanically. The relation of insulation material life to temperature generally can be predicted by:

$$\text{life} = A \exp (B/T)$$

where A and B are constants that are properties of the material and T is the absolute temperature

Data is usually taken by subjecting many test samples of a given material to a fixed voltage (electric field) with temperature as a parameter. The resulting measurements of breakdown are usually presented in an Arrhenius plot such as shown in Figure 7-11 (Ref. 7-24). As can be seen in Figure 7-11, the logarithm of life (time to failure or breakdown) is a straight line that is inversely proportional to temperature, as would be expected if the equation given above is valid. Also illustrated is the fact that there is a normal distribution of data in time to breakdown.

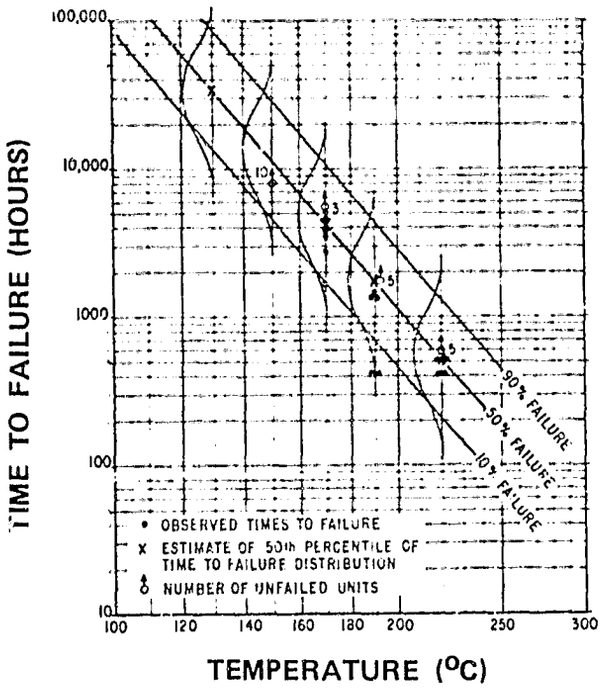

Figure 7-11 TYPICAL ARRHENIUS PLOT OF INSULATION LIFE DATA

As indicated by the distribution shown for the data in Figure 7-11, there is a spread in the measured time to failure for a given temperature. This type of data is often presented on a Wiebull plot such as shown in Figure 7-12 (Ref. 7-5). Figure 7-12 serves to illustrate a typical spread for this type of test data and the large number of samples that must be tested to accurately determine mean life.

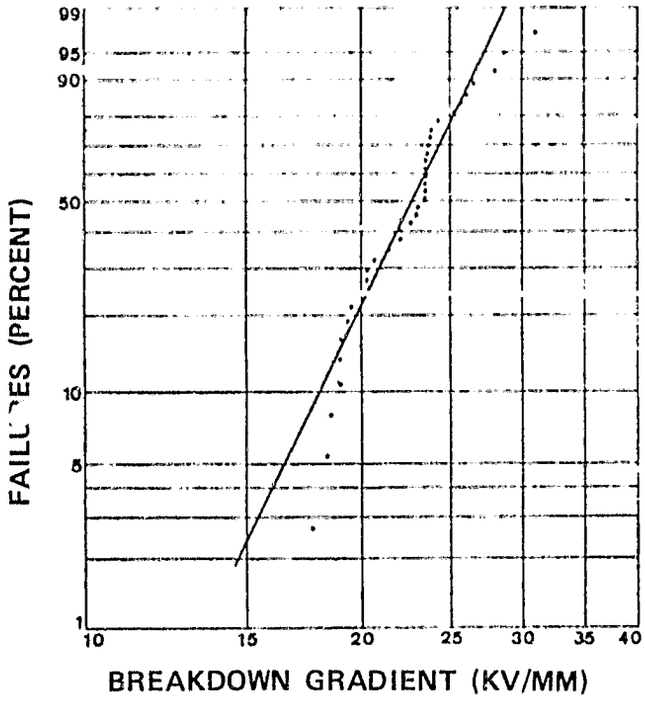

Figure 7-12 WEIBULL PLOT OF EPR INSULATION LIFE DATA

Most researchers in this field caution about extrapolating absolute values of life or voltage endurance much beyond the time periods used in the testing. Several common insulation materials have proven field service lives that exceed the value predicted by temperature accelerated aging tests. The greatest value of such testing appears to be in providing comparisons of the life of alternate materials in various temperature environments.

Voltage. Life (time to breakdown) has been found to be inversely proportional to applied electrical stress. Investigators have arrived at the following expression to describe voltage aging:

$$\text{life} \times (\text{electric field})^{N} = \text{constant}$$

where N is a property of the material

The equation indicates that a plot of life (time to breakdown) versus electric field on log-log paper will be a straight line with a slope of $-1/N$. In many cases, measured data bears out this relationship. In other cases the line may exhibit a change in slope (change in the value of N) at some point in time, which indicates a change in the failure mechanism such as the onset of corona. This is illustrated by Figure 7-13 which shows the ac breakdown voltage for a Mylar sample (Ref. 7-8).

As shown in the figure, the life versus electric field curve is a straight line up to about 100 hours. At this point, the slope changes and the line follows a curve which appears to approach 1000 volts as an asymptote. The researchers, Starr and Endicott, accommodated the curvature of the greater than 100 hours line segment by subtracting a constant voltage (1 kV). The voltage endurance behavior of the sample, (five layers of 0.002 in. thick Mylar) is then given by:

$$\text{Life} \times V^{4.8} = 8 \times 10^5 \qquad \text{Life} < 100 \text{ hours}$$

$$\text{Life} \times (V-1)^{1.44} = 3 \times 10^4 \qquad \text{Life} > 100 \text{ hours}$$

where V = applied voltage in kV rms and Life is in hours

The researchers hypothesized that the change in slope occurring at about 100 hours results from differences in the failure mechanisms between what they called high- and low-voltage corona. It is also possible that a completely different failure mechanism, such as dielectric heating, was responsible for the failures occurring in less than 100 hours.

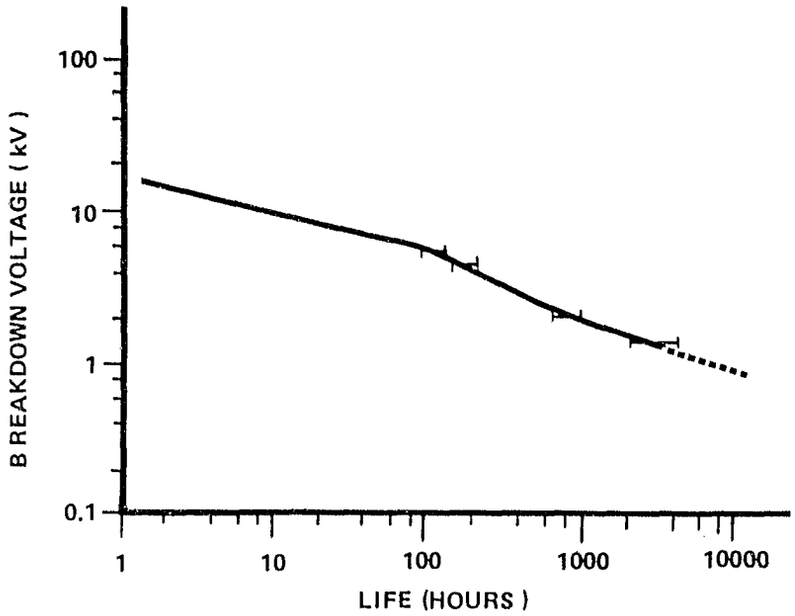

Figure 7- 13 LONG-TIME LIFE OF MYLAR (60 Hz)

It is also interesting to note that the apparent 1000 volt asymptote of the long-time (>100 hours) curve agrees reasonably well with the minimum corona starting voltage of the Mylar sample. It might be inferred from this that at voltages below 1000 volts the sample would not undergo corona degradation and that failure would result from a different mechanism. The new mechanism might be ultraviolet light or any other mechanism either not introduced by the researchers or one that requires a longer time period than was used during testing.

The change in failure mechanism with level of applied electrical stress serves to illustrate the potential for error when short-time test data is extrapolated or when testing time is accelerated by raising the stress level.

Combined Factors. In general, very little successful work has been done to predict aging or voltage endurance for two or more factors acting on an insulator simultaneously (for example, temperature and voltage level). This is due in part to the lack of sufficient knowledge to model various aging effects with at least the accuracy of the chemical-rate effect of temperature. Also, multiple factors can combine to synergistically accelerate aging. Several studies (Refs. 7-9 and 7-10) have shown that sequential testing with two factors gives results that differ from those obtained from the simultaneous application of the same two factors. Whether life is under- or overestimated by sequential testing appears to depend both on the aging factors involved and the particular insulating material.

7.2.3 Design Procedures

In order to establish guidelines for evaluation of the electrical insulation performance of module encapsulation systems, Bechtel conducted a review of existing industry design practices and experience. The results of this review indicate that, in some respects, insulation design is still more of an art than an exact science. The design of successful insulation systems, for specific applications and using specific insulating materials, generally requires an iterative procedure involving initial design, laboratory testing and feedback of real time performance data.

As discussed in Section 7.2.2, the present lack of understanding with regard to aging effects (especially combined effects) on insulation performance makes it difficult to extrapolate existing performance data to new designs, such as solar cell encapsulating systems. In addition, the design of many electrical insulation systems have, in the past, been governed by mechanical and other nonelectrical considerations. This is illustrated in Figure 7-14, which presents maximum allowable ac stress specified by the Insulated Power Cable Engineers Association (IPCEA) for the manufacture of insulated wire and cable using various solid dielectric insulating materials.

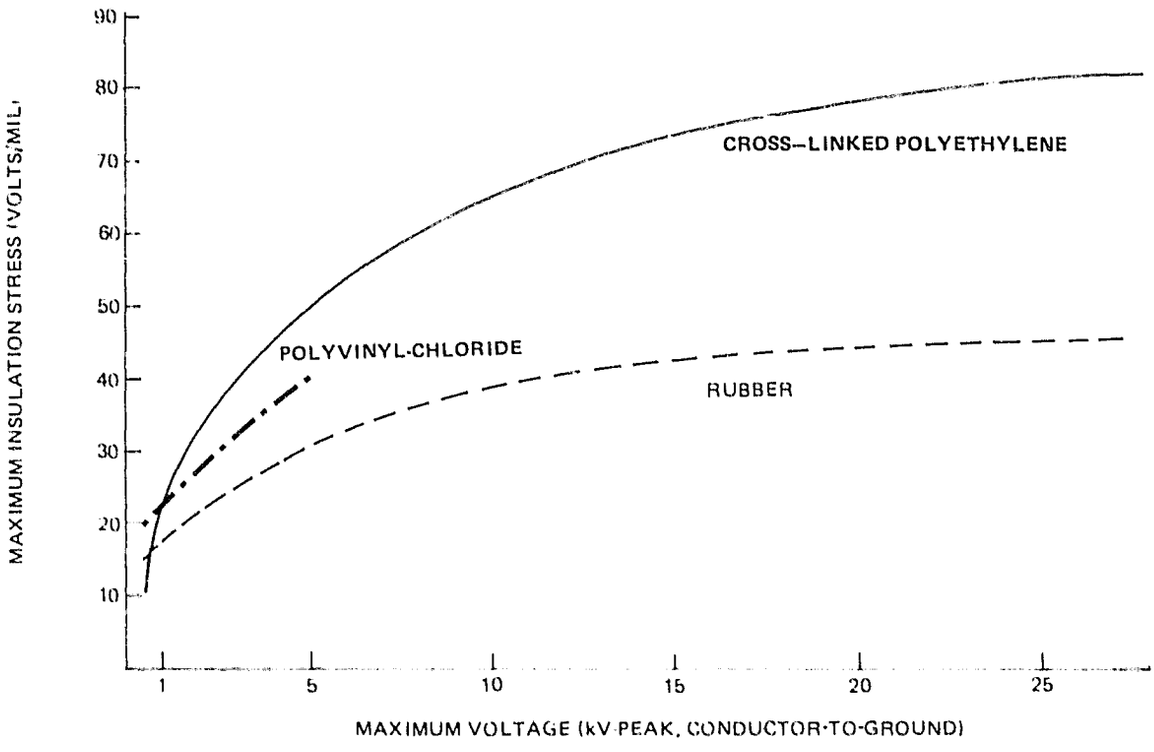

Figure 7-14 MAXIMUM ALLOWABLE AC STRESS FOR CABLE INSULATION

The relatively low allowable stress levels for cables designed to operate at less than 1000 volts results from minimum insulation

thickness required to resist cracking, abrasion, and other mechanical damage that can occur during installation or operation. As can be seen in Figure 7-14, allowable stress levels increase with increasing cable voltage rating. However, above about 15 kV, stress levels become relatively constant at a maximum value which appears to be dependent on the electrical properties of the specific material being used. The fact that the allowable stress levels for cable insulation reach a maximum value implies that, at the higher voltage levels, mechanical considerations are outweighed by electrical concerns (voltage endurance) and that material thickness is determined by electrical performance requirements.

The data in Figure 7-14 apply to ac applications and it is likely that the maximum allowable stress levels are influenced by the corona inception voltage. In other words, the stress must be kept below the level at which corona will result in significant material degradation during the life of the insulation. In ac applications where corona can be reduced or eliminated, such as in oil-filled, paper-insulated high voltage cables, allowable stress can be significantly higher. For example, high-pressure oil-filled cable designs often used stress levels (equivalent peak stress to ground) in the range of 15 kV/mm (381 volts/mil). The higher acceptable stress levels result primarily from the fact that the oil fills any voids in the solid insulating material which might otherwise act as sites for corona discharge and material degradation.

Although the experiences of the cable industry in the design of solid dielectric ac insulation systems are interesting and informative, the emphasis of this study is on the design of module insulation systems, which are primarily a dc application. Acceptable stress levels for a specific material are generally higher for dc applications than for ac, when all other operating conditions remain constant. Various cable manufacturers have indicated that cables insulated with solid dielectric insulation could be safely operated under continuous dc stresses of between 2.5 and 3 times the maximum allowable stress levels for ac operation.

In the past, requirements for high voltage dc cables, where electrical stress levels would likely govern insulation design, have been limited to a few specialized types of applications. For example, a cable designed for supplying high voltage dc power to x-ray tubes uses approximately 7.9 mm (311 mils) of ethylene-propylene rubber between the inner conductor and the cable jacket. The cable is rated for a maximum voltage of 75 kVdc. This results in an average stress level in the insulation of about 9.5 kV/mm (241 volts/mil). The relatively high stress level (five times higher than indicated in Figure 7-14 for ac cables) likely results from the intermittent nature of voltage application inherent in the operation of most x-ray systems.

A recent study (Ref. 7-11) illustrates the degree of uncertainty with regard to the voltage endurance, at high stress levels, of

dielectrics in dc fields. The study investigated design requrements for a 600 kV dc rated cable. For that design example, oil-impregnated paper was selected as the dielectric material primarily because substantial information exists for this insulation in high voltage ac cables. For design purposes, the investigators assumed a safety factor of 3. That is, the maximum working stress level is one-third of the measured short-time breakdown values. This resulted in a maximum design stress (in a uniform field) of about 35 kV/mm (900 v/mil) for the oil-impregnated paper insulation at 25°C.

The authors conclude by stating "Should a more comprehensive future study of the long-time dielectric behavior disclose that the 'safety-factor' of one-third is conservative, a reduction in the above insulation thickness will be possible" (Ref. 7-11). One might also consider that additional long-time performance data might demonstrate the need for reduced stress levels (increased safety factor).

The design examples and safety factors presented in this section illustrate the relatively wide range of practices currently in use by designers of electrical insulation systems. Evaluation of these data result in several conclusions, as follows:

- Electrical insulation systems are designed to operate at stress levels below the measured short-time breakdown levels.
- The ratio between short-time breakdown stress and maximum working stress (safety factor) can

be significantly influenced by both material properties and operating environment and the degree of design conservatism.

- Operation in dc fields is generally less severe (in terms of aging effects) than operation in ac fields of equivalent stress and, all other things being equal, results in somewhat higher permissable working stress levels.

However, considering the variety of encapsulating materials and module configurations, as well as the nature of the module operating environment, it is not considered prudent at this time to speculate on acceptable safety factors for the design of module encapsulation/insulation systems. Estimation of acceptable safety factors for a specific module configuration is discussed briefly in Section 7.5.1, Design Example.

7.3 ELECTRICAL PROPERTIES OF MATERIALS

The electrical properties of many materials can be obtained from handbooks, manufacturers' literature and from the results of research published in various technical journals. However, electrical properties data of interest for the various materials that are either in use or being considered for the manufacture of modules are not tabulated in any one source document. Also, much of the available data is for 60 Hz.

Table 7-1 lists typical published values for electrical properties of representative encapsulating materials. The data listed should be considered approximate and used with caution.

TABLE 7–1

ELECTRICAL PROPERTIES

Material	Dielectric Strength (volts/mil)	Dielectric Strength Comments	Relative Dielectric Constant ε	Relative Dielectric Constant Comments	Volume Resistivity Ω-cm	Volume Resistivity Comments	Surface Resistivity Ω-cm	Surface Resistivity Comments	Source Reference No.
Bakelite, BT-48-306 (100% Phenol Formaldehyde)	277	25°C 1/8" thick	8.6	24°C, 60 Hz	–	–	–	–	7-2
Bakelite, BT-48-306 (100% Phenol Formaldehyde)	–	–	8.0	24°C, 100 Hz	–	–	–	–	7-10
Phenol Formaldehyde	300	–	5	25°C, 10^6 Hz	2×10^6	22°C 22°C	8×10^{15}	22°	7-11
Phenol Formaldehyde (cast)	75-450	–	5-15	25°C, 10^6 Hz	–	–	8×10^{15}	22°	7-12
EVA (Ethylene vinyl acetate, 28% VA)	1,100	60 Hz .014" thick	2.5	60 Hz	10^{12}	ASTM D257	–	–	7-21
EVA (Ethylene vinyl acetate, 28% VA)	2,500	DC .014" thick	–	–	–	–	–	–	7-21
EVA (Ethylene vinyl acetate, 28% VA)	620-780	1/8" thick	2.5-3.2	–	10^9	–	10^{15}	50% RH, 23°C	7-21
Glass, Borosillicate 7740	12,000	.0039" thick, intrinsic	4.8	10^6 Hz, 20°C	10^{15}-10^{16}	25°	10^{15}	40% RH (10[illegible]	7-24
Glass, Soda Lime 0080	11,000	.0039" thick, intrinsic	7.5	10^6 Hz, 20°C	10^{13}	25°	10^{12}	40% RH (10^7 [illegible]	7-24
Glass, Soda Lead	8,000	.0039" thick, intrinsic	8.2	10^6 Hz, 20°C	10^{14}	25°	–	–	7-24
Mylar (Polyethylene Teraphalate)	3-4000		2.0	60 Hz	–		–	–	7-14
Mylar (Polyethylene Teraphalate)	5,000		–		4×10^{15}		4.8×10^{11}	100% RH	7-22
Mylar (Polyethylene Teraphalate)	7,500	60 Hz, ASTM D149 & D2305	3.3	25°C, 60 Hz	10^{18}	60 Hz ASTM D257	–	–	7-11
Mylar (Polyethylene Teraphalate)	5,000	60 Hz, 150°C	3.7	150°C, 60 Hz	10^{13}	–	–	–	7-11
Mylar (Polyethylene Teraphalate)	14,000	25°C DC, 500 V/sec, .001"			–		–	–	7-13
Mylar (Polyethylene Teraphalate)	8,000	150°C DC, 500 V/sec, .001"	–		–		–	–	7-13
Mylar (Polyethylene Teraphalate)	7,500	25°C, 60 Hz ASTM 149 & D2305	3.3	25°C, 60 Hz, ASTMP 150	10^{18}	25°C ASTM D257	10^{16}	25°C	7-3
Mylar (Polyethylene Teraphalate)	6,000	150°C	3.7	150°C, 60 Hz	10^{13}	150°C	10^{12}	150°C	7-3
Polyethylene	600	0.10" thick	2.26	25°C, 60 Hz	–		–	–	7-2
Polyethylene	460-470	–	2.3	–	10^{10}-10^{11}	–	–	–	7-2
Polyethylene	1,000	–	2.3	–	–		–	–	7-13
Polyethylene	1,000	–	2.3	–	10^{19}	–	–	–	7-14
							–	–	7-15
PVB (Polyvinylbuteral)	350	60 Hz, .125" thick	5.6	60 Hz	5×10^{10}	50% RH, 23°C	–	–	7-23
Sylgard 184	550-600	ASTM 149, 500 V/sec, 1/16"	2.6-2.75	60 Hz, ASTM 150	10^{14}	ASTM 257	–	–	7-17
Tedlar (Polyvinyl Fluoride)	3,400	25°C, 60 Hz	8.5	10^3 Hz, ASTM D-150	4×10^{13}	23°C ASTM D257	–	–	7-19
Tedlar (Polyvinyl Fluoride)	–	–	–	–	2×10^{10}	100°C ASTM D257	–	–	7-19
Tedlar (Polyvinyl Fluoride)	3,500	60 Hz	9.9	10^3 Hz, ASTM 150	7×10^{14}	ASTM D257	10^{16}	–	7-19
Tedlar (Polyvinyl Fluoride)	–	–	–	–	1.5×10^{11}	100°C	–	–	7-19

Preferrably, current data on the material properties should be obtained from the manufacturer or from testing. As can be seen, not all sources give the same values for properties of the same material. In addition, material properties can vary, depending on the exact formulation of a material that is imprecisely described by a generic name (for example, EVA). Also, as discussed, dielectric strength decreases with time at a rate that is dependent on specific material characteristics and the service environment. Properties, such as resistivity, are also subject to variations, particularly with changes in relative humidity and moisture.

Although data on short-time dielectric strength, relative dielectric constant, and volume and surface resistivities are generally available, data on long-time voltage endurance of candidate module materials has generally been found to be unavailable. In addition, care must also be exercised when using the published short-time data. For example, dielectric strength is often given without reference to the test method or conditions used in obtaining the data and therefore diminishes its usefulness.

The use of material electrical properties for module design calculations is illustrated in Sections 7.4 and 7.5.

7.4 MODULE DESIGN AND TESTING

This section presents a discussion of several factors affecting module insulation design and testing.

7.4.1 Module Potential

The voltage withstand or insulation requirements of a module depend, of course, on the system or branch circuit voltage. However, the insulation level required also depends on the branch circuit configuration and the location of the module within that configuration. Figure 7-15 shows a simplified schematic of a generic branch circuit with 2N modules connected in series. Parallel connections, if any, are assumed to be at the branch circuit level or within the module. The circuit illustrated is floating (ungrounded except for module frames).

As indicated by the figure, the potential difference between modules and between each module and ground is a function of location within the branch circuit. The potential across the insulation of the two end modules (1 and 2N) is equal to one-half of the branch circuit voltage ($V_s/2$). The potential decreases uniformly along the branch circuit and reaches zero at the electrical midpoint of the branch circuit (N and N+1). Actually, there is a small difference within each module due to the module voltage, but module voltages are negligibly small compared to the

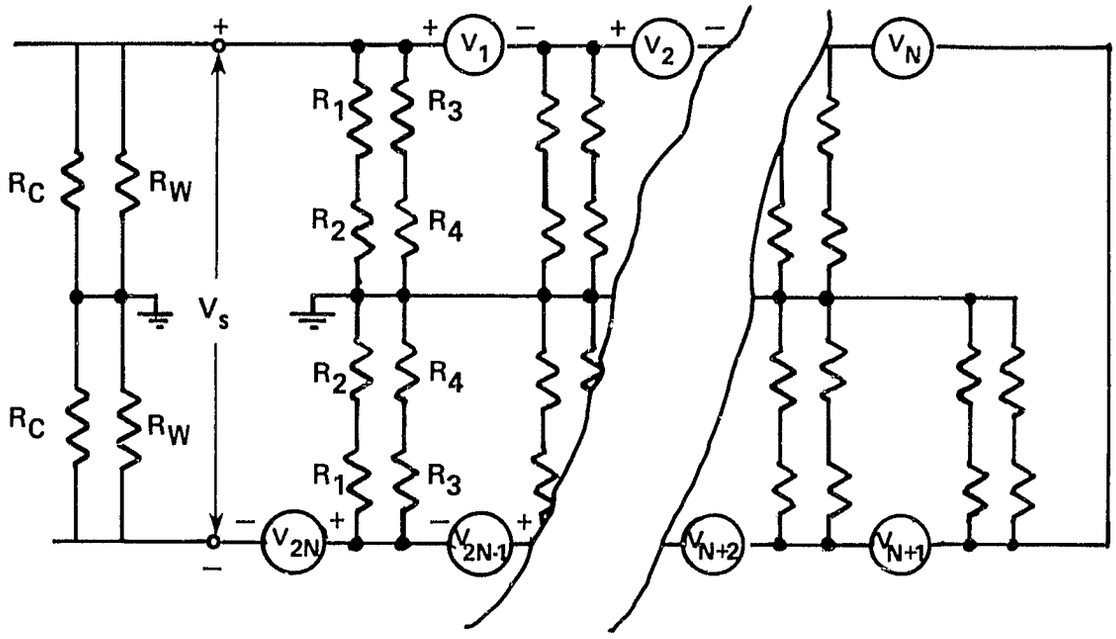

V_N — MODULE (OR CELL) VOLTAGE

V_S — BRANCH CIRCUIT VOLTAGE

R_1 — VOLUME RESISTANCE OF MODULE SUPERSTRATE

R_2 — SURFACE RESISTANCE OF MODULE FRONT COVER

R_3 — VOLUME RESISTANCE OF MODULE SUBSTRATE

R_4 — SURFACE RESISTANCE OF MODULE BACK COVER

R_W — WIRING LEAKAGE RESISTANCE

R_C — CONVERTER LEAKAGE RESISTANCE

Figure 7–15 BRANCH CIRCUIT SCHEMATIC

branch circuit voltage in large systems having many modules wired in series.

The potential distribution for a center grounded branch circuit configuration is the same as for the floating configuration.

If the branch circuit were grounded at one pole (not illustrated), the maximum potential difference would increase to V_S. For example, grounding the negative pole would result in a potential difference, across the insulation of module number one, equal to the branch circuit voltage (for the schematic shown in Figure 7-15). As with the ungrounded configuration, the potential difference decreases uniformly along the branch circuit, reaching zero for the last module at the negative pole.

It is assumed that all modules will be identical within manufacturing tolerances. It is likely that any savings accruing from reduced insulation for modules near the electrical midpoint (graded insulation) would be offset by increased production, installation, and maintenance costs. Although for large high voltage systems, several discrete insulation levels might be considered.

7.4.2 Insulation Voltage Distribution - DC

For many module designs, the encapsulation/insulation system consists of a laminate of two or more materials. In such cases, the dc voltage is distributed across the material in proportion to the ratio of the volume resistivities of the individual laminate constituents. Therefore, the electric field is not simply the voltage (cell to ground, see Section 7.4.1) divided by the laminate thickness as is the case for a single material.

The resistance of each layer of material is given by the expression for Rn as follows:

$$Rn = \frac{\rho n \times Ln}{S}$$

where ρn is the volume resistivity of material n
Ln is the thickness of material n
S is the laminate area

The distribution of a dc voltage across the laminate is given by:

$$Vn/V = Rn/(R_1 + R_2 + -- R_X)$$
$$= \rho nLn/(\rho_1 L_1 + \rho_2 L_2 + -- \rho_X L_X)$$

where, Vn is the voltage across material n
V is the voltage across the laminate and
R_X is the volume resistance of each material layer 1 through x.

The resulting electric field across material n is then Vn/Ln.

In some laminates most of the field can be across one of the materials. This has been illustrated in a previous Bechtel report (Ref. 2-1) and is reproduced here as Figure 7-16.

Of interest is the possibility of large electric fields occurring across very thin layers of adhesives, primers, or thin front or back cover films, resulting in high stress levels. However, to date, little interest has been shown in the electrical properties of primers and such data does not appear to be available.

The discussion of electrical stress in module encapsulants has thus far assumed a uniform field between parallel conductors. Although this is a useful approximation, actual values for the maximum electric field will be higher due to field intensification (see Section 7.1.1). Inspection of Figures 7-2 and 7-3 shows that electric fields will be higher than those calculated for flat electrodes due to sharp corners on cells and interconnects, raised metal tips from poor soldering or similar items. Sharp edges on a metal module frame can result in similar intensification if in close proximity to cells. Also, lumps of solder or raised cell interconnects would result in reduced insulation thickness which would further increase stress levels. Areas of high field concentrations are likely sites for insulation failure, as are material imperfections such as voids and impurities.

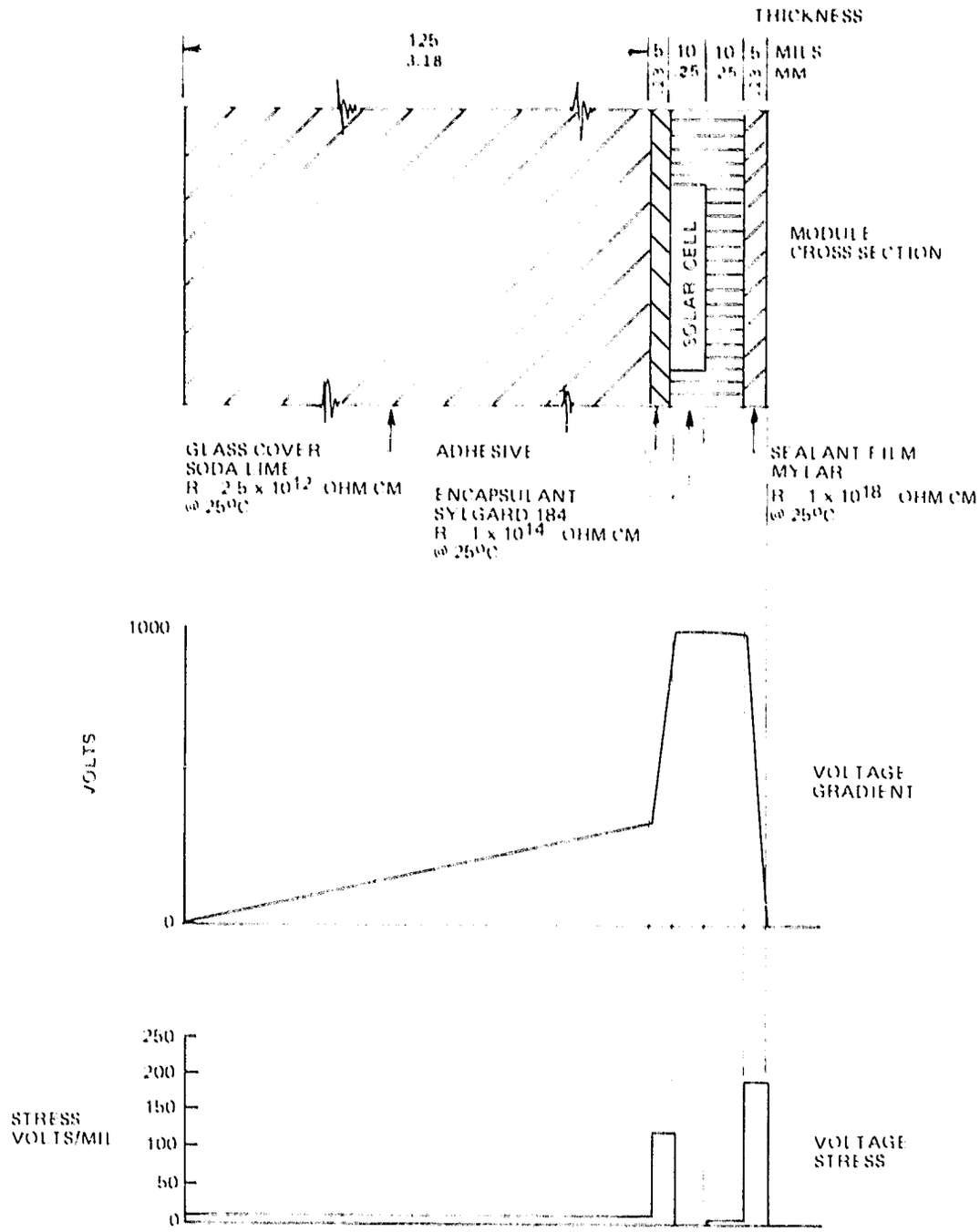

Figure 7-16 VOLTAGE GRADIENT AND STRESS DISTRIBUTION FOR GLASS SUPERSTRATE MODULE DESIGN

7.4.3 Insulation Voltage Distribution - Transient

During the course of its life, a module will likely be exposed to transient voltages. Transient voltages can result from lightning surges or from the converter. Transients may also occur during module testing. Under transient conditions, the voltage distribution in a module can differ significantly from the steady-state dc distribution discussed in Section 7.4.2.

As previously discussed, for two or more insulators in series, the distribution of steady-state dc voltages is a function of the resistivities of the materials and their relative thicknesses. For transient voltages, the distribution is a time dependent function of both material permittivities and resistivities as well as thickness.

Figure 7-17 presents a simplified configuration of a two material laminate and its equivalent circuit, as well as equations representing the voltage distribution and electric fields in the materials with the application of a transient step function. The equations shown in the figure can be expanded to the general case of n laminates. As before, the voltage is obtained by assuming an exponential solution and solving for the constants. The voltage across the "m"th laminate (normalized to the applied voltage) is given by:

$$V_m / V = (A_m - B_m) e^{-KT} + B_m$$

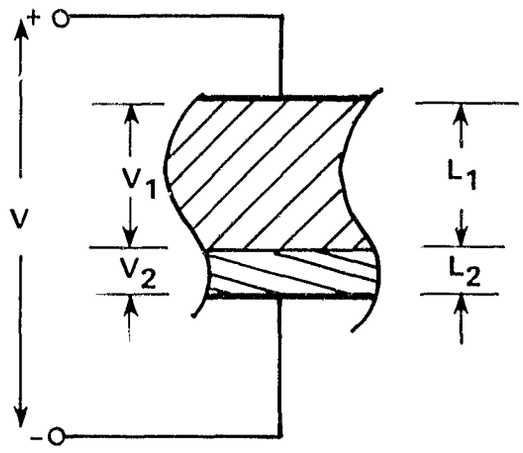

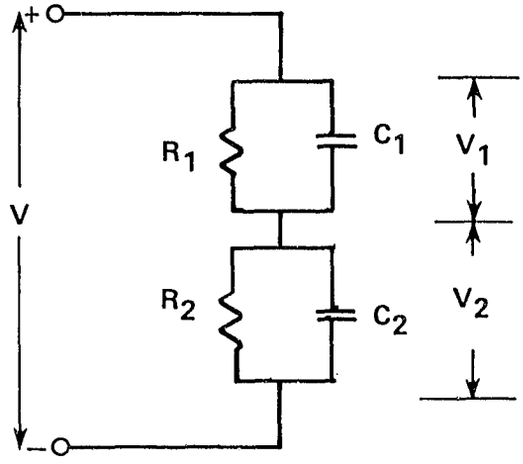

V = APPLIED VOLTAGE

V_N = VOLTAGE ACROSS MATERIAL N

S = ELECTRODE AREA

L_N = THICKNESS OF MATERIAL N

ρ_N = RESISTIVITY OF MATERIAL N

ϵ_N = PERMITTIVITY OF MATERIAL N = $\epsilon_R \epsilon_O$

ϵ_R = RELATIVE DIELECTRIC CONSTANT

ϵ_0 = PERMITTIVITY OF FREE SPACE
$10^{-9}/36\pi$ FARADS/METER

E_N = STRESS IN MATERIAL N

$$C_N = \frac{\epsilon_N S}{L_N}$$

$$R_N = \frac{\rho_N L_N}{S}$$

$$V_1/V = (A - B)e^{-KT} + B$$

$$V_2/V = 1 - V_1/V$$

$$K = \frac{\left(\frac{1}{\rho_1 L_1} + \frac{1}{\rho_2 L_2}\right)}{\left(\frac{\epsilon_1}{L_1} + \frac{\epsilon_2}{L_2}\right)}$$

$$B = \frac{\rho_1}{\rho_1 + \rho_2 L_2/L_1}$$

$$A = \frac{\epsilon_2}{\epsilon_2 + \epsilon_1 L_2/L_1}$$

$$E_1 = V_1/L_1$$

$$E_2 = V_2/L_2$$

Figure 7—17 SERIES DIELECTRIC PARAMETERS

where:

$$K = \sum_{N=1}^{N} 1 / (\rho_N L_N) / \sum_{N=1}^{N} \epsilon_N / L_N$$

$$A_m = (L_m / \epsilon_m) / \sum_{N=1}^{N} L_N / \epsilon_N$$

$$B_m = \rho_m L_m / \sum_{N=1}^{N} \rho_N L_N$$

and the electric field in the "m"th laminate is:

$$E_m = V_m / L_m$$

The time constant of the material laminate is governed by all three parameters and can vary over four orders of magnitude for material combinations used in present module designs. For steady-state dc voltages, the distribution is governed by material resistivities and thicknesses as given by the equation for "B".

There are many combinations of materials and thicknesses used in present and proposed module designs (for both sub- and superstrate configurations). Examples of the response of several encapsulation configurations to a 1000 Vdc step (as might be applied during testing) are shown in Figures 7-18 through 7-21.

Material properties presented in Table 7-1 and the equations presented in Figure 7-17 were used for the calculations. In these figures, the steady-state dc field distribution is that shown at t=∞. As can be seen by comparing the time scales on these four figures, there can be considerable variation in time constants.

This indicates the need to allow adequate time for the current to reach steady-state during module testing. The time required for the charging current to decay to a sufficiently small value so as not to impair the measurement of steady state (dc) values (sometimes called the soak time), can vary from milliseconds to minutes, depending on the insulation characteristics, as shown by Figures 7-18 through 7-21.

7.4.4 Insulation Voltage Distribution - AC

A module may also be exposed to ac voltages from converter ripple or dither type maximum power tracking circuits. In addition to depending on insulation material properties, the ac voltage distribution in a multilaminate system is a function of the frequency of the applied voltage.

To obtain the volgate distribution under ac excitation (with a radian frequency w), the equivalent circuit shown in Figure 7-17 can be viewed as a simple impedance divider. The voltage across the "m"th laminate in an n laminate system is simply the ratio of

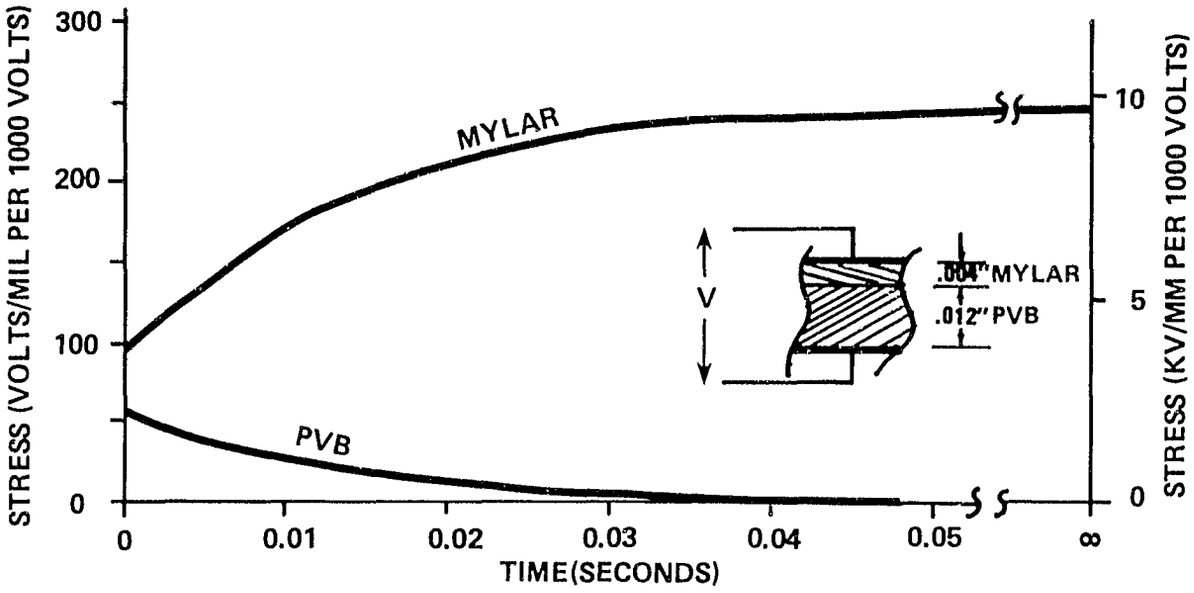

Figure 7—18 STRESS IN MYLAR/PVB LAMINATE

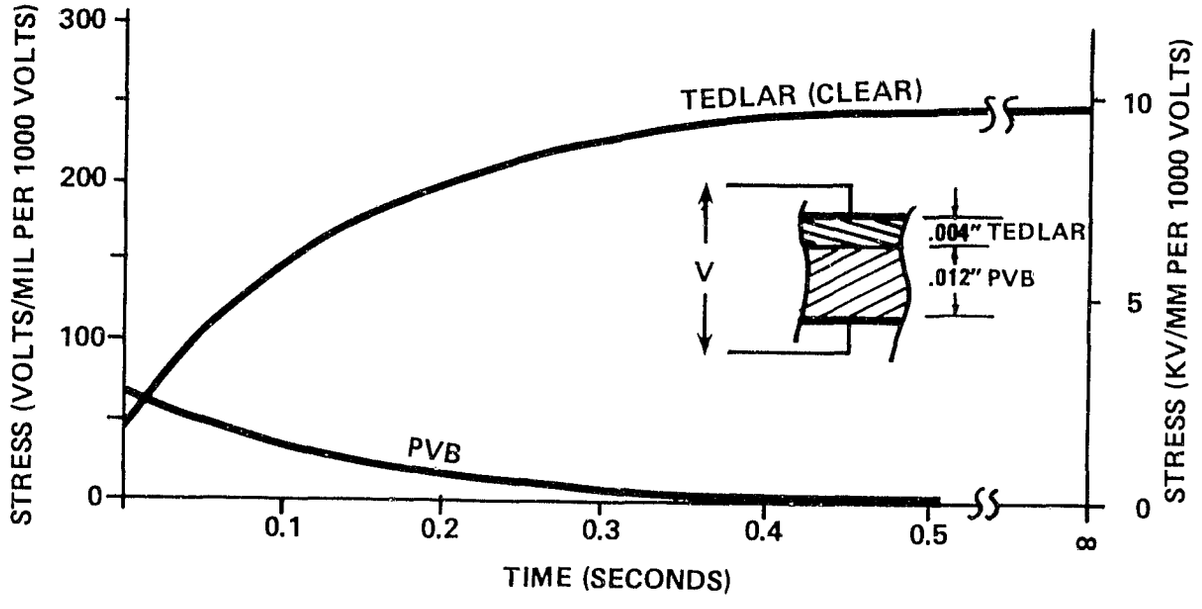

Figure 7-19 STRESS IN CLEAR TEDLAR/PVB LAMINATE

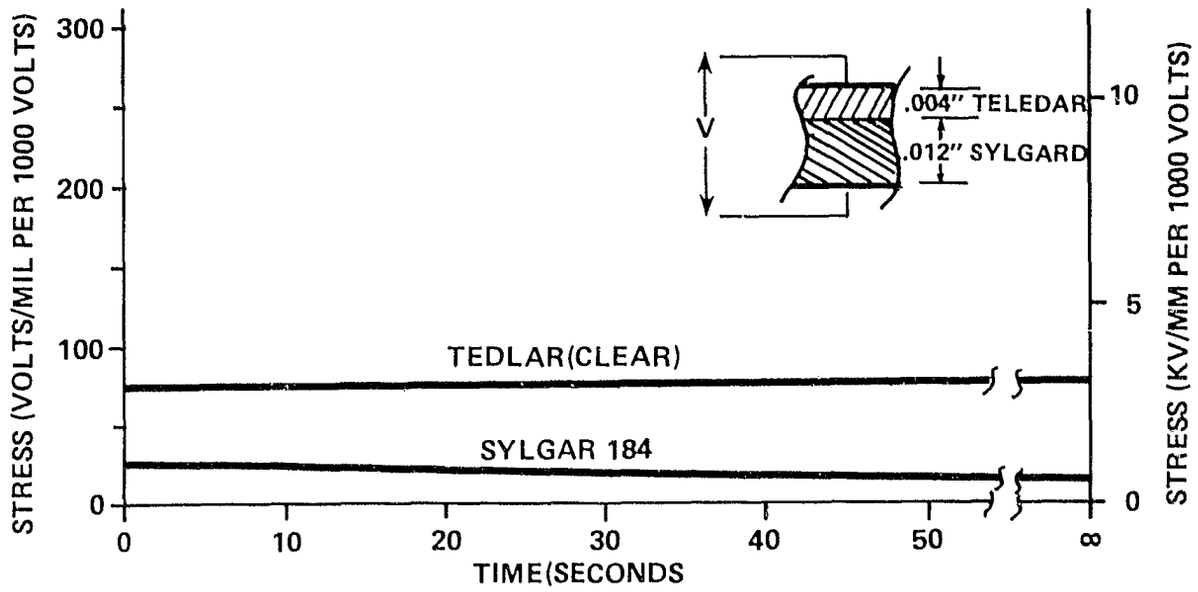

Figure 7—20 STRESS IN CLEAR TEDLAR/SLYGARD LAMINATE

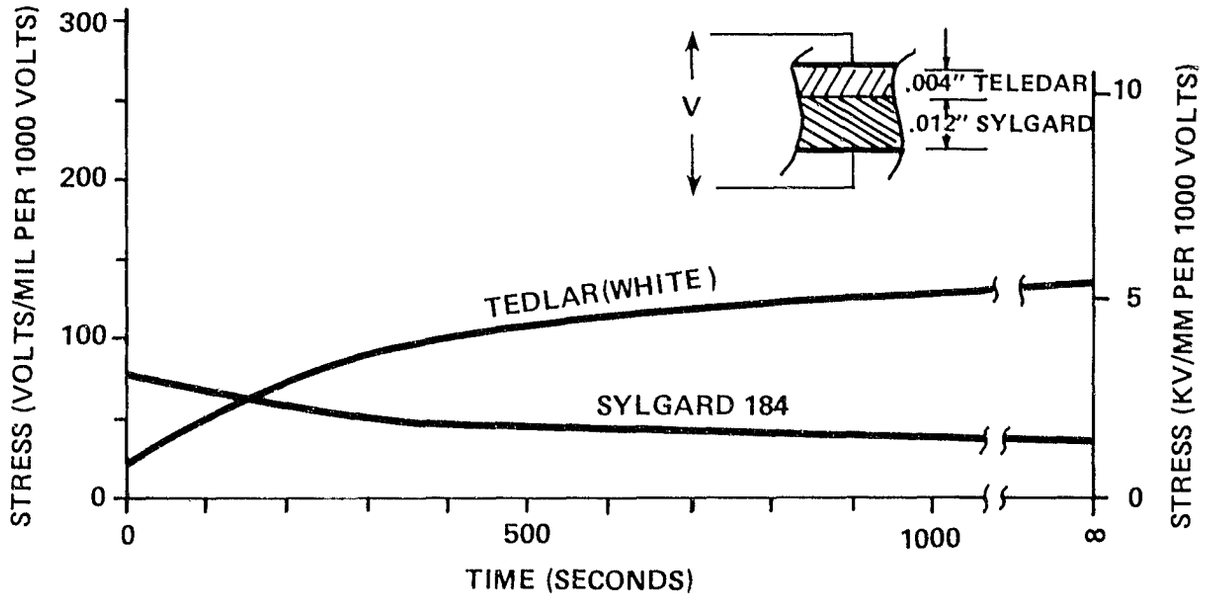

Figure 7—21 STRESS IN WHITE TEDLAR/SYLGARD LAMINATE

its impedance to the total impedance and can be expressed as follows:

$$V_m / V = Z_m / \sum_{N=1}^{N} Z_N$$

where the complex impedance of each element is given by:

$$Z_N = (1 / R_N + j\omega C_N)^{-1} = (R_N - j\omega C_N R_N^2) / (1 + \omega^2 C_N^2 R_N^2) = (\rho_N L_N - j\omega \epsilon_N \rho_N^2 L_N) / (1 + \omega^2 \epsilon_N^2 \rho_N^2)$$

and the normalized electric field in the "m"th laminate is:

$$E_m = V_m / L_m$$

Depending on the applied frequency, the stress distribution in a two laminate system will vary between that shown for t=0 and t= ∞ in Figures 7-18 through 7-21. Thus it can be seen that testing with an ac voltage will not (usually) produce the same stress distribution as dc.

7.4.5 Module Leakage Resistance

Figure 7-22 illustrates sections of several typical module configurations and a simplified electrical equivalent circuit of the module insulation. As indicated by Figure 7-22, there are essentially two parallel electrical leakage paths through the

module encapsulation/insulation system, through the substrate and through the superstrate.

Present module testing requirements include measuring electrical leakage resistance between the cells within a module and its exterior metal framework (or mounting structure if the module does not contain any exposed metal surfaces).

The following discussion explains why the present procedures should be modified to provide a better measure of leakage resistance in order to facilitate evaluation of both personnel safety and leakage power losses.

Personnel Safety. Personnel safety hazards may result from either excessive leakage currents flowing in the support structures or from insufficiently insulated exposed module surfaces.

As shown in Figure 7-22, electrical leakage paths occur in both the superstrate and the substrate. Each leakage path is in turn composed of a volume resistivity and a surface resistivity. Therefore, the measured value of leakage resistance depends on the materials' resistivities and the module configuration.

Evaluation of the module configuration presented in Figure 7-22A (conductive edge frame with insulating super-and substrates), using the surface and volume resistivities of commonly used encapsulating materials (Table 7-1), indicates that present

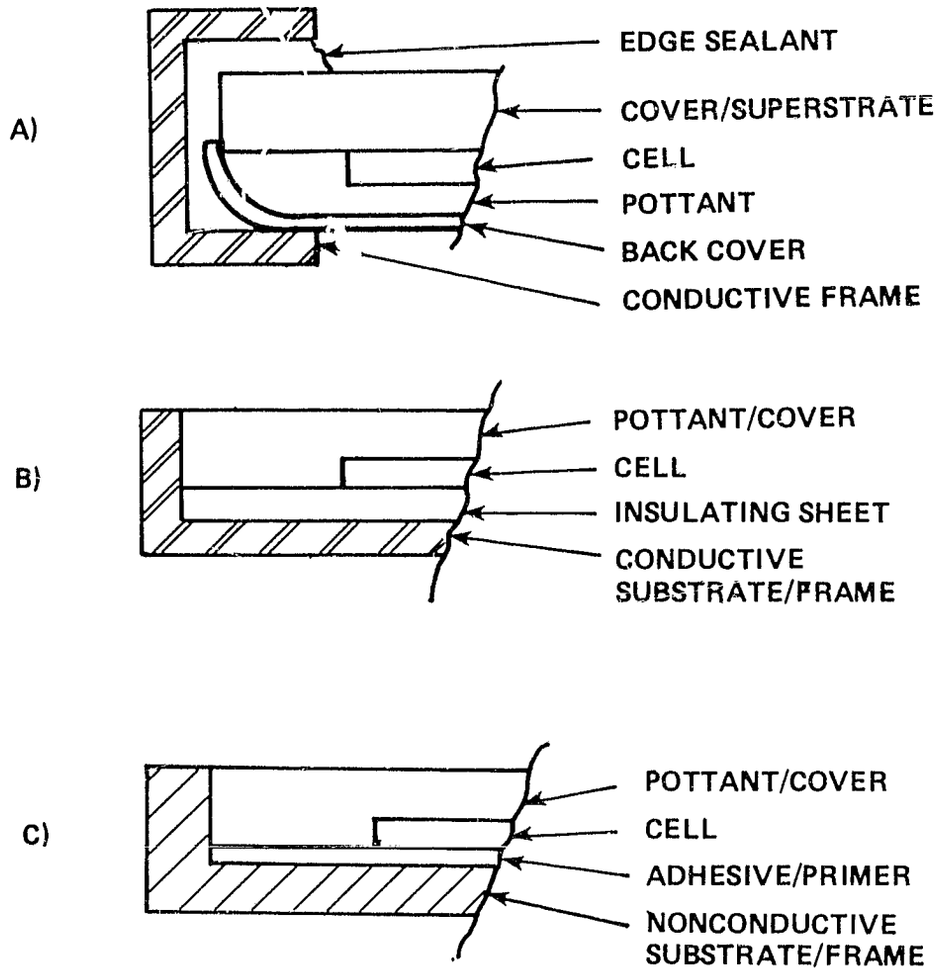

R_S – ELEMENT OF SURFACE RESISTANCE = $\frac{\text{(SURFACE RESISTIVITY) (GAP LENGTH)}}{\text{(ELEMENT PERIMETER)}}$

R_V – ELEMENT OF VOLUME RESISTANCE = $\frac{\text{(VOLUME RESISTIVITY)(THICKNESS)}}{\text{(ELEMENT AREA)}}$

Figure 7–22 MODULE INSULATION CONFIGURATIONS

measurement techniques essentially measure the leakage resistance of the area near the edges of the module. This is because the surface resistance component of the super and substrate leakage resistances increases with distance from the module frame. However, in service the module surface resistivities can be significantly reduced due to the effects of dirt accumulation, high humidity, dew or other factors. The result can be a significant increase in the magnitude of the system leakage current, when compared to that which would be calculated using the laboratory measured value for module leakage resistance.

Further, after the modules are installed in a high voltage array, personnel may come in direct contact with the surface of a module. In this important instance, the surface resistance does not contribute to the insulation system. Most research on personnel electrical safety has been conducted at the power line frequency of 60 Hz. At that frequency, the internal resistance between major extremities is about 500 ohms. Voltages above 250 volts are likely to puncture the skin. Below about 250 volts, shock currents are limited by contact resistance. This property varies greatly among individuals and is on the order of 10^5 ohms for dry skin but may be as low as 1000 ohms for wet skin.

For the module configuration illustrated in Figure 7-22B (conducting substrate) the substrate surface resistivity would effectively be zero, however, the superstrate surface resistance

would have the same effect on the module leakage resistance as described for Figure 7-22A.

The leakage resistance of the configuration illustrated in Figure 7-22C (no exposed conducting parts) is subject to the same considerations discussed for Figure 7-22A. In addition, the measured leakage resistance would be affected by the extent of contact and the method of connection between the module and conducting parts of the test frame.

It is therefore proposed that present test procedures be modified, as follows, to take these factors into account. Resistance and electrical breakdown tests should be made with a conductor covering all insulated module surfaces and connected to the frame. The conductor may be a pool of conducting liquid (such as a salt solution or mercury) or a conductive rubber foam sheet (such as Emerson and Cumming, Inc. Eccoshield SV-F). This technique would allow measurement of any personnel safety hazard that may exist. It would also tend to show up defects such as encapsulant material pinholes, voids, trapped impurities, protruding (or nearly protruding) cell interconnects or similar problems that might go undetected by measuring breakdown between the module frame and cells.

The testing of modules with film (smooth) back covers could utilize a conducting sheet electrode. Modules with a ribbed

nonconducting substrate might require use of a conducting liquid test electrode.

Power Losses. As previously discussed, insulators have a high but finite resistance. Thus, modules operating in a photovoltaic power system will have a finite leakage current. Module leakage currents are governed by the module resistance to ground (R) and the module potential to ground (electrical position in the branch circuit as discussed in Section 7.4.1). Branch circuit leakage current is the sum of the module leakage currents. For example, consider a branch circuit configuration that has one pole grounded and that is made up of N modules of voltage V connected in series, to produce a system voltage $V_s = NV$. The total leakage current for the branch circuit is given by:

$$i = (V_s - V)/R + (V_s - 2V)/R + \cdots + (V_s - NV)/R$$

$$i = 1/R \sum (V_s - xV)$$

$$i = V/R\,(N^2 - N(N+1)/2)$$

$$i \approx VN^2/2R \qquad \text{for } N >> 1$$

where R = module leakage resistance.

The module and branch circuit current for a single series string (no parallel modules) is given by:

$$I = P/V = \eta QA/V$$

where η is the module efficiency
Q is the insulation and
A is the module area.

Thus the branch circuit leakage current, expressed as a fraction of the total current, is given by:

$$F = i/I = V_S^2 / (2\pi Q RA)$$

As shown, leakage current increases with the square of the system voltage. The equation also illustrates that module resistance per unit area, rather than module resistance, is a more significant parameter for evaluating the total photovoltaic system. This is because, for equal module resistances, the use of several small modules in parallel can result in a lower equivalent leakage resistance (higher leakage current) than if a single, larger, module were used. The conclusion is the same whether grounded or ungrounded branch circuits are considered.

The required level of module resistance may also restrict material choices, especially for larger modules, as illustrated in Figure 7-23.

For example, previous JPL specifications have required a minimum module resistance of 10^8 ohms (Ref. 7-22). As shown in Figure 7-23, to meet this requirement a 1.2 by 2.4 m (4 by 8 ft) module would require an encapsulation thickness in the range of 0.0025 cm (0.98 mil) for a material with a volume resistivity of 1×10^{15} ohm-cm. A thickness of 0.076 cm (30 mil) would be required for a material with a volume resistivity of 6×10^{13} ohm-cm. However, to meet the requirement of 10^8 ohm module

resistance, a 1.2 by 2.4 m (4 by 8 ft) module using EVA (volume resistivity = 10^{12} ohm-cm) with an aluminum foil vapor barrier as the back encapsulation system would require about 2.97 cm (1170 mils) of EVA. This is clearly impractical and implies that: a high resistivity backing film (such as Mylar) is required, the 10^8 ohm leakage resistance requirement should be reevaluated, or both. A more recent specification (Ref. 7-23) reduced the leakage resistance requirement to 4 x 10^7 ohms per module. However, this would still require about 1.19 cm (468 mils) of EVA.

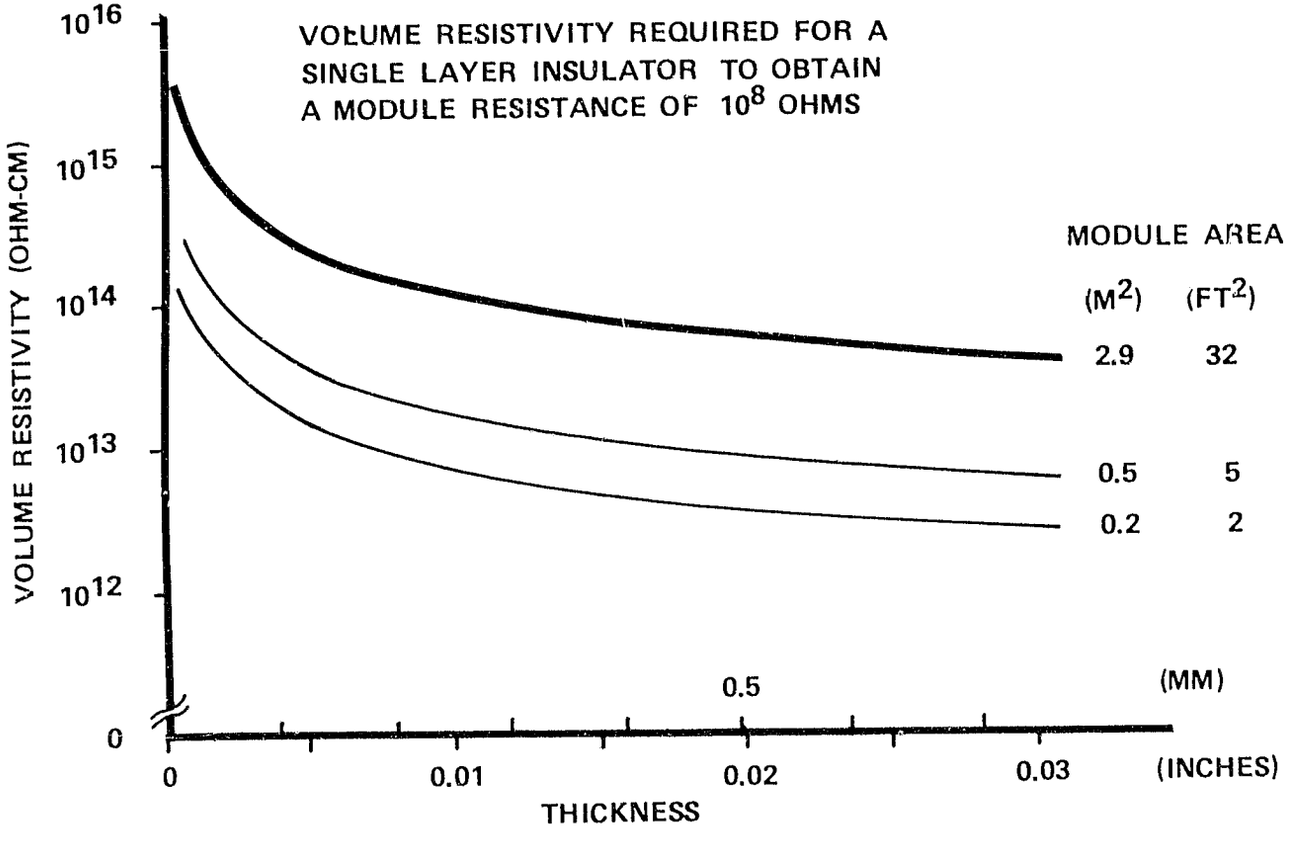

Figure 7-23 VOLUME RESISTIVITY REQUIREMENTS

Power losses due to dielectric heating by ac ripple currents are expected to be on the order of a tenth of a percent or less. Thus, this aspect of leakage current does not appear to be significant. However, if branch circuit leakage resistance is not maintained at acceptable levels, excessive power loss, ohmic heating and shifts in branch circuit peak power operating point may result.

Therefore, module leakage resistance requirements should be further evaluated in order to establish acceptable levels for various module sizes, system sizes, voltage levels and system configurations.

7.5 MODULE DESIGN IMPLICATIONS

This section illustrates the considerations and design procedures necessary to ensure adequate voltage endurance for a specific encapsulation system. The implications of system voltage level on design requirements and, therefore, the cost of the encapsulation system are also discussed.

As discussed in Section 7.4.1, the voltage across a module's insulation is influenced by the location of the module within the branch circuit. However, if all modules within a system are to be manufactured to a common specification, the highest voltage must be designed for. This is the branch circuit voltage for

circuits with one pole grounded and half that amount for floating or center grounded systems.

It is likely that the principle materials and physical arrangement for a specific encapsulation design will be selected based on considerations other than voltage endurance requirements. These considerations will probably include material cost, as well as long-time mechanical and optical performance. Voltage endurance (as well as leakage resistance) considerations may then impose additional design requirements. Working stress is determined by first calculating the uniform field across the material or material laminates (as discussed in Section 7.3). This uniform stress must then be increased by a factor to account for the field intensification due to edges on the cells and cell interconnect buses. The calculated value of working stress in the encapsulant materials can then be used to predict the voltage endurance of the module. However, due to the present lack of long-time voltage endurance data for typical encapsulant materials, material selection and determination of required material thicknesses are difficult. In particular, the derating of short-time voltage breakdown values (safety factor) is likely the greatest source of inaccuracy at present and points out the need for further programs to obtain long-time voltage endurance data for typical module materials and operating environments.

7.5.1 Design Example

Factors affecting module insulationn design are discussed further by way of an example. For purposes of illustration, a glass-superstrate/EVA/aluminized Mylar module is considered. The configuration is essentially as shown in Figure 7-16, except that EVA is used instead of Sylgard 184 and the Mylar has an aluminum coating to further increase moisture resistance.

In analyzing this design the following assumptions are made:

- The nominal encapsulating system consists of (from front to back) 3.18 mm (125 mil) soda-lime glass superstrate/0.38 mm (15 mil) EVA adhesive/solar cell assembly/ 0.38 mm (15 mil) EVA encapsulant/aluminized Mylar back cover sheet.
- The configuration of the bus and electrical feedthroughs do not limit the module voltage breakdown. This is a separate element of the design problem.
- Primers or similar very thin layers of material do not affect the insulation system design. This assumption is forced by the present lack of available data for such materials, but should be investigated further.
- The nominal voltage across the encapsulation system is 1000 volts dc (representing either a 1000 V system with one pole grounded or a 2000 V system either floating or center grounded).
- The dc voltage is assumed to be free of ac ripple, which might otherwise result in corona degradation. This assumption is included to simplify the following design example. However, the actual effects of inverter induced ac ripple on module insulation life should be further investigated.

- The cells, interconnects and intramodule buses are planer, with no raised areas due to interconnects or solder. For actual module designs such factors must be taken into account to ensure that material design thicknesses are maintained at all locations.

- The Mylar and EVA are free of voids and impurities. For actual modules this may not be a valid assumption in that voids may be introduced during material manufacturing and/or module encapsulating processes. Thicknesses are minimum values and account for production tolerances.

- The surface resistance of the glass superstrate is assumed to be sufficiently reduced by accumulated dirt so that it can be ignored during stress distribution calculations.

- A 20 year life is desired.

Significant characteristics for the encapsulation materials are summarized in Table 7-2.

TABLE 7-2

DESIGN EXAMPLE MATERIAL CHARACTERISTICS

Material	Thickness (mm)	Thickness (mils)	Volume Resistivity (ohm-cm) (1)
Superstrate			
Soda-lime glass	3.18	125	10^{13}
EVA	0.38	15	10^{12}
Substrate			
EVA	0.38	15	10^{12}
Aluminized Mylar	to be determined		10^{18}

1) From Table 7-1

It should be noted that both the super- and substrates are laminated layers, each containing two different materials. Therefore, working stress levels must be determined based on the ratios of thicknesses and volume resistivities, as discussed in Section 7.4.2.

The voltage across the superstrate materials is calculated to be 988 volts across the glass and 12 volts across the EVA. This results in a uniform stress level of about 0.31 kV/mm (8 V/mil) in both the glass and EVA. Assuming a stress concentration factor of 2 results in a maximum working stress of only 0.62 kV/mm (16 V/mil). Therefore, the voltage endurance of the superstrate appears to be more than adequate.

Examination of the thicknesses and volume resistivities for the substrate materials indicate that, in this laminate, virtually all of the voltage will appear across the Mylar.

Long-time voltage endurance data for Mylar under dc stress was not found to be available. Therefore, maximum allowable working stress was estimated based on available ac data and appropriate safety factors. From Figure 7-13, it was assumed that the ac voltage endurance of a 0.25 mm (10 mil) thick Mylar sample is about 1000 volts in a uniform field. Based on the discussion presented in Section 7.2.3, this value was increased by a factor of 3 to account for the generally higher voltage endurance of materials in dc fields. This results in a dc voltage endurance,

for 0.25 mm (10 mil) thick Mylar, of 3000 Vdc or 12 kV/mm (300 V/mil) in a uniform field. Using a stress concentration factor of 2 results in an equivalent maximum stress of 6 kV/mm (150 V/mil) for a 0.25 mm (10 mil) thick sample. As a final factor, examination of Figure 7-4 shows that in the region of interest, breakdown stress in Mylar varies inversely with the square root of thickness. Acceptable working stresses and equivalent voltage levels are illustrated in Figure 7-24 as a function of Mylar thickness.

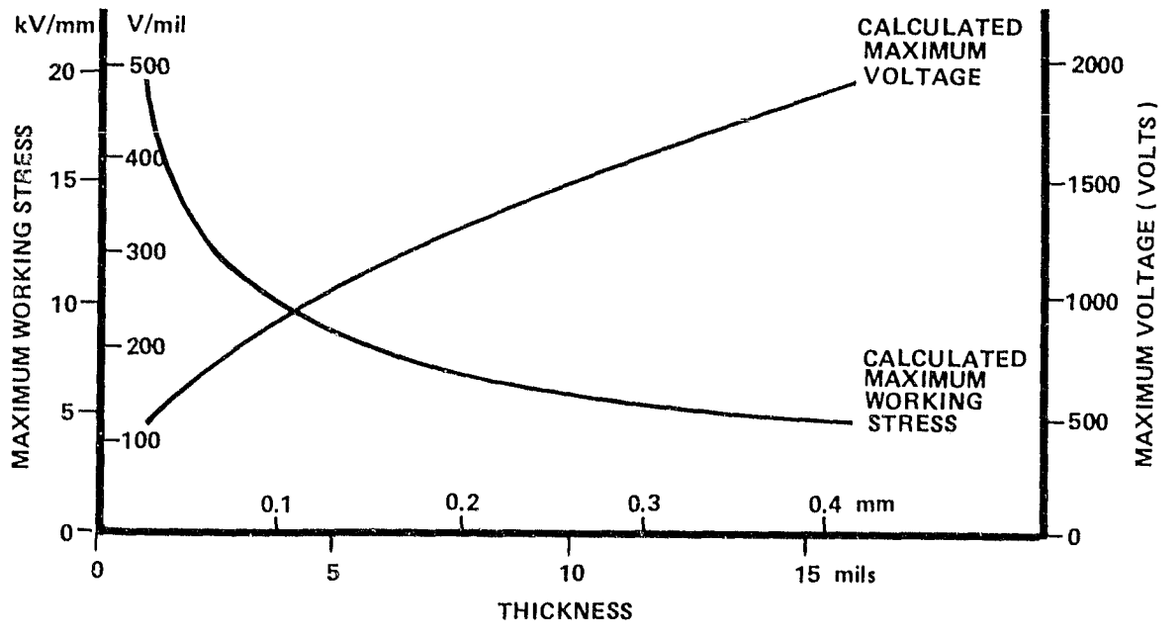

Figure 7-24 REQUIRED MYLAR THICKNESS AS A FUNCTION OF VOLTAGE

For the nominal 1000 volt level used in this example, Figure 7-24 indicates that the required Mylar thickness would be on the order of 0.125 mm (5 mils).

7.5.2 Cost Implications

Estimates of the cost implications of module insulation requirements as a function of branch circuit voltage are presented in Figure 7-25. These estimates are based on the approximations and design example from Section 7.5.1. Since the data used to determine long-time voltage endurance may contain large errors, the estimates should only be regarded as an indication of cost trends rather than a measure of absolute costs.

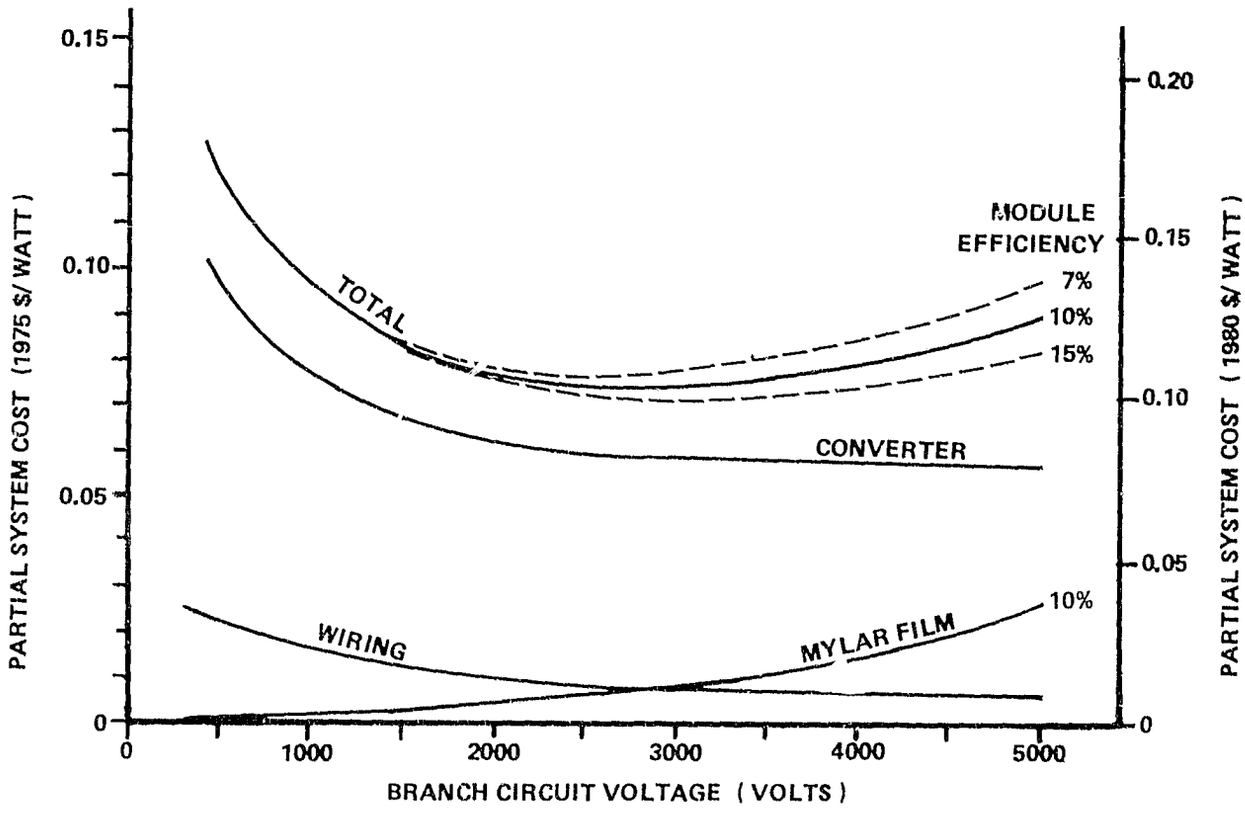

Figure 7-25 COST SENSITIVITY TO VOLTAGE

Essentially, the only system component costs affected by dc voltage level are the converter, the dc wiring and the module encapsulation costs. Figure 7-25 illustrates the behavior of

these individual component costs, as well as partial system cost, as a function of voltage level.

To simplify presentation of the data in Figure 7-25, it was assumed that the availability and cost of Mylar occurs as a smooth function of thickness rather than in discrete steps. The cost data for wiring and converters are from a previous Bechtel study (Ref. 3-1) and are for large central station power plant purchase quantities. Several general conclusions can be derived from the data presented in Figure 7-25, including:

- Dc voltage dependent photovoltaic power system costs are dominated by converter cost characteristics.
- For high-power systems, there exists an optimum branch circuit voltage that results in minimum system cost.
- Module efficiency is not a strong factor insofar as the effect of the incremental cost of insulation on total system cost.

One other conclusion is that for large systems, branch circuits with one pole grounded require higher levels of insulation and are therefore more expensive.

7.6 TESTING REQUIREMENTS

Data on the long-time voltage endurance of materials being used as module encapsulants does not appear to be readily available. It is suggested that JPL initiate a program to obtain and correlate data relating to the voltage endurance of encapsulating materials and modules.

This section presents recommendations regarding the establishment of such a testing program. In addition, several suggestions relating to module design requirements and qualification testing are also presented.

7.6.1 Voltage Endurance Testing

Various studies and programs have produced extensive lists of candidate module materials. Insofar as possible, data should be collected on the long-time voltage endurance of such materials. However, during the conduct of the present study, it was found that this data is generally not available. Further, available data is usually for 60 Hz rather than dc.

It is likely that dc voltage endurance data on module materials will have to be obtained from a program established for this specific objective. Initial efforts should be with a limited number of materials that show the most promise for future use (perhaps Mylar, Tedlar, PVB and EVA).

Data should be obtained from:

- Existing sources
- Real-time testing
- Accelerated aging

Existing Sources. There appears to be little existing data in the literature regarding the voltage endurance of candidate module encapsulating materials, especially under module operating conditions. However, it may be possible to obtain aged samples of various materials (for example, Mylar from old greenhouses) which could then be tested for dielectric strength, volume resistivity and other relevant parameters. Comparison of these results with published and/or measured values for new material would provide an important first step towards the evaluation and verification of module voltage endurance.

In addition, existing modules, such as the Block II and Block III designs, which have been installed in operating systems should be acquired for testing. Such testing will provide insight into the voltage endurance of encapsulating materials and encapsulation systems under actual operating conditions.

Test procedures should be in accordance with those described by the ASTM, particularly ASTM D-149 for dielectric strength and ASTM D-150 for conductivity data.

Real-Time Testing. The experiences of the cable industry (such as treeing-initiated failures in high voltage extruded dielectric cable) indicate the need for real-time testing to verify the voltage endurance of specific insulation (encapsulation) systems. It is therefore considered prudent that a real-time aging program

be established to evaluate the voltage endurance of present and proposed module encapsulation systems.

This program should include the assessment of dielectric strength, leakage resistance and other relevant parameters for encapsulating materials and modules exposed to actual operating conditions. Operating conditions normally include: temperature cycling, ultraviolet (sunlight) exposure, humidity and moisture, dc system voltage (including diurnal and seasonal variations resulting from peak power point tracking), transient and superimposed ac ripple voltages as well as other parameters appropriate for specific operating environments. Such testing should involve stressing modules at various voltage levels and periodically measuring dielectric strength or breakdown level (point C on Figure 7-10). Other types of measurements, such as simply measuring leakage current at one voltage, may give a less accurate indication of decreases in breakdown level (a shift to the left for area D on the curve in Figure 7-10).

Real-time testing should be conducted in conjunction with an accelerated aging program to provide data for correlating real-time and accelerated test results.

Accelerated Aging. Initial tests should be for accelerated aging due to voltage, exposure to concentrated sunlight and, perhaps, temperature. At first, these tests should be conducted with only one variable (accelerated aging parameter) acting on a given set

of samples.

After establishing confidence in correlating single variable accelerated aging data with real-time performance, attempts should be made to evaluate the effects of applying two or more accelerated aging parameters simultaneously. As discussed in Section 7.2.2, much work remains in the area of accelerated aging under actual operating conditions (multiple accelerated aging parameters) before complete confidence is established.

Further testing might include evaluation of various sample thicknesses, other materials, laminated materials (or material-primer laminates), other variables (such as ozone or atmospheric pollutants), the effect of varying temperature and/or voltages (to simulate diurnal cycles), transient withstand of aged samples and 60 Hz (to correlate with existing data that may be available).

7.6.2 Design Requirements and Qualification Testing

A proposed revision to the present module testing procedure has been discussed in detail in Section 7.4.4. Essentially, it consists of using a conductive foam rubber sheet on the module surface during electrical breakdown testing in order to better identify possible personnel hazards, insulation voids, imperfections, raised interconnects, etc., on modules with either conductive or nonconductive frames.

A second item under module testing (as discussed in Section 7.4) is to consider module resistance per unit area rather than total module resistance when evaluating system leakage current. No change in measurement technique is involved.

Section 8

CONCLUSIONS

This section presents major conclusions derived from the conduct of this study.

8.1 CURVED GLASS MODULE ARRAY COSTS

Comparison of installed costs for otherwise equivalent flat and curved glass module array configurations indicated potential cost savings for the curved glass configuration.

Specifically, savings of up to $10.00/m^2$ in 1980 dollars ($7.14/m^2$ in 1975 dollars) may be realized with regard to foundation/support structure/panel costs for a curved glass module array designed for a maximum 2.4 kPa (50 psf) loading. These savings are for an array having a 2.4 m (8 ft) slant height and using 1.2 by 2.4 m (4 by 8 ft) panels. Foundation/support structure/panel cost savings for a curved glass module array having a slant height of 4.8 m (16 ft) and using 2.4 by 4.8 m (8 by 16 ft) panels are about 20 percent less ($8.00/m^2$ in 1980 dollars) at a loading of 2.4 kPa.

These costs, however, do not include the premium for curving the glass. Estimated fabrication (bending) costs obtained during this study range from about $18.00 to $30.00/m² (1980 dollars) for a production volume of 4.6 x 10^5 m²/year (5 x 10^6 ft²/year). Therefore, reductions in foundation/support structure/panel costs do not appear sufficient to offset the glass bending costs as presently estimated.

Although presently estimated glass bending costs appear unacceptable, larger production volumes could result in significant per unit cost reductions. This is because automated glass manufacturing equipment is capital intensive and the attainment of low unit production costs requires that the equipment capital costs be amortized over many units. Therefore, it is conceivable that higher production volumes (for example, in the range of 9 x 10^6 m²/year) could result in attractive "total installed costs" for the curved glass module array. This is discussed further in Section 9, Recommendations.

8.2 CURVED GLASS MODULE DESIGN

Linear analyses of stress and deflections in the curved glass module, using finite element techniques, generally provide an acceptable level of accuracy for design loads of up to ±2.4 kPa (±50 psf).

The curved glass module design consisting of a 1.2 x 2.4 m (4 by 8 ft) 0.48 cm (0.187 in.) thick glass plate appears to be structurally sound for design loadings of up to ±2.4 kPa (±50 psf).

The use of 15 cm (6 in.) long support clips results in relatively high stress concentrations at the edges of the support clips for 2.4 kPa (50 psf) loading conditions. Extending the clip length to 30 cm (12 in.) reduces the stresses to acceptable levels.

Fabrication and testing of prototype curved glass superstrate modules should be considered in order to facilitate verification of the analytical results, as well as optimization of the support clip design.

8.3 FOUNDATION COSTS

In general, foundation design requirements and, therefore, foundation costs are dependent on site soil conditions.

For rocky soil conditions, where drilling costs would be prohibitive, or for loose sandy soil conditions, where casing and installation costs would be large, spread-footings are preferrable to caisson type foundations. However, caisson foundations may have a lower cost if the soil is sufficiently cohesive so as to permit installation without the need for

casings (to prevent the hole from collapsing during construction).

For example, when casings are not required, caisson foundations result in a cost saving of about $11.00/m² (1980 dollars) over equivalent spread-footing type foundations at a design loading of 2.4 kPa (50 psf).

Optimization of present construction techniques and/or equipment might extend the range of soil conditions for which caisson foundations are economically attractive.

8.4 ELECTRICAL INSULATION REQUIREMENTS

In addition to providing mechanical support and environmental protection of the solar cells, the module encapsulation system will most likely be required to provide electrical isolation of energized modules. Therefore, the encapsulating system must maintain acceptable electrical insulating properties throughout the useful life of the module.

Existing industry experience in the design and long-time performance characteristics of solid-dielectric insulating systems results primarily from the cable industry. The majority of this experience relates to operation with ac fields (60 Hz).

The electrical properties of materials are affected by both the physical configuration of the insulation system and the effects of aging. In addition, corona, ultraviolet light, temperature, and other ambient conditions tend to reduce dielectric strength with time (aging). Therefore, adequate safety factors must be used in the design of the system. This is necessary to ensure that stress levels in the material are sufficiently below those that would cause failure during the life of the module.

The required safety factor is somewhat dependent on material properties, configuration and ambient conditions. Although safety factors for module insulation, operating primarily in a dc field, will likely be somewhat lower than those used for ac insulation, present experience is not sufficient to formulate definite values.

Calculation of stress levels within module encapsulation systems must account for field intensifications resulting from sharp edges on solar cell interconnects and other conducting surfaces. In addition, for series dielectrics (laminates) ac stress distributes in proportion to the materials' permittivities and their relative thicknesses, while for dc fields the stress distributes in proportion to the materials' resistivities and thicknesses. Therefore, it is possible to develop high stress levels in thin material layers such as primers, adhesives, or cover films. Also, chemical reactions can occur between insulating materials and other materials, such as primers and

adhesives, and may result in severe reduction in the dielectric strength of the insulator.

In addition to dielectric strength, the encapsulation system must maintain an acceptable level of leakage resistance. This requirement becomes more significant as module size increases and/or for increasing system voltages. Some of the candidate encapsulating materials (such as EVA) appear to have relatively low volume resistivities, so that it may be necessary to provide an additional layer of high resistance material (such as a Mylar sheet).

Previous attempts, primarily by the cable industry, to predict long-time insulation performance by means of accelerated aging tests have, at best, been only partially successful. This is especially true with regard to the effects of multiple aging parameters, which are likely to be present in the modules' operating environment. Therefore, it appears prudent that a testing program be established to evaluate the voltage endurance of module encapsulating systems under actual operating conditions.

Section 9

RECOMMENDATIONS

In view of the potential cost savings for the curved glass module array configuration, large volume glass bending costs should be further evaluated. The evaluation should include identification of potential fabrication methods as well as equipment capital costs and required production volumes.

Present glass industry manufacturing capabilities should also be evaluated to assess the potential effects of future photovoltaic glass requirements on industry production capacity. Such an evaluation should consider sheet fabrication, tempering and all other manufacturing processes necessary to produce glass sheets suitable for use in photovoltaic modules.

If large volume glass fabrication costs appear to be acceptable, a test program should be conducted to experimentally verify the technical feasibility of the curved glass module design. The test program should include the fabrication of several full sized curved glass module/support clip assemblies. The assemblies should be subjected to simulated uniform wind loading conditions and should be appropriately instrumented so as to permit measurement of stress distributions and deflections.

The testing program should also include optimization of the support clip design with regard to location, length, gasket material and other design variables.

In view of the sensivity of foundation design requirements and hence, foundation costs, to site soil conditions, future array design and cost studies should better account for these variations.

Construction technques and equipment required for installing caisson foundations in sandy, or otherwise noncohesive, soils should be investigated. This could extend the range of soil conditions for which caisson foundations are economically attractive.

Module design programs should include evaluation of the electrical performance of the encapsulation system. Important considerations include stress concentrations and distributions, voltage endurance and leakage resistance. These will become more important for larger modules and/or higher system voltages likely to be used in large systems.

A testing program should be established to evaluate and identify the long-time electrical characteristics of encapsulating materials and encapsulation systems under actual operating conditions. The program should include real-time aging of material and module samples, with periodic measurement of

dielectric strength (not just leakage current), volume resistivity and other significant parameters.

An accelerated aging program should be conducted in parallel with the real-time testing. This will facilitate correlation of data as well as identification of reliable accelerated aging techniques for the evaluation of long-time electrical isolation performance under actual operating conditions.

Module leakage resistance should be specified per unit module area rather than for the total module. In addition, module leakage resistance should be measured using a conducting sheet over the module surface. This will facilitate identification of possible material defects and/or personnel safety hazards.

Section 10

NEW TECHNOLOGY

No reportable items of new technology have been identified by Bechtel during the conduct of this work.

REFERENCES

2-1 Bechtel National, Inc., Module/Array Interface Study, Final Report, prepared for the Jet Propulsion Laboratory under contract number 954698, August 1978

3-1 Bechtel national, Inc., Terrestrial Central Station Life-Cycle Analysis Support Study, Final Report prepared for the Jet Propulsion Laboratory under contract number 954848, August 1978

3-2 Bechtel Corporation, Engineering Study of the Module/ Array Interface for Large Terrestrial Photovoltaic Arrays, Final Report prepared for the Jet Propulsion Laboratory under contract number 954698, June 1977

3-3 Bechtel Corporation, A Conceptual Design of a Photovoltaic Central Station Power Plant, Final Report prepared for Spectrolab, Inc., under subcontract 66725, July 1976

4-1 Review of World Experience and Properties of Materials for Encapsulation of Terrestrial Photovoltaic Arrays, Final Report, work performed by Battelle Columbus Laboratories, Columbus, Ohio, for ERDA, under contract no NAS-7-100-954328, July 21, 1976

4-2 Process Development for Automated Solar Cell and Module Production - Task 4: Automated Array Assembly, Annual Report, MB Associates, prepared for the Jet Propulsion Laboratory under contract no. 954882, June 12, 1979

4-3 Roark, R.J., Formulas for Stress and Strain, 4th Edition, McGraw-Hill, 1965

4-4 Timoshenko, S.P. and Gene, J.M., Theory of Elastic Stability, 2nd Edition, McGraw-Hill, New York, N.Y.

4-5 Melosh, R.J. and Al'amundil, M.Y., "Educing Alternate Equilibrium States in Mechanics Simulation," to be presented at the "Symposium on Computation Methods in Nonlinear Structural and Solid Mechanics," Washington, D.C., October 6-8, 1980

5-1 Bechtel National, Inc., Design of Low-Cost Structures for Photovoltaic Arrays, prepared for Sandia Laboratories under contract number 05-6195, San Francisco, CA, April 1979

6-1 D. Moore, Cyclic Pressure-Load Developmental Testing of Solar Panels, JPL Report No. 5101-19, February 28, 1977

7-1 Fink and Carroll, Standard Handbook for Electrical Engineers, Tenth Edition, McGraw-Hill, 1969

7-2 Reference Data for Radio Engineers, International Telephone and Telegraph Corporation, Fourth Edition, 1962, p. 921

7-3 Du Pont, Technical Information Bulletin M-4D -- Electrical Properties Mylar Polyester Film, E.I. Du Pont De Nemours and Company (Inc.) Wilmington, Delaware

7-4 Underground Power Transmission, A Study prepared by Arthur D. Little Inc., for the Electric Research Council, ERC Publication No. 1-72, October 1972, pp. 7.8-1.9 and 7.12

7-5 L. Simoni and G. Pattini, A New Research Into the Voltage Endurance of Solid Dielectrics, IEEE Transactions on Electrical Insulation, Volume EI-10 No. 1, March 1975

7-6 ABC of Motor and Generator Insulation, Electric Machinery Mfg. Company E-M Synchronizer 100-SYN-73, p. 28

7-7 E.L. Brancato, Insulation Aging - A Historical and Critical Review, IEEE Transactions on Electrical Insulation, Volume EI-13 No. 4, August 1978

7-8 W.T. Starr and H.S. Endicott, Progressive Stress - A New Accelerated Approach to Voltage Endurance, Paper #61-243 presented at the AIEE Winter General Meeting, New York, January 1961

7-9 E.M. Port and H.E. Pietsch, Aging of Insulation by Thermal and Electrical Stress, Electrical/Electronics Insulation Conference Proceedings, IEEE Publication No. 75 CH 1014-0-EP54, November 1975

7-10 F.J. Campbell, Combined Environments versus Consecutive Exposures for Insulation Life Studies, IEEE Transactions, Volume NS-11, 1964

7-11 R.A. LaBozetta, The Development of a High Voltage dc Cable, Final Report, prepared by the Okonite Company for Electric Power Research Institute, Research Project 7818, Report EL-606, January 1978

7-12 A.R. von Hippel, Dielectric Materials and Applications, The MIT Press, Cambridge MA, 1966

7-13 Handbook of Chemistry and Physics, 33rd Edition, Chemical Rubber Publishing Company, Cleveland, OH

7-14 Design of Safe Electrical Equipment for Research, Los Alamos Scientific Laboratory, Informal Report No. LA-7597-MS prepared under DOE Contract No. W-7405-Eng-36, April 1979

7-15 Battelle Columbus Laboratories, Review of World Experience of Materials for Encapsulation of Terrestrial Photovoltaic Arrays, Final Report to JPL under contract no. NA9-7-100-954328, July 21, 1976

7-16 Du Pont, Technical Information Bulletin TD-1A, October 1977

7-17 Dow Corning Bulletin for Sylgard 184 Resin

7-18 D.C. Miles and J.B. Briston, Polymer Technology, Chemical Publishing Company, New York 1965

7-19 Properties of Glasses and Glass-Ceramics, Corning Glass Works, Corning, New York, August 1973

7-20 Modern Plastics Encyclopedia, McGraw-Hill, 1979

7-21 Du Pont Sales Office

7-22 User Handbook for Block III Silicon Solar Cell Modules, JPL Document No. 5101-82, November 15, 1979

7-23 Block IV Solar Cell Module Design and Test Specification for Intermediate Load Center Applications, JPL Document No. 5101-16, November 1, 1976

7-24 W. Nelson, A Survey of Methods for Planning and Analyzing Accelerated Tests, IEEE Transactions on Electrical Insulation, Volume EI-9 No. 1, March 1974

7-25 DuPont, Technical Brochure - Design Data for Teflon, A66426, June 1970